GEOLOGY OF THE GRANVILLE HARBOUR AREA

AND

MINERALIZATION IN THE GOURLAYS CREEK PROSPECT

by

R. G. Norris, B.Sc.

Submitted in partial fulfilment
of the requirements for the degree
of Bachelor of Science with Honours.

UNIVERSITY OF TASMANIA

December, 1985

LANDSAT IMAGE OF GRANVILLE HARBOUR AND THE AREA IMMEDIATELY TO THE NORTH.

ABSTRACT

The dominantly (meta-)sedimentary sequence of the Granville Harbour area ranges in age from Late Proterozoic to Devonian. Five phases of deformation are recognized in these sequences; two are correlated with the Late Proterozoic Penguin Orogeny, one with the Upper Cambrian Jukesian Movement, and two with the Early to late-Middle Devonian (Tabberabberan) Orogeny. Lower greenschist facies metamorphism accompanied the Penguin Orogeny.

Faulted against the Oonah Formation and unconformably underlying the Mt Zeehan Conglomerate are 415 m of interlayered schists, phyllites, quartzites and dolomites. This sequence is a probable lithostratigraphic correlate of the Crimson Creek Formation and has been named the Duck Creek Sequence. Minor metavolcanics contained within the Duck Creek Sequence, Oonah Formation and Whyte schist are defined chemically as ocean-floor tholeiite basalts.

Within the Gourlays Creek Prospect, the Oonah Formation hosts two distinct styles of mineralization:

(i) syngenetic banded iron formation of chemical origin, and

(ii) calcic, garnet-pyroxene, metasomatic infiltration exoskarn.

The banded iron formation is a stratabound and stratiform horizon consisting of massive and banded magnetite-pyrite-(quartz) and magnetite-barite mineralization. This chemical exhalative, banded iron formation is a probable analogue of the (Recent) Red Sea metalliferous sediments and is the only recognized deposit of its type in Tasmania. Sulphur isotopes from this horizon give $\delta^{34}S$ values for pyrite in the range of −7.6 to +15.5‰ and for barite, +35.8‰. A combination of inorganic reduction of Precambrian seawater, ($\delta^{34}S$ = +20 to +25%), with isotope disequilibrium, and biogenic reduction is required to explain the range in pyrite $\delta^{34}S$ values.

Intrusion of the Devonian Heemskirk Granite was accompanied by the formation of a garnet- pyroxene skarn. The dominantly calcic mineralogy of the skarn is suggestive of a lime-rich protolith. The deposition of magnetite-pyrrhotite-chalcopyrite and pyrite occurred during retrograde skarn alteration.

Sulphur isotope studies of skarn-associated sulphides indicate a source fluid with a $\delta^{34}S$ value of +7 to +15‰. Such high values indicate an inhomogeneous source consisting of barite from the banded iron formation, primary pyrite and/or magmatic sulphur. From fluid inclusion studies, homogenization temperatures for garnet and late-stage, retrograde quartz are >500°C and 330-340°C respectively. Deposition of sulphides during retrograde skarn alteration is inferred to occur at temperatures of 350-360°C, pressures of 13-35 MPa and from a 20-21 wt% equiv. NaCl solution. Minor tin (<0.35%) mineralization is considered to be associated with retrograde skarn formation.

CONTENTS

LIST OF FIGURES

LIST OF TABLES

CHAPTER 1
INTRODUCTION

The main aim of this study was originally to investigate the style of mineralization in the Gourlays Creek Prospect, a CRA/Geopeko Joint Venture project located approximately 1 km north of Granville Harbour. Detailed mineralogical and petrological studies, with fluid inclusion and sulphur isotope work are incorporated in this investigation to support interpretations of the mineralization. Since the initiation of this project, the aims have been broadened to include stratigraphic, metamorphic and structural studies of the dominantly sedimentary lithologies exposed in the area. Minor associated metavolcanics are investigated by petrological and geochemical techniques.

1.1 LOCATION, ACCESS, PHYSIOGRAPHY, MAPPING, SAMPLING AND FIELD CONDITIONS

Granville Harbour is a coastal shack settlement located 27 km WNW of Zeehan in Western Tasmania (Fig. 1.1). Access to the area is by the Lower Pieman Dam Road via Zeehan. A total of four weeks was spent in the field using Granville Harbour as a base and another week was spent logging drill core at Burnie. Follow-up work has been undertaken over a period of approximately six months.

The best exposures in the area are along a narrow coastal platform extending 7 km northwards from Granville Harbour. Sediments ranging in age from Late Proterozoic to Devonian in age are exposed along this coastal section. It is from these exposures that most of the stratigraphic, metamorphic and structural interpretations are based. The coastal lowlands are dominated by impenetrable teatree scrub, swamp and Quaternary cover with no exposures of the pre-Devonian lithologies. Inland, approximately 1 km west of the coastal section, the physiography is defined by a low, undulating, Tertiary basalt plateau. Two streams, the Gourlays and Vincents Creeks, have cut through this basalt plateau exposing the underlying sediments of the Oonah Formation (Fig. 2.1). The mineralized horizons occur within these basalt windows. Minor exposures of both mineralization and sediments of the Oonah Formation are confined to the creek beds and along bulldozed grid lines. The southern part of the field area is dominated by the Devonian Heemskirk Granite, a small apophysis of which intrudes the grid area.

Surface geological mapping of the coastal exposures was undertaken using 1:6500 aerial photos and 1:5000 photocopied enlargements of these photos. Grid and stream mapping was done on 1:2500 grid maps of the

CRA/Geopeko Joint Venture. A summary 1:5000 geological and structural interpretation map of both areas is presented in appendix A.6. All other field maps are reduced from this base map.

Co-ordinates of surface localities referred to in the text are given to the nearest 10 m. For coastal outcrops, the localities refer to the 100 km square grid CO of the Australian Map Grid (AMG), Zone SK-55. All co-ordinates for the Gourlays Creek Prospect are CRA/Geopeko grid co-ordinates. Its relationship to the AMG is shown in figure 2.1 and appendix A.6. Throughout the thesis all bearings (i.e. strike of bedding, etc.) are for grid north on the AMG.

CRA/Geopeko exploration diamond drill holes are referred to as DDH CGA, DDH GCB and DDH GC3. Co-ordinates and orientations of drill holes and summary drill core logs are given in appendix A.2. Due to poor exposures of the mineralized horizons in the grid area, most samples and interpretations of the mineralization are from drill core. All specimens sampled from both surface outcrops and drill core are referred to by their UTGD (University of Tasmania, Geology Department) number and have been stored and catalogued in the Geology Department rock store. A list of specimens, their sample locations and a brief description are given in appendix A.1.

1.2 PREVIOUS EXPLORATION AND LITERATURE

The lead into exploration in the Granville Harbour district came by the way of a field investigation during 1979-1980, by a CRA/Geopeko joint venture, into a 3.5 km long 2000 nT aeromagnetic anomaly first defined in a survey for Rio Australia Exploration in 1956. A grid was cut in 1980 and further extended in 1982. After this preliminary work, the potential for replacement-style Sn mineralization within banded calcsilicate rocks was realized. Intrusion of the Devonian Heemskirk Granite caused metasomatism of the carbonate sediments within the sequence. The grid area has been termed the Gourlays Creek Prospect by the exploration companies.

The bulk of the airborne anomaly was attributed to two conformable, parallel and relatively narrow bodies containing abundant magnetite. These bodies strike N-S in the southern part of the anomaly and are folded to an E-W strike in the north (e.g. Fig. 2.1). On the basis of this aeromagnetic anomaly and Sn-Cu-Fe bedrock geochemistry, a total of three holes were drilled. Drill core samples indicated anomalous concentrations of Sn and Cu to be associated with an upper pyroxene-garnet skarn horizon and anomalous Cu but negligible Sn concentrations to be associated with a lower banded magnetite-rich horizon. A possible syngenetic origin for the lower horizon

has been suggested. CRA/Geopeko progress reports on this area include Porter (1980), Perring (1983) and Kendall (1984).

Excepting exploration progress reports, the only previous literature of any consequence on the Granville Harbour area is a Geological Survey of Tasmania Explanatory Report of the Zeehan area (Blissett, 1962). The stratigraphy as defined by Blissett is used as a basis for this study. However, significant modifications have been made.

1.3 TIN-TUNGSTEN DEPOSITS IN TASMANIA

All known primary Sn(-W) deposits in Tasmania occur in rocks ranging in age from Late Proterozoic to Upper Devonian, and are spatially and genetically related to the emplacement of post-kinematic granites of Upper Devonian to Early Carboniferous age (Solomon, 1981). The distribution of major Sn(-W) deposits is shown in figure 1.2. In northeastern Tasmania, Sn mineralization occurs predominantly in greisens, and W in sheeted vein systems. In northwestern Tasmania there is a paucity of greisen deposits but an abundance of Sn(-W) replacement and skarn mineralization (Collins, 1983). The massive pyrrhotite-cassiterite replacement deposits of western Tasmania account for the bulk of Tasmania's tin production. Skarn deposits tend to be of low grade (<0.5% Sn), much of the Sn occurring in silicates, e.g. Moina (Kwak and Askins, 1981), St Dizier (Purvis, 1978) and Mt Lindsay (Kwak, 1983). The tungsten-bearing skarns contain no significant tin mineralization, e.g. King Island (Kwak and Tan, 1981) and Kara (Barrett, 1980). In comparison to the massive pyrrhotite-cassiterite replacement deposits (e.g. Renison - Paterson **et al.**, 1981; Mt Bischoff - Groves **et al.**, 1972; and Cleveland - Collins, 1983), the skarns are proximal to the granite intrusive.

1.4 REGIONAL GEOLOGY

The following discussion of the regional geology is based on the Geological Survey of Tasmania report for the Zeehan area (Blissett, 1962), a summary by Solomon (1981), a review of the regional geology in the Cleveland area (Collins, 1983), and others as quoted.

The oldest rocks exposed in the Granville Harbour area are the Late Proterozoic Whyte Schist. According to Gee (1967), the Whyte Schist forms part of an 8 km wide belt, termed the Arthur Lineament, consisting of pelitic schist, greenschist and amphibolite in the lower to middle greenschist facies. The Whyte Schist in the south are considered to correlate with the Keith Metamorphics in the north. In the southwest, apparently stratiform but disrupted lenses of magnetite-pyrite

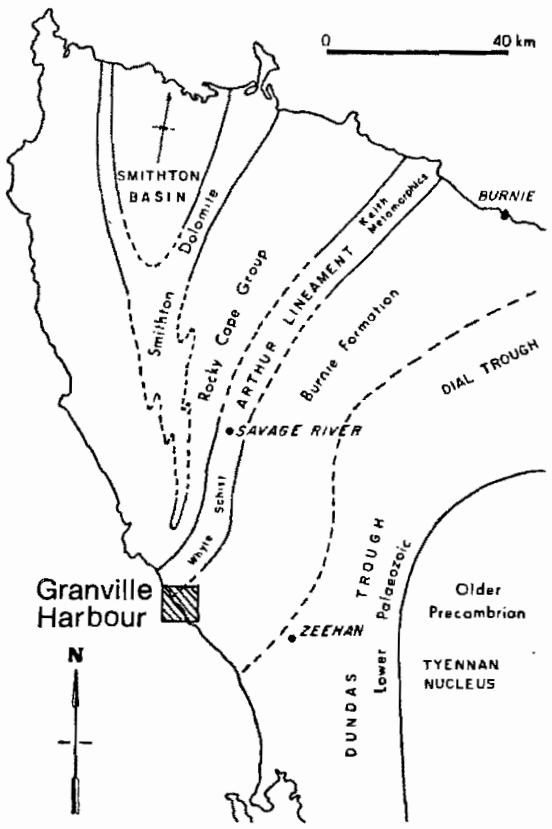

Fig. 1.1 Major Precambrian and Early Palaeozoic structural elements of NW Tasmania (after Gee, 1967). Field area is defined by hatched area labelled "Granville Harbour".

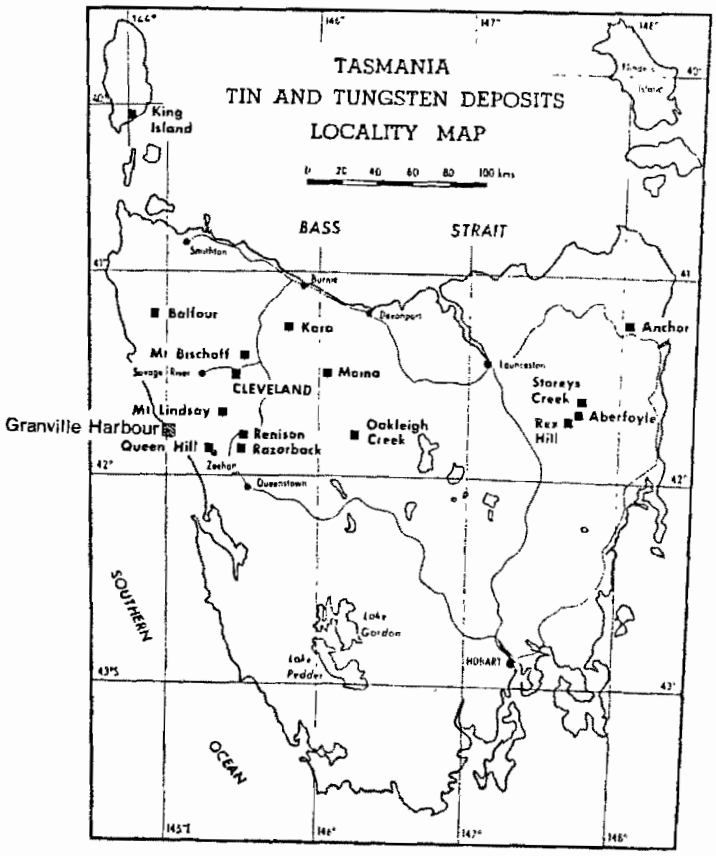

Fig. 1.2 Major Sn(-W) deposits of Tasmania (after Collins, 1983). Granville Harbour defined by cross hatched area.

mineralization of the Savage River Mine occur within a suite of metamorphosed tholeiitic basalt, andesitic tuff and gabbroic intrusives (Coleman, 1975).

West of the Arthur Lineament (Fig. 1.1), the Rocky Cape Group consists of unmetamorphosed laminated mudstone and super-mature orthoquartzite sequences with minor turbiditic greywacke and rare occurrences of basaltic lava and mafic tuff. East and southeast of the Arthur Lineament is a complexly folded sequence of interbedded slaty mudstone, siltstone, quartzite and turbiditic quartzwackes. These rocks comprise the Burnie Formation in the north and the Oonah Formation in the south. Folding and the development of the metamorphic belt is attributed to the Penguin Orogeny. During the course of the tectonic movements, the Rocky Cape Group and Burnie Formation were separated by a high angle shear zone now represented by the Arthur Lineament (Gee, 1967).

The Rocky Cape region is flanked by a meridional belt of Eo-Cambrian and Cambrian rocks (Dundas Trough and associated igneous rocks), within which five major stratigraphic lithologies may be distinguished:

(i) Late Precambrian (or Eo-Cambrian) orthoquartzite-shale sequence with minor dolomite (Success Creek Group);

(ii) mudstone-greywacke sequences with basaltic volcanic rocks and minor chert and limestone (Crimson Creek Formation;

(iii) ultramafic and mafic complexes;

(iv) fossiliferous Middle to Late Cambrian mudstone-greywacke-conglomerate sequences (Dundas Group); and

(v) dominantly acid to intermediate volcanic rocks with felsic intrusives (Mt Read Volcanics).

The eugeosynclinal-type sedimentation that characterized much of the Eo-Cambrian, terminated in the Late Cambrian and was replaced by deposition of siliceous conglomerate and sandstone. The main siliceous clastic sequence is the Owen Conglomerate, and the Mt Zeehan Conglomerate in the Zeehan area. The clastic sequence is followed conformably by up to several hundred metres of shallow-marine Middle to Late Ordovician Gordon Limestone. Conformably overlying the limestones is the Silurian to Early Devonian Eldon Group, which consists of shallow-marine interbedded mudstone and quartz sandstone. In the Zeehan area, the Eldon Group obtained a maximum thickness of 1800 m, (Blissett, 1962).

Between the Early Devonian and late Middle Devonian there occurred a widespread, major period of deformation (the Tabberabberan Orogeny) which affected all Early Palaeozoic rocks and to a lesser extent, rocks of the Rocky Cape and Tyennan regions (Williams **et.al.**, 1975; Williams, 1979). In

Western Tasmania, two main phases of folding are recorded. During the Late Devonian there occurred a major period of emplacement of post-tectonic granitoid intrusions (e.g. Heemskirk Granite, Meredith Granite, Granite Tor massif) probably representing the final phase of the Tabberabberan Orogeny.

Acknowledgements

The author is indebted to Dr. R.R. Large firstly for suggesting the topic and for the guidance and supervision graciously provided throughout the year. CRAE kindly allowed the author to work on the Gourlays Creek Prospect, to sample the drill core and provided copies of the previous exploration reports. Thanks must also go to Dr's. R.F. Berry and A.J. Crawford for fruitful discussions and their help regarding the topics of structural geology, metamorphism and igneous petrology. Dr. M.R. Banks is thanked for the identification of fossils. Finally I would like to thank G. Davidson for proof reading much of the manuscript and to June Pongratz for her typing expertise.

CHAPTER 2

STRATIGRAPHY

The stratigraphy in the Granville Harbour area as shown in figure 2.1 is dominated by a sedimentary sequence ranging in age from Upper Proterozoic to Devonian. A generalized stratigraphic column as defined in this study is shown in figure 2.2 and a schematic geological cross-section is given in figure 2.3.

The only previous stratigraphic work of consequence in this area is that of Blissett (1962) who discusses the formations of the Eldon Group in detail and the other units to varying degrees of completeness. During the course of this study, the area has been remapped and the stratigraphy redefined. Modifications include the inclusion of the Duck Creek Sequence, a possible Late-Middle Cambrian Crimson Creek correlate, and the redefining of 120 m of micritic limestone exposed to the north of Duck Creek as belonging to the Devonian Florence Quartzite. Blissett (1962) previously defined these micritic limestones as Gordon Limestone.

2.1 PROTEROZOIC

WHYTE SCHIST

One kilometre of sediments and subordinate metavolcanics of the Whyte Schist are exposed in the most northern section of the field area (Fig. 2.1). The sequence is faulted against micritic limestone of the Florence Quartzite to the south and covered by beach sands to the north. Gee (1967) indicates these sediments to be part of the Arthur Lineament. Both the Whyte Schists and the Oonah are considered to be affected by the Penguin Orogeny which according to Adams **et.al.**,(1985) occurred between 700 and 750 Ma. ago. Blissett (1962) considers the Oonah Formation to be younger than the Whyte Schists.

The sequence dominantly consists of green and black schists with subordinate quartzites, phyllites, dolomites and spilites. All the lithologies contain abundant disseminated pyrite and the quartzites have a weathering pattern suggestive of high carbonate contents. Mineral assemblages are consistent with lower greenschist facies metamorphism.

Oonah Quartzite and Slate

Sediments of the Oonah Formation are the dominant lithology in the Granville Harbour area outcropping along 4 km of coastline and, to a limited extent, within the grid area of figure 2.1.

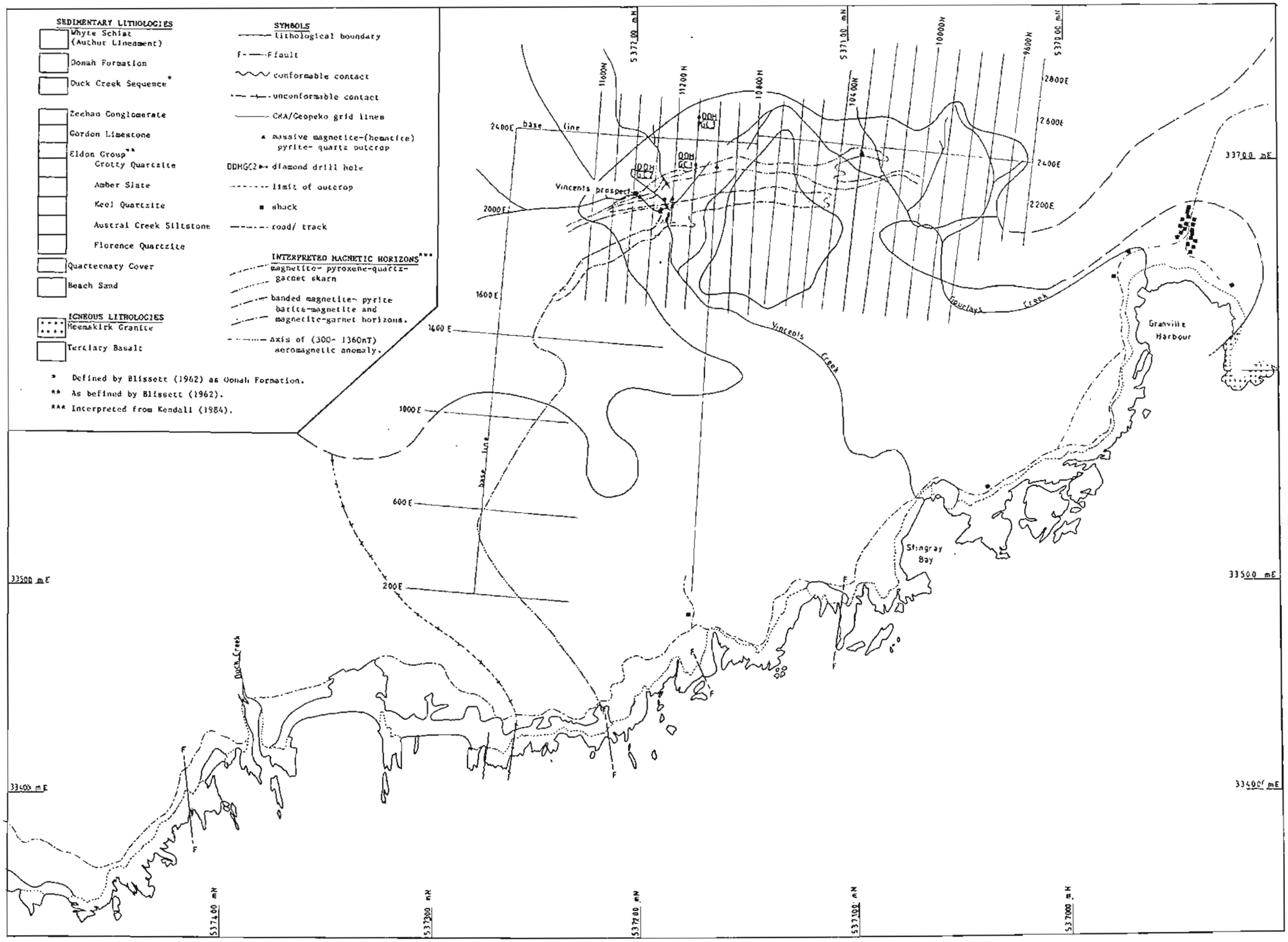

Fig. 2.1 Simplified field map of the Granville Harbour area. The grid area is part of a CRA/Geopeko Joint Venture exploration lease and is referred to as the Gourlays Creek Prospect (Kendall, 1984). For a detailed 1:5000 copy of this map refer to appendix A. .

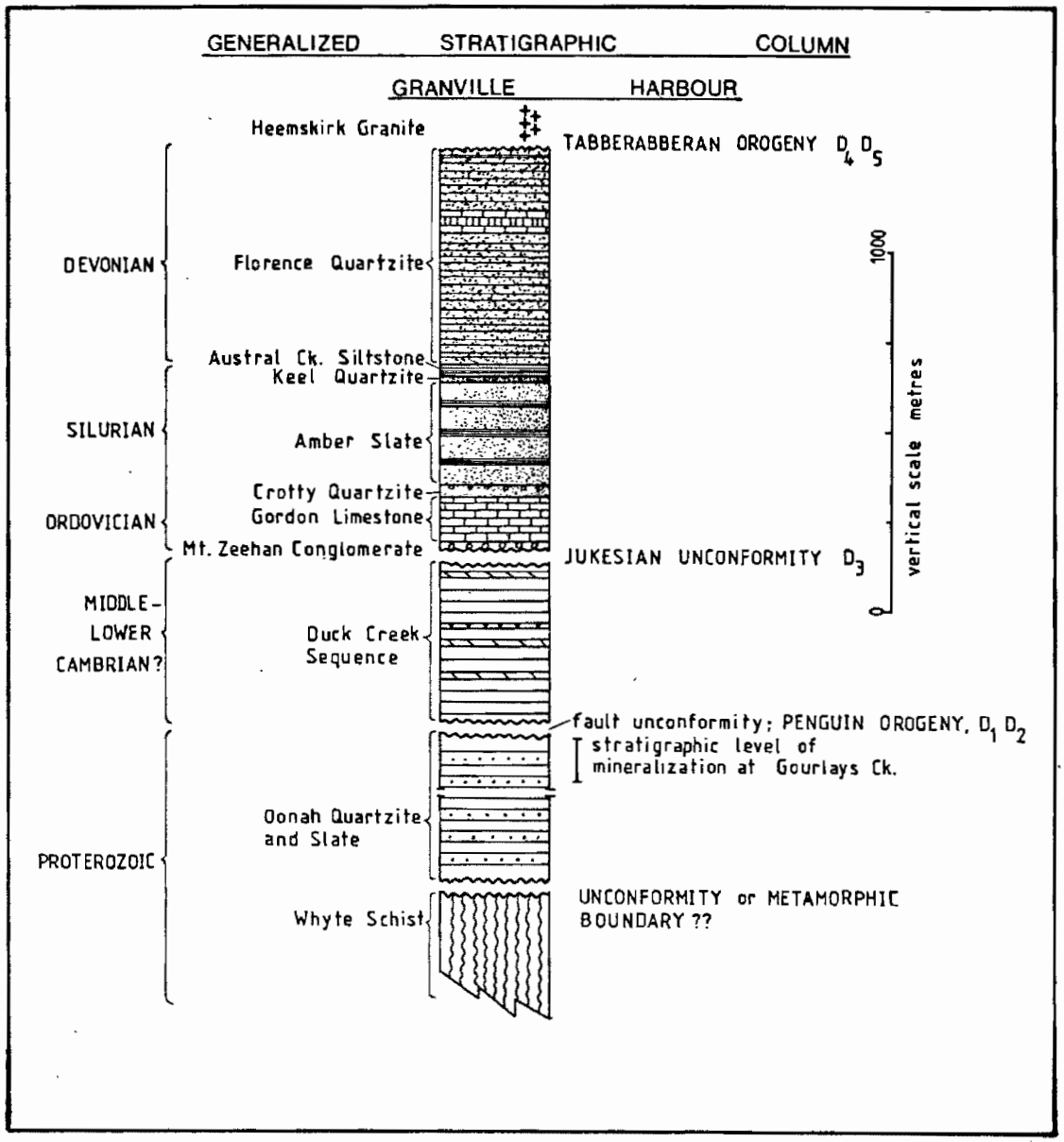

Fig. 2.2 Generalized stratigraphic column for the Granville Harbour area. Symbols for the Cambrian to Devonian sequences are given in Fig. 2.3 (modified from Blissett, 1962).

Along the coastal section, the Oonah Formation consists of interlayered quartzites, schists, phyllites and hornfels. At Granville Harbour, fine grained quartz hornfels are dominant while to the north, massive medium-coarse grained quartzites with subordinate interlayered chloritic schists and phyllites prevail. Minor development of calcsilicate hornfels is noted south of Stingray Bay.

Based on lithology, as investigated during this study, the sediments outcropping at Granville Harbour and along the coastal section to the north are considered to correlate with the Oonah Formation as observed to the east of the field area and along the Pieman Dam road. The high proportion of schists and common spilitic metavolcanics observed in the Whyte Schist, makes a correlation with this sequence unlikely. Apparent disparities between the coastal rocks at Granville Harbour and the Oonah Formation as observed at other localities are a result of progressive induration and hornfelsing associated with intrusion of the Heemskirk Granite in the south of the field area (Fig. 2.1).

Outcrop in the grid area is poor. However, the sequence may be subdivided into an eastern zone consisting of interlayered micaceous and chloritic siltstones and quartzites, and a western zone, dominated by chloritic quartzites. Minor stratabound massive magnetite and pyrite and stratiform banded hematite-quartz outcrops have been mapped along with significant calcsilicate hornfels and unreplaced carbonate (e.g. Fig. 2.1).

2.2 EARLY CAMBRIAN (?)

DUCK CREEK SEQUENCE

Interbedded schists, phyllites, quartzites and carbonates belonging to this sequence outcrop along 415 m of coastline north of Granville Harbour. The sequence is faulted against the Oonah Formation in the south and unconformably underlies the Mount Zeehan Conglomerate in the north.

Most of the quartzitic sediments are chloritic. The schists consist dominantly of fine grained muscovite (>60%) and have a strong slaty cleavage. In general, the schists are finely laminated with interlayered dolomite-rich and brown quartz sandstone bands 1-5 mm in width. Dolomite also occurs in four distinct units 1-2 m thick (Fig. 2.3). The most southern dolomite unit is strongly silicified.

Underlying the unconformity between the Mount Zeehan Conglomerate and Duck Creek Sequence is 10 m of purple stained hematitic quartzite and grit representing an ancient erosional surface or a soil horizon. The angular unconformity is thus not only representative of a tectonic discontinuity but also of an extensive period of non-deposition.

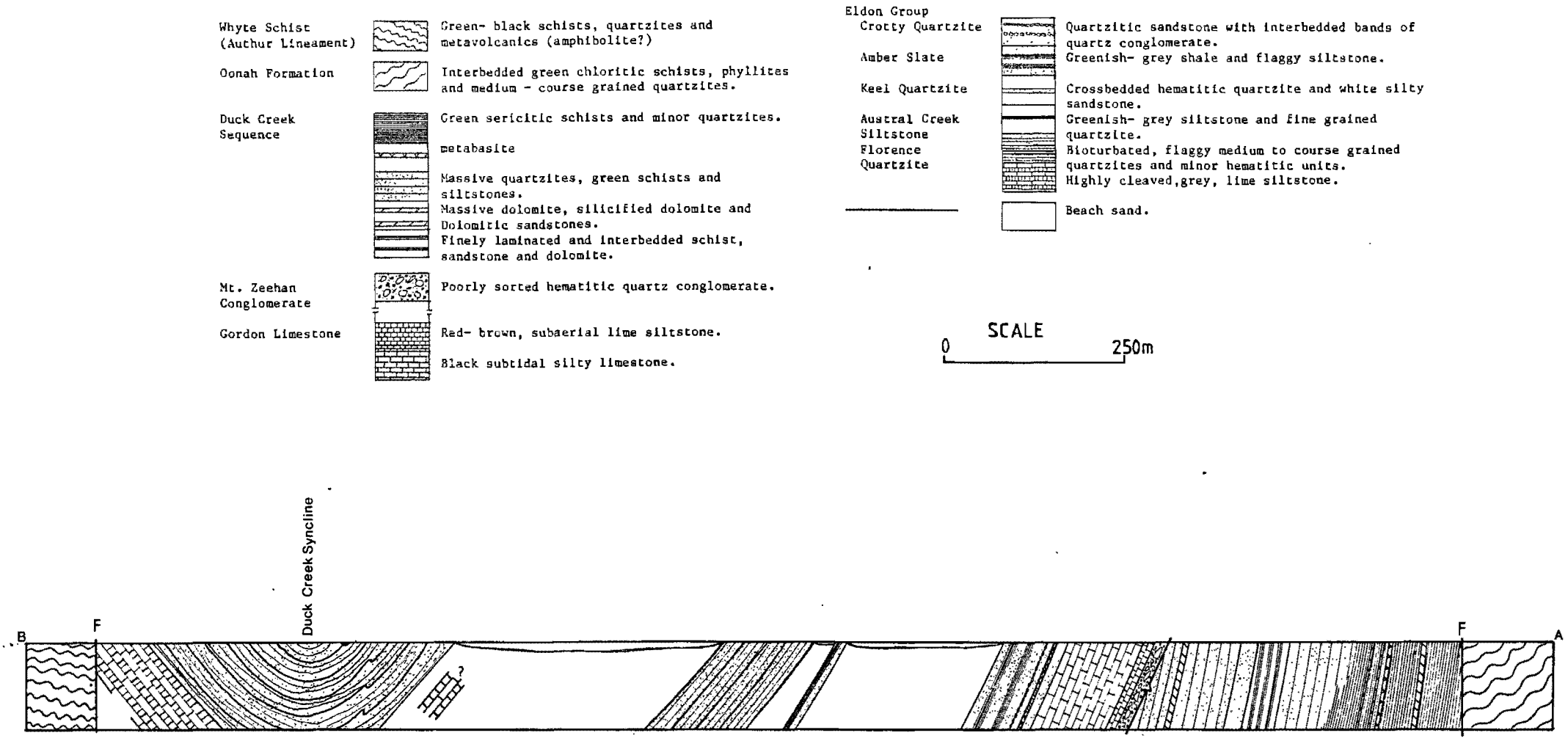

Fig 2.3 Geological crossection of coastal section A(537424mN,33389mE) to B(537206mN/ 33440mE) projected along strike onto N-S grid lines. The subdivision of the Eldon Group into its formations is from Blissett (1962).

Lithologically this sequence may correlate with the Early Cambrian Crimson Creek Formation which according to Blissett (1962), conformably overlies the Oonah Formation elsewhere in the Zeehan district. Blissett (1962) tentatively defined the sediments along the coast as belonging to the Oonah Formation but also suggested that at least some of the succession to correlate with the Whyte Schist to the north. Williams (1976), similarly correlates these sediments with the Whyte Schist.

2.3 Ordovician

MOUNT ZEEHAN CONGLOMERATE

The Mount Zeehan Conglomerate rests unconformably on sediments of the Duck Creek Sequence and grades progressively into the Gordon Limestone. Blissett (1962) suggested the contact between the Mount Zeehan Conglomerate and the underlying sediments to be a fault contact and the conglomeratic sediments to correlate with the Moina Sandstone. From this study, no evidence of faulting was found and the sediments are correlated with the Mount Zeehan Conglomerate.

A total of 12 m of conglomeratic sediments are exposed along the coastal section north of Granville Harbour. The conglomerate is a purple stained hematitic quartz conglomerate with poorly sorted angular quartz clasts ranging in size from 1-50 mm. The lower part of the sequence is dominated by bedded conglomerate with individual beds being defined by variable clastic and hematite contents and by graded bedding. The clasts are dominantly milky white vein(?) quartz and minor hematite-rich siltstone. The source of the clastic content of the conglomerates remains an enigma in that the clasts are very angular suggesting a proximal source yet only minor milky white vein quartz is observed in the Oonah Formation and Duck Creek Sequence.

The mean grainsize of the Mount Zeehan Conglomerate becomes progressively finer in its upper beds with quartz sandstones and shaly beds becoming dominant. The top of the sequence is dominated by fine grained, red-brown calcareous siltstones and minor white conglomerate units.

GORDON LIMESTONE

Approximately 115 m of Gordon Limestone is exposed along the coastal section. The lower contact is gradational to the Mount Zeehan Conglomerate and is defined by red-brown silty limestone. The colouration is due to minor disseminated hematite representating oxidizing environments of deposition. The next 100 m of succession is defined by highly cleaved,

black lime mudstones. Thin section 68275, from these sediments, is defined as a dolomitized micritic limestone.

2.4 SILURIAN- DEVONIAN

ELDON GROUP

The Eldon Group sediments outcrop along 1.6 km of coastal section (Fig. 2.3) and occupy the core of the Duck Creek Syncline. The total thickness represented here is 950 m assuming an average dip of 50°. Blissett (1962) has further subdivided the coastal sequence into five formations of the Eldon Group.

Crotty Quartzite

The Crotty Quartzite overlies the Gordon Limestone conformably and is represented by 26 m of massive pale grey quartz sandstone and minor interbedded conglomerate, siltstones and fine grit beds. The conglomerate is a white, close-packed quartz conglomerate with subrounded, poorly sorted quartz and minor limestone clasts 5-10 mm in diameter.

Amber Slate

The Amber Slate conformably overlies the Crotty Quartzite and is represented by 40 m of interbedded shales and flaggy siltstones and sandstones. The sediments are moderately sheared and have a green colouration. The weathering pattern in some of these units indicates a minor carbonate component.

The next 230 m of the succession is covered by beach sand. Blissett (1962) interprets this to be all part of the Amber Slates.

Keel Quartzite

The Keel Quartzite is represented by 2 m of cross-bedded, purple stained, hematitic quartzite and grit beds. The lower contact with the Amber Slate is obscured by beach sands.

Austral Creek Siltstone

Seven metres of interbedded greenish-grey siltstone and fine grained quartz sandstone, of the Austral Creek Siltstone, conformably overlies the Keel Quartzite to the south of Duck Creek. The next 30 m of the succession is covered by beach sand but is defined by Blissett (1962) as part of this Formation.

Florence Quartzite

Sediments of the Florence Quartzite occupy the core of the Duck Creek Syncline (Fig. 2.3). The dominant lithologies are flaggy pale-grey quartzites, laminated siltstones and light blue-green, fine-grained, friable sandstone. Individual beds tend to be massive and range in thickness from

10-20 cm to over 2 m. Minor purple stained hematitic sandstones and grits also outcrop in the core of the Duck Creek Syncline.

The most northern exposure of the Florence Quartzite is defined by 120 m of strongly sheared grey micritic limestones (68276). A coral (68277) from this lithology has been tentatively defined as Favosites moonbiensis Etheridge, giving an age of Early to Middle Devonian (M.R. Banks, pers. comm.). Strong recrystallization makes a positive identification difficult. Blissett (1962) previously defined these sediments as belonging to the Ordovician Gordon Limestone.

Much of the Florence Quartzite, especially the lower exposures, is strongly bioturbated. Worm burrows are everywhere perpendicular to bedding indicating shallow marine conditions of deposition. Minor occurrences of soft sediment deformation folds have been observed. In figure 2.4, individual folds are contained within a thick sandstone bed. Folds are defined by siltstone and mudstone that has enveloped medium grained sandstone. Such folds are interpreted to have a slump or dewatering type origin.

Fig. 2.4 Slump or dewatering folds within a medium grained sandstone unit in the Florence Quartzite.

2.5 IGNEOUS ROCKS

Spilites and Metabasites

Fine to medium grained tholeiitic spilites are common to the Whyte Schist. They are deep green, strongly chloritic and are associated with abundant magnetite in veinlets and as disseminations. Due to the contrasting weathering effects, the spilites generally sit above the low-lying platform of the host schists. Individual units may not be followed along strike. Spry (1964) and Coleman (1975) consider metavolcanics from within the Whyte Schist to be intrusive in origin.

Two samples of tholeiitic metabasite (68245, 68246) have been obtained from the Oonah Formation. Both samples are drill core sections and their relationship with the host rocks is uncertain. Another sample of metabasite (68242) was also sampled from a 1 m wide unit in the Duck Creek Sequence. This metabasite unit is everywhere conformable with bedding suggesting it to be either a sill or flow. All these metavolcanics are discussed in detail in Section 4.1.

Heemskirk Granite

The Heemskirk Granite outcrops along the southern shore of Granville Harbour and within the grid area of figure 2.1. The main body of granite is defined as a tourmaline-rich muscovite granite with tourmaline occurring as either rounded, 5-10 cm diameter nodules or in veins. Within 2-3 m of the granite contact with the Oonah Formation it is a fine grained aplitic granite with local greissen development. Both granite types are the white granites of Klominsky (1972). A post-Tabberabberan age for this massif has been given. Skarns, including the Gourlays Creek skarn and the St Dizier skarn, and hornfelsing of the country rocks are associated with this granite intrusion.

Tertiary Basalt

Olivine- and magnetite-bearing Tertiary basalt forms a low undulating plateau which covers up to 20% of the grid area. Vincents and Gourlays Creeks have eroded through this basalt exposing the Oonah Formation through two windows (Fig. 2.1).

CHAPTER 3

STRUCTURAL GEOLOGY

Five phases of deformation are recognised from the Precambrian and Palaeozoic sediments exposed along the coastal section north of Granville Harbour. Four phases are recognised in the Oonah Formation, two in the Duck Creek Sequence and two in the post-Cambrian lithologies. The relative sequence of deformation has been determined by

(i) overprinting relationships, and

(ii) the distribution of various phases between the stratigraphic units.

Preliminary mapping of the Whyte Schist defined three phases of deformation. Tentative correlations of these deformation events are made with the structure in the Oonah Formation.

3.1 OONAH FORMATION

S_0 ; differentiated layering/bedding

Since no sedimentary structures in the Oonah Formation have been recognized, compositional layering is simply referred to as layering. Most of the layering represents metamorphic differentiation but probably subparallels the primary bedding.

The distribution of layering orientations indicate a shallow SE-plunging fold system (i.e. B_4, Fig. 3.3a). This correlates with the average orientation of B_4 folds. The significant spread of readings away from the great circle is attributed to D_5 deformation.

D_1; first phase deformation

The only evidence of D_1 deformation in the Oonah Formation is the development of a spaced cleavage in coarse grained psammite units. Preferential weathering along S_1 has enhanced this cleavage. At 537210mN /33440mE (Fig. 3.1), the S_1 cleavage is orientated at a high angle to layering suggesting this area to be in the hinge of a B_1 fold. Outside this area, recognizable S_1 cleavages are rare.

D_2; second phase deformation

Second phase deformation produced folds with contrasting styles; (i) B_2^0, second phase folds of the S_0 layering and; (ii) B_2^1, second phase folds of the S_1 cleavage. This phase of deformation is restricted to the Precambrian units with closures being recognized at Granville Harbour (e.g. 536920mN/ 33630mE) and in the vicinity of the most northern exposures of the Oonah Formation (e.g. 537230mN/ 33440mE).

Fig. 3.1 Domain analysis of the Oonah Formation based on differentiated layering orientations. Contoured equal area plots of layering (contours at 1, 2, 4 and 8%) labelled A to E correlate with domains A to E respectively, (redrawn from the 1:5000 geological interpretation map, Appendix A.6)

Structural Interpretation Map of Granville Harbour

LEGEND

- Whyte Schist
- domain
  - A
  - B
  - C — Donah Formation
  - D
  - E
- Duck Creek Sequence
- Mt Zeehan Conglr / Gordon Limestone
- Eldon Group
- Heemskirk Granite

- bedding
- cleavage
- form line
- F — F fault
- unconformity
- conformable contact / domain boundary
- minor fold
- major syncline
- anticline

SCALE 1:10 000

by R C Norris

Granville Harbour

Stingray Bay

Duck Creek

5 370 00 mN

5 371 000 mN

5 375 000 mN

5 374 00 mN

5 373 00 mN

5 372 00 mN

5 269 00 mN

336 00 mE

335 00 mE

334 00 mE

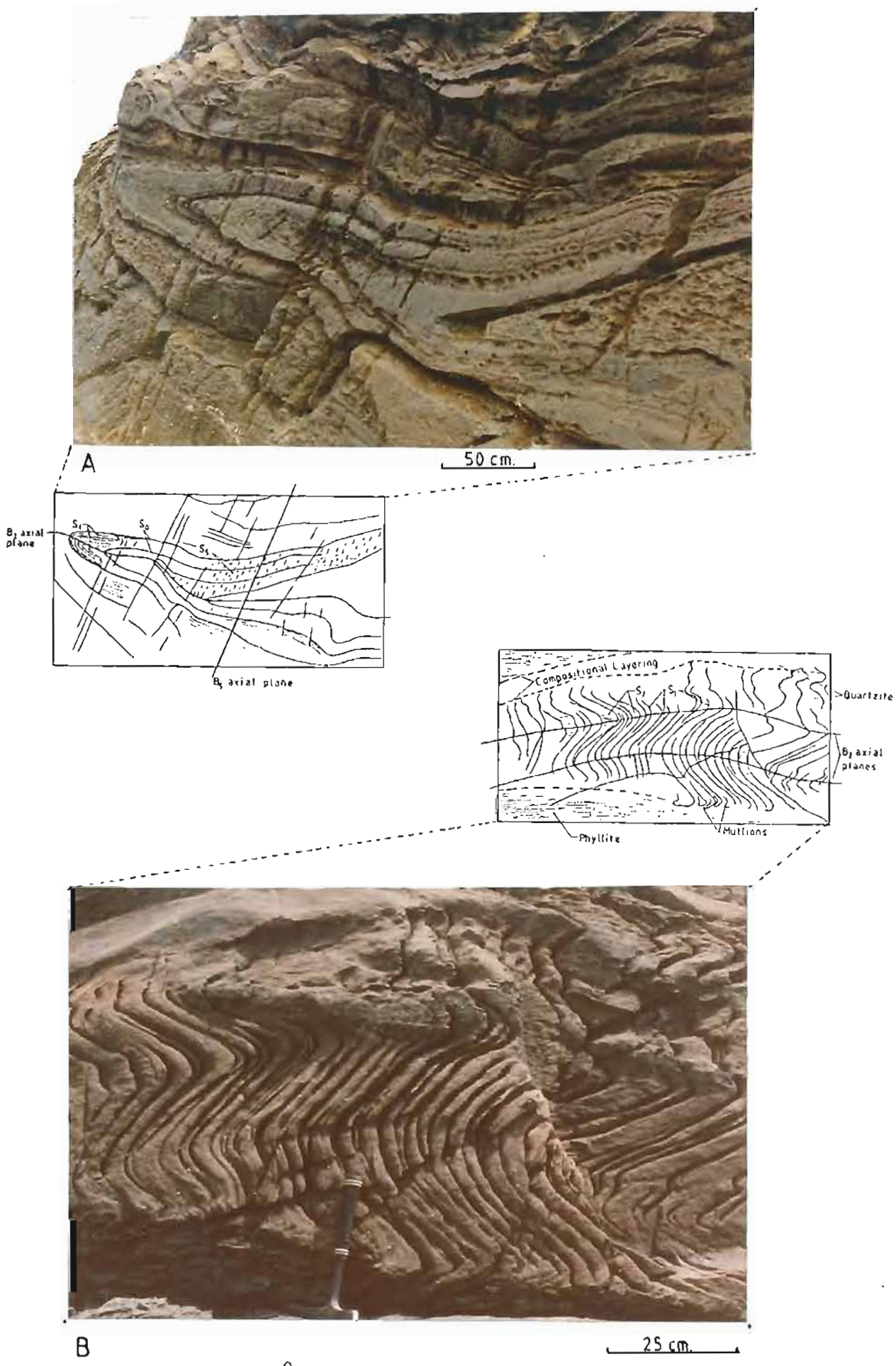

Fig. 3.2 (a) Recumbent B_2^0 fold in the Oonah Formation. Note that S_1 is sub-parallel to S_0 and the folding of S_1 in the hinge zone; (b)B_2^1 folds in course grained psammite units with minor mullion structures developed at the base of this psammite unit.

B_2^0 folds are similar, recumbent to plunging inclined, tight to isoclinal and with angular closures (Fig. 3.2a). Asymmetry of B_2^0 folds is defined by greater attenuation of the lower limb and hinge thickening. In comparison, the style of B_2^1 folds is largely dependent on the orientation of the S_1 cleavage. Where S_1 is parallel to the layering, B_2^1 folds are indistinguishable from B_2^0 folds (Fig. 3.2a). Where S_1 is at a high angle to layering, B_2^0 folds are completely contained within individual coarse grained psammite units with the lower contact being defined by mullions (Fig. 3.2b insert). The consistency in the distribution of these mullions (i.e. the lower contact) is suggestive of graded bedding indicating north facing and for the layers to be the right way up. The style of these B_2^1 folds is open, rounded and plunging inclined.

Both B_2^0 and B_2^1 folds have resulted in the development of an axial plane cleavage. In thin section 68223, this cleavage is defined as a crenulation cleavage while in hand specimen, in all but the most hornfelsed rocks, it is recognized as a moderate to strong schistosity. Throughout most of the coastal section this cleavage is subparallel to the layering and has been refolded by later deformation.

The mean orientation of measured B_2 fold hinges is 30° ---> 310° (Fig. 3.3b) while B_2 axial planes strike E-W and dip moderately shallowly to the north (Fig. 3.3d). S_2 cleavages measured in the vicinity of tHe most northern exposures of the Oonah Formation indicate refolding by a shallow E- plunging fold system (Fig. 3.3c). Mapping also supports refolding in this area.

D_3; third phase deformation

No structures within the Oonah Formation may be confidently assigned to the third phase of deformation.

D_4; fourth phase of deformation

B_4 folds attributed to D_4 deformation are typically open, concentric and plunging normal in style. The dominant orientation of B_4 folds is shallowly SE- plunging or shallowly NW- plunging. Significant scatter of B_4 fold hinges around a great circle is defined in figure 3.3g. Axial planes to B_4 folds are near vertical, strike NW-SE and are tightly clustered (Fig. 3.3f). The causes of this clustering, compared with the scattering of the hinge lines orientations, are twofold. Firstly due to measurement difficulties caused by the open style of many of these folds, not all axial planes were measured. This is especially the case for the S to SE- plunging fold systems. Secondly, much of the variability in orientation of B_4 fold axes is the direct result of overprinting on older fold systems and not from refolding. This conclusion is supported by the

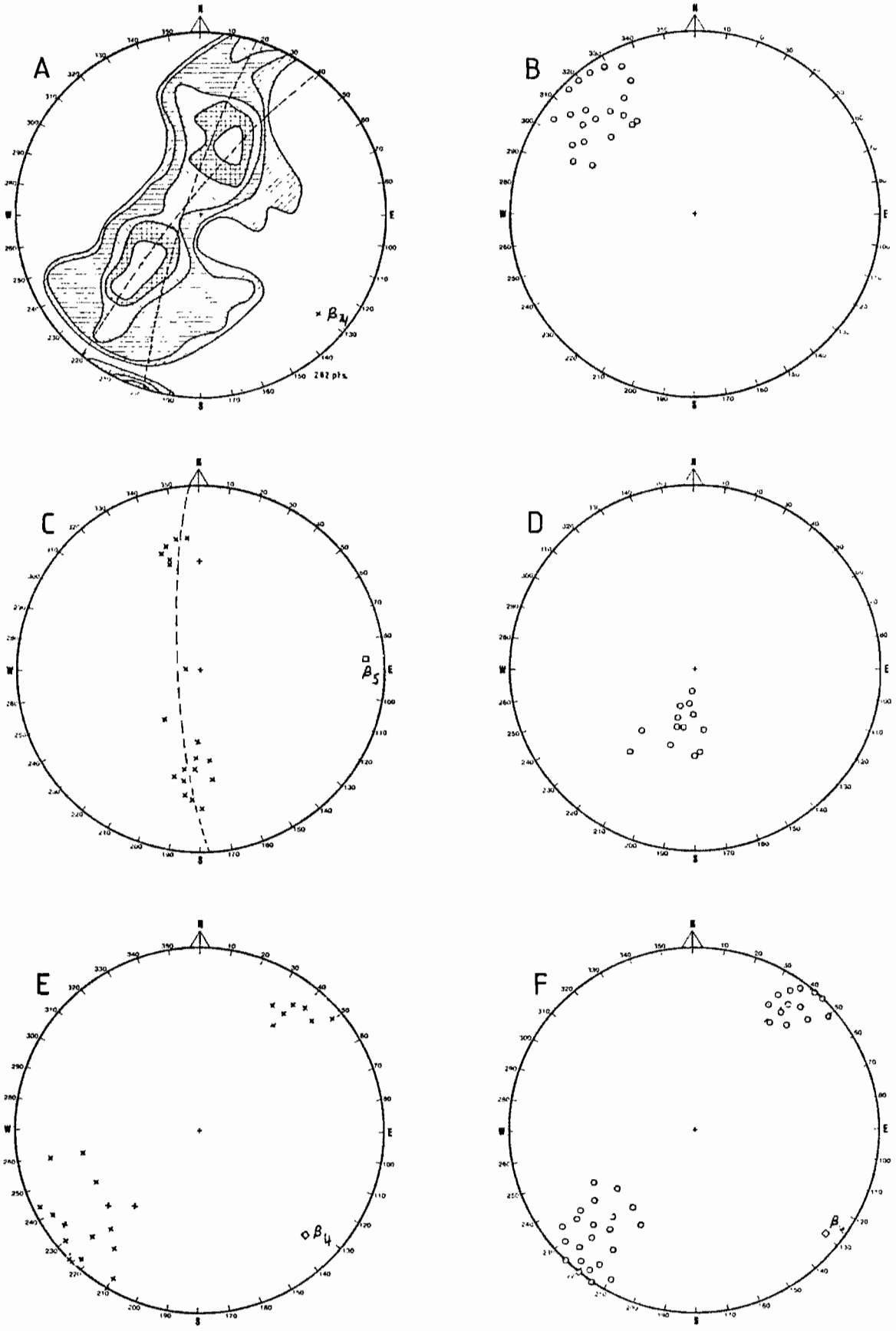

Fig 3.3(a-k). Equal area plots of planes and lineations in the Oonah Formation; (a) poles to differentiated layering, contours at 0.5, 1, 2, 3 and 5%. (b) B_2^0 and B_2^1 hinge line orientations; (c) poles to S_2 cleavage; (d) poles to B_2 axial planes; (e) poles to S_4 cleavage; (f) poles to B_4 axial planes;.....

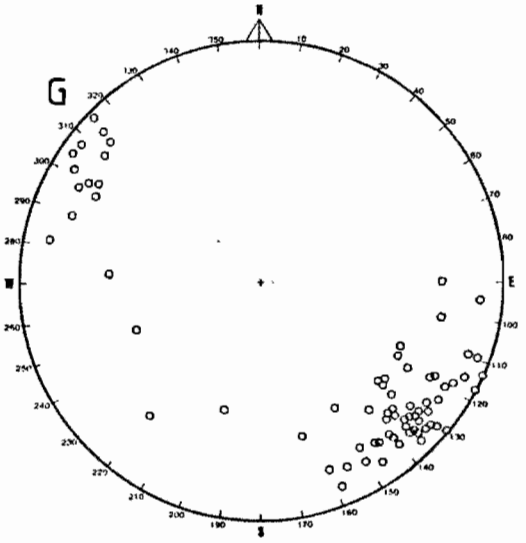

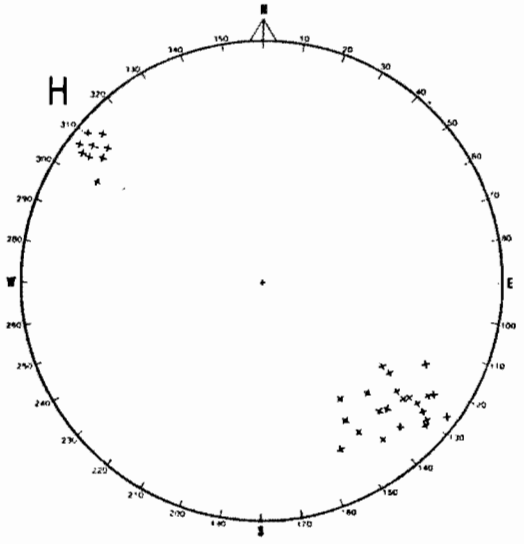

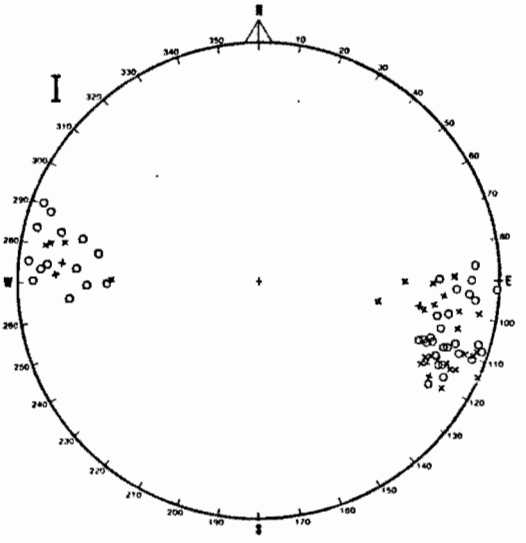

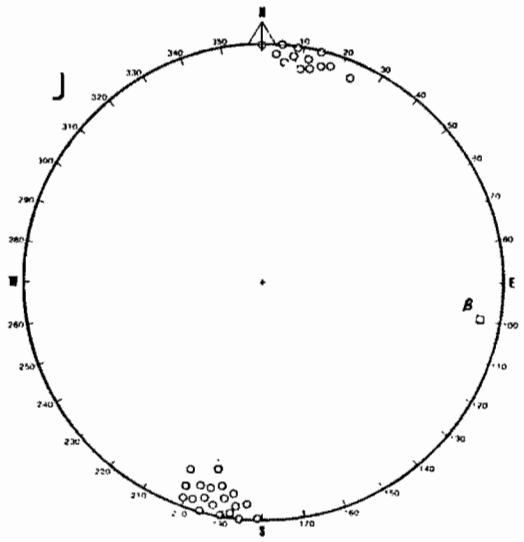

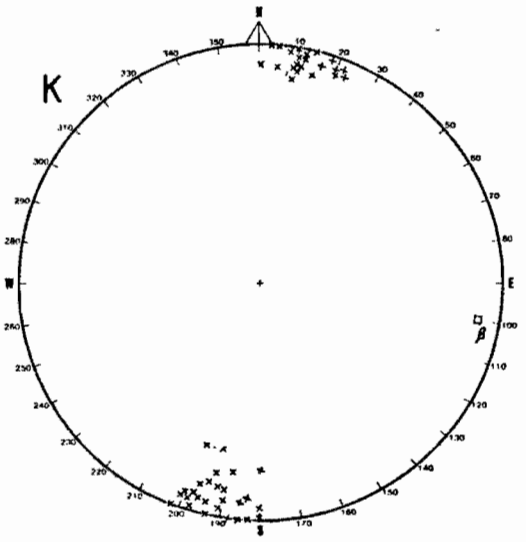

Fig 3.3 contd. (g) B_4 hinge line orientations; (h) S_4/ S_0intersection lineations; (i) o B_5 hinge line orientations, x S_5/ S_0 intersection lineations; (j) poles to B_5 axial planes; (k) poles to S_5 cleavage.Where apprropiate the distribution of readings is defined in terms of great circles. The poles to these great circles, B_4 and B_5, have a similar orientation to fourth and fifth generation folds respectively.

fact that most reversals in plunge of B_4 folds occur in areas of strong D_2 deformation. Associated with B_4 folds is an axial plane spaced cleavage which clearly cuts and often displaces both the S_2 schistosity and layering (Fig. 3.4a).

The scale and style of mesoscopic B_4 folds vary dramatically from kinks with wavelengths in the order of several centimetres and with angular closures to large, open, basinal structures outcropping at the northern headland of Granville Harbour. Some of these variable B_4 fold styles are represented in figure 3.4. On a regional scale, the dominant B_4 fold is a large, gentle to open, SE- plunging syncline. The hinge of of this syncline is exposed in near-horizontal layering just south of Stingray Bay (Fig. 3.1).

D_5; fifth phase deformation

D_5 deformation becomes progressively stronger to the north of Stingray Bay as shown by domain analysis (Fig. 3.1). B_4 and B_5 folds have very similar styles, the latter however, consistently trend E-W and are horizontal to weakly plunging normal,(Fig. 3.3i). The tight clustering of B_5 axial planes and field evidence suggest that reversals in plunge of B_5 fold axes are a direct result of overprinting on older fold systems.

Unique to D_5 deformation is the development of an E-W striking axial plane crenulation cleavage (Fig. 3.5a). This cleavage crenulates the S_2 schistosity and is distinct on the S_2 cleavage surface of most phyllites, schists and some schistose quartzites.

To the north of Stingray Bay (domain D, Fig. 3.1), folds of both D_4 and D_5 generations are recognized while overprinting relationships prove conclusively the given sequence of deformation. Firstly overprinting of B_5 on B_4 has resulted in reversals of B_5 fold axes while retaining a constant B_5 axial plane orientation. In comparison, B_4 axial planes are gently folded by the B_5 folds. Secondly, the S_4 cleavage is crenulated by the S_5 cleavage and is folded by B_5 folds.

The major regional B_5 fold in the area is an open, shallowly east-plunging antiform that outcrops in the vicinity of the most northern exposures of the Oonah Formation (537200mN/ 33450mE, Fig. 3.1, domain E). Reversals of plunge are common in this area due to overprinting on D_1 and D_2 structures. The northern limb of this antiform is faulted against the Duck Creek Sequence.

Domain Analysis

Domain analysis of layering was carried out in an attempt to define the changing character of deformation in the Oonah Formation and to obtain a better understanding of the regional structure. Two of the important

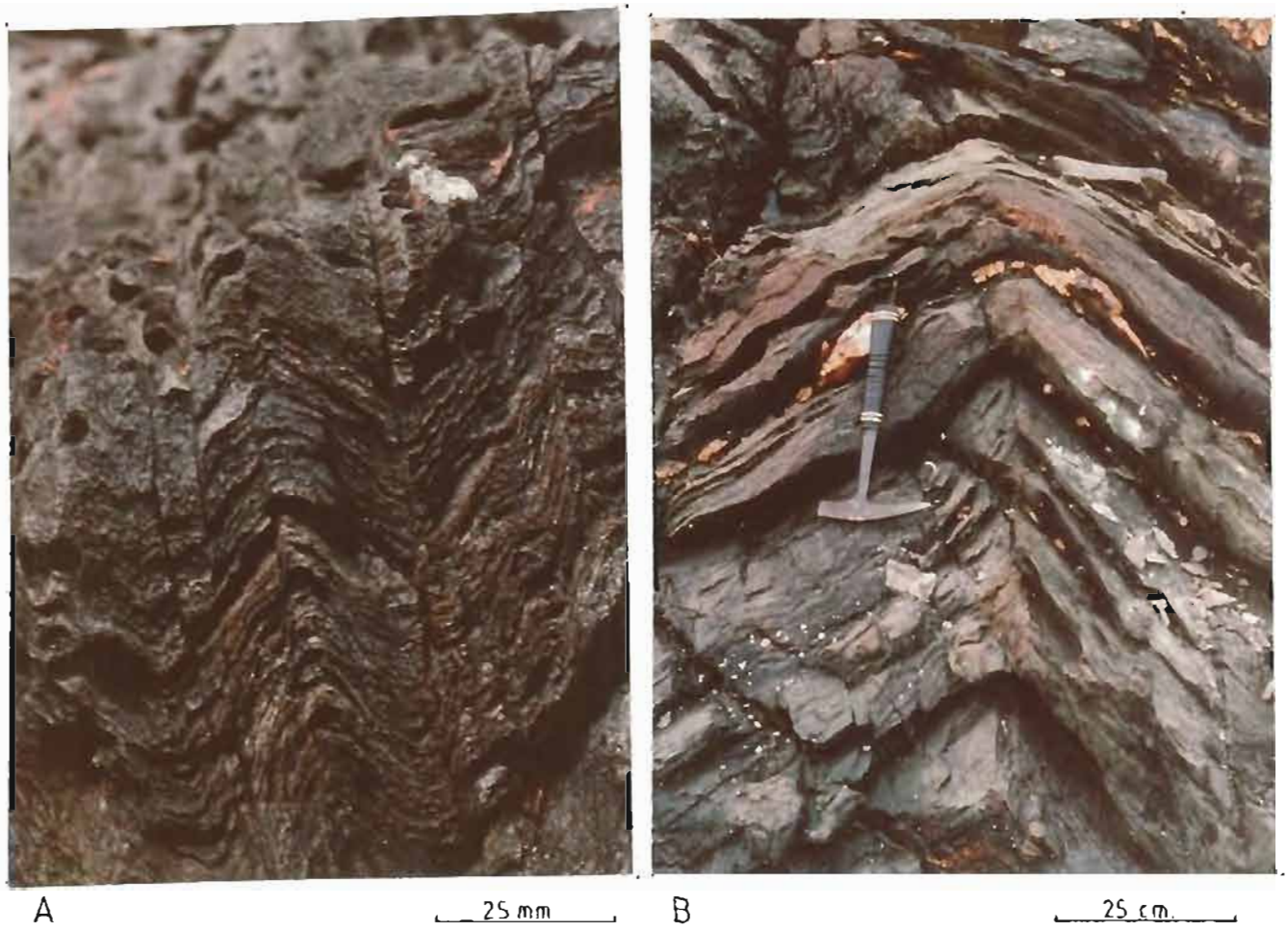

Fig. 3.4 B_4 fold styles in the Oonah Formation; (a) macroscopic B_4 folds of the S_2 cleavage. Note the development of an axial plane fracture cleavage; (b) relatively angular B_4 fold in interlayered phyllites and quartzites; (c) large open B_4 fold in quartzite.

A

5 cm.

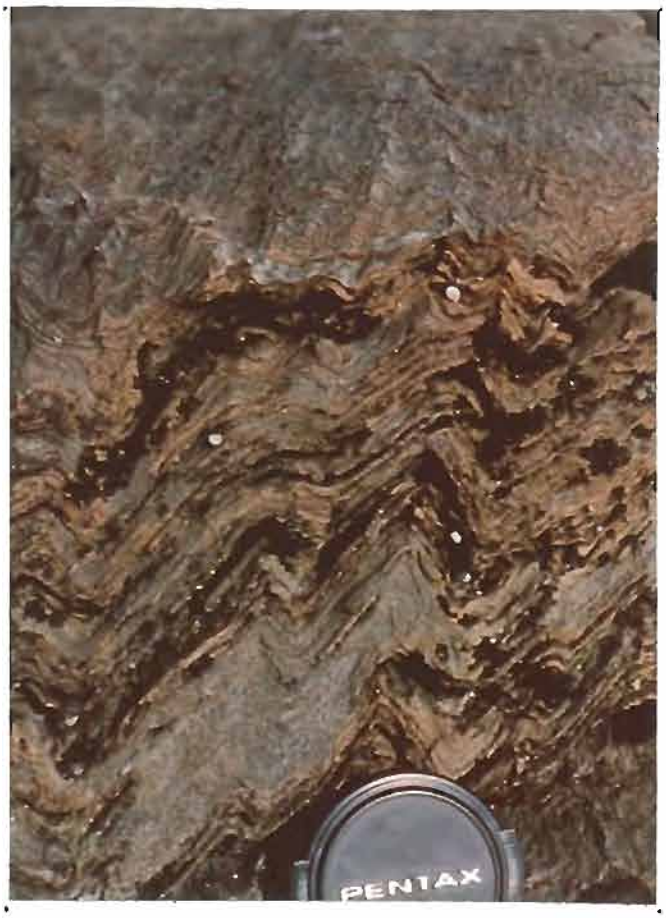

B

5 cm.

Fig. 3.5 D_5 deformation styles in the Oonah Formation; (a) strong crenulation cleavage in phyllites; (b) B_5 kinks of the S_2 cleavage and the sub-parallel compositional layering in schistose quartzites.

regional structures defined by domain analysis are the B_4 synform in the Stingray Bay area and the B_5 antiform near the most northern exposures of the Oonah Formation. Due to the open nature of both these fold systems, domain boundaries do not necessarily correlate with a particular hinge line. The domain analysis is shown in figure 3.1.

Domain A is an area dominated by short wavelength B_4 folds and significant D_2 deformation. The mean trend of fold axes, as defined by the distribution of poles to bedding, is shallow to the SSE. Domain B is transitional to the former domain but from field description, is not affected by B_2 folding.

A regional B_4 synform is exposed within domain C. The gentle to open nature of this fold system is reflected by the spread of layering orientations. It must be noted that boundaries of this domain are not fixed by any particular structural feature and that this domain is in fact transitional between the NW dipping B_4 limb of domain B and the south dipping $B_{4/5}$ limb of domain D. However, since no fold closure could be assigned to this synform, domain C is included to indicate this area to be the hinge zone of a large open SE- plunging fold system.

An increase in dominance of D_5 deformation is represented in domains D and E. The orientation of layering readings in domain D is consistent with both the SE trending B_4 fold system and the E trending B_5 fold system. It is within this area that overprinting relationships between these two fold systems are observed. Domain E is dominated by E-W trending B_5 folds. Variable layering orientations and reversals of plunge of fold axes in this area are attributed to strong D_1 and D_2 deformation.

3.2 DUCK CREEK SEQUENCE

The dominant control on plane orientations in the Duck Creek Sequence is D_5 deformation. Minor fold hinges exhibit variable plunges to 105^{o} (Fig. 3.6b) while the spread of bedding readings (Fig. 3.6a) defines a similar trending fold system.

The boundary relationship between the Duck Creek Sequence and the overlying Ordovician sediments is an angular unconformity representing a minimum contact angle of 30^{o}. Since both the Duck Creek Sequence and the overlying sediments exhibit evidence of D_4 and D_5 deformation, this unconformity necessitates the inclusion of a pre-Ordovician deformation event (i.e. D_3).

Unique to the Duck Creek Sequence is the development of a moderately strong slaty cleavage that subparallels layering. This E-W striking cleavage (Fig. 3.6c), is axial planar to minor B_5 fold hinges but is unlike

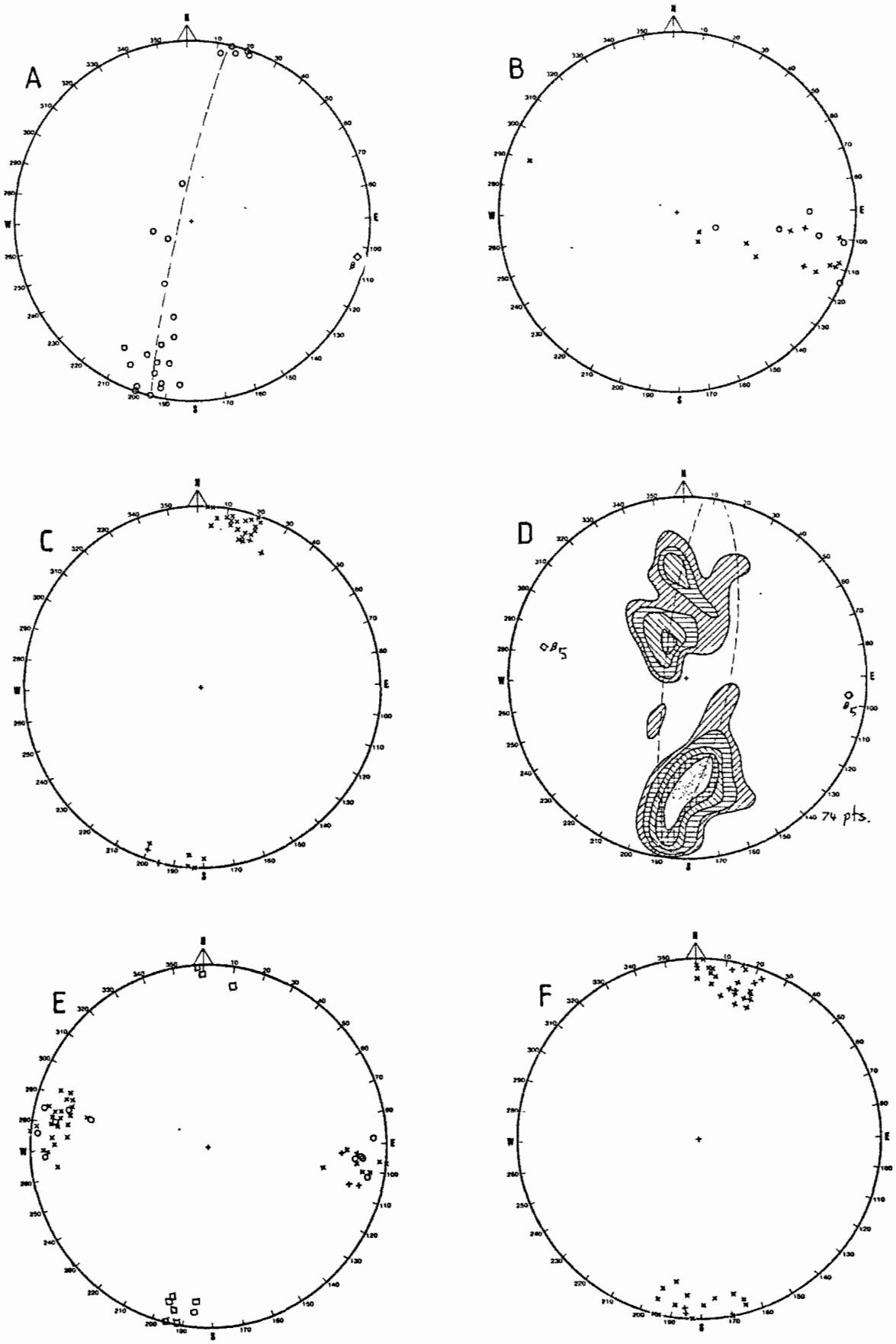

Fig. 3.6(a-f). Equal area plots of planes and lineations from Palaeozoic lithologies, (a-c) Duck Creek Sequence: (a) poles to bedding, the spread of readings defines a shallow east plunging fold system; (b) o B_5 hinge line orientations, x S_5/ S_0 intersection lineations; (c) poles to the S_5 cleavage. (d-f) Zeehan Conglomerate, Gordon Limestone and Eldon Group: (d) poles to bedding, contours at 0.5, 1, 2, 4, and 8%; (e) o B_5 hinge line orientations, x S_5/ S_0 intersection lineations, □ poles to B_5 axial planes; (f) poles to the S_5 cleavage.

the S_5 cleavage, in neither morphology nor apparent strength, to that observed in other lithologies. It is suggested this cleavage formed during D_3 deformation and was rotated and reactivated by D_5 deformation. Other evidence of D_3 deformation is given by the E-W spread of B_5 hinge line orientations. This spread probably resulted from overprinting on B_3 and/or B_4 folds. Evidence of these earlier fold systems is obscured by the penetrative nature of D_5 deformation.

At 536260mN/33430mE a minor post-S_5 foliation strikes 20°N of S_5 (i.e. approximately 070°). This cleavage is sub-parallel to the bounding fault between the Oonah Formation and the Duck Creek Sequence. Based on these observations, faulting is tentatively defined as being syn-post D_5 deformation.

3.3 MT ZEEHAN CONGLOMERATE, GORDON LIMESTONE, ELDON GROUP

Bedding and sedimentary structures are distinct and easily recognized in the Palaeozoic lithologies. Primary structures include cross bedding, graded bedding and sedimentary dewatering or slump folds.

The dominant control on bedding orientations in the above units is the shallow east and west plunging Duck Creek Syncline. The hinge of the syncline outcrops within the Florence Quartzite, 10 m north of the mouth of Duck Creek (Fig. 3.1). Within the hinge zone, folds tend to be concentric, horizontal to shallowly plunging normal and open. Away from the hinge zone, fold closures are rare and poorly defined. The style and orientation of these folds is consistent with D_5 deformation in the Oonah Formation.

Axial planar to the B_5 folds is an E-W striking cleavage which varies in morphology from a weak spaced cleavage to a moderately strong schistosity within some units of the Florence Quartzite. Analysis of the S_5/S_0 intersection lineations (Fig. 3.6e) indicates a distinct change of plunge across the Duck Creek Syncline with shallow westerly plunges to the south and shallow easterly plunges to the north. Within the hinge of the syncline, both orientations of bedding cleavage intersection lineations and fold axes are observed in association with mesoscopic dome and basin structures. Mapping indicates that an open, cross cutting southeast trending B_4 fold hinge outcrops in this area thus explaining the reversals in plunge of D_5 lineations. The B_4 fold is gentle to open, rounded and lacks an axial plane cleavage.

Like the regional B_5 antiform in the Oonah Formation (Fig. 3.1), the northern limb of the Duck Creek Syncline is faulted. The fault which also defines the northern contact of the Florence Quartzite against the Whyte Schist is a left lateral strike slip fault, striking at 070°. A lineation

parallel to this fault may be mapped as far south as Duck Creek. Northwards, towards the fault, the S_5 cleavage is rotated into parallelism to this fault-related lineation. Such rotation of S_5 is attributed to shear strain proving faulting to be syn- to post-D_5 deformation.

3.4 WHYTE SCHIST

Three generations of deformation are recognized in the Whyte Schist. The two older events are tentatively correlated with D_2 and D_4 deformation in the Oonah Formation. The youngest deformation event D_5, may be positively correlated to similar deformation in the Oonah Formation and Palaeozoic sediments to the south.

D_2; second phase deformation

D_2 deformation resulted in the development of tight reclined folds with rounded closures and a style intermediate between concentric and similar. Significant spreading of B_2 hinge lines and axial planes (Fig. 3.7c) is attributed to later deformation. Unique to D_2 deformation is the development of a strong axial plane schistosity. This cleavage generally parallels layering (Fig. 3.7 a & b), except in the hinges of rare B_2 folds.

D_4; fourth phase deformation

B_4 folds fold the S_2 schistosity and the sub-parallel layering but exhibit no significant development of an axial plane cleavage. Macroscopic B_4 folds with wavelengths of less than 2-3 m are plunging normal and open with closures varing from moderately angular in the pelite units to markedly angular in the more competent psammite units.

Overprinting relationships between D_4 and D_5 structures offer no unique interpretation of the relative sequence of deformation in the Whyte Schists. Based on the similar styles, tentative correlations are made to D_4 deformation in the Oonah Formation. The mean orientation of five B_4 folds measured in the Whyte Schists is 40° ---> 180° (Fig. 3.7d), a more detailed mapping program would likely show a more significant spread of readings.

D_5; fifth phase deformation

Folds and cleavage characteristic of this phase of deformation may be mapped from Devonian sediments in the south, across the previously defined boundary fault and into the Whyte Schists. A positive correlation is therefore established.

B_5 folds are generally open to tight, rounded and plunging normal with a parallel style. The mean trend of B_5 hinge lines, 40° ---> 090° (Fig. 3.7e), is subparallel to the trend of the Duck Creek Syncline. An E-W striking crenulation cleavage (Fig. 3.7f) has developed axial planar to

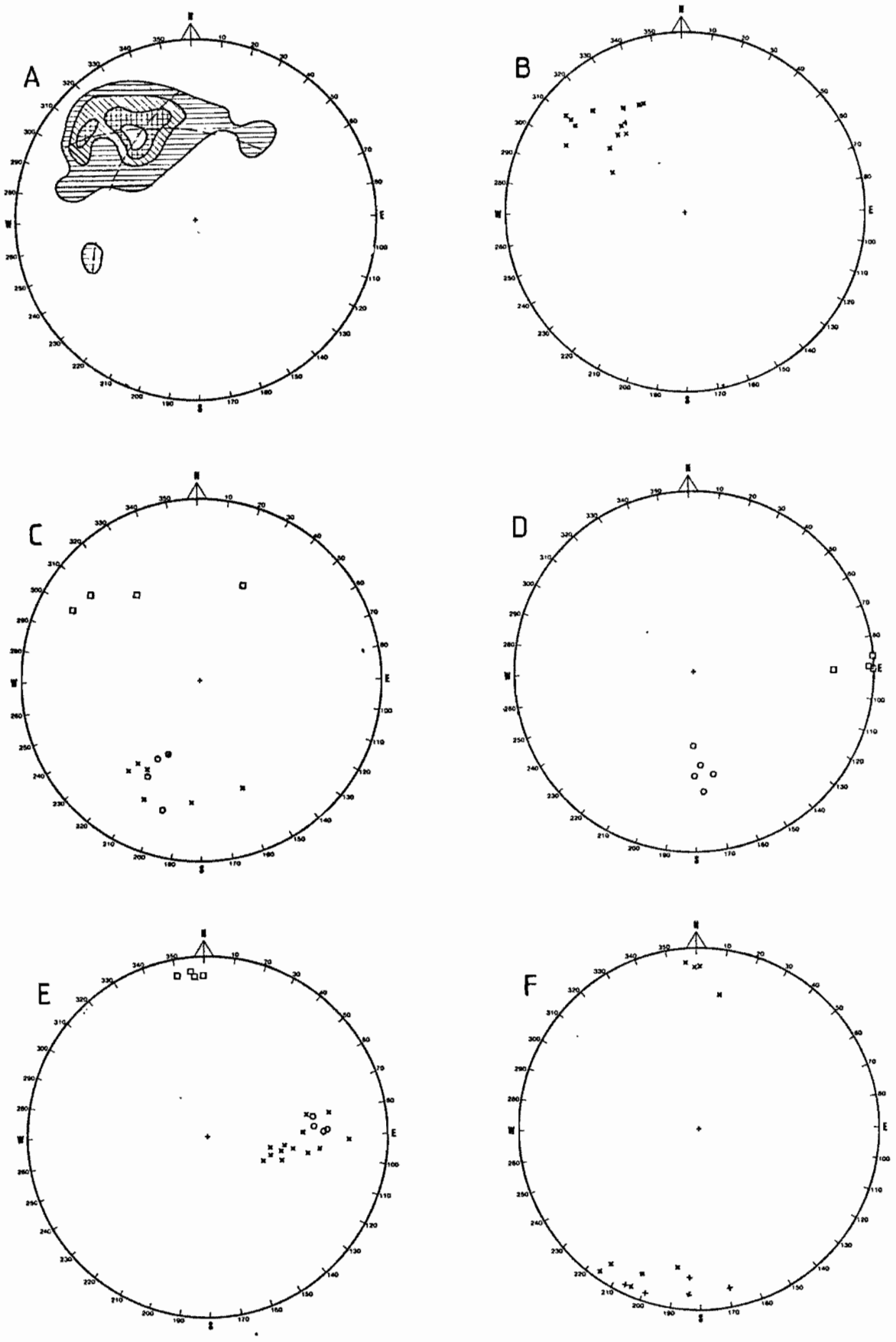

Fig 3.7(a-f). Equal area plots of planes and lineations from the Whyte Schists. (a) poles to differentiated layering, contours at 1,2,3 and 10%; (b) poles to S_2 cleavage; (c-e) ○ B_X hinge line orientations, × S_X/ S_0 intersection lineations and □,poles to axial planes of B_2, B_4 and B_5 folds respectively; (f) poles to S_5 cleavage.

the B_5 folds. This cleavage is strongest in the pelitic units and is similar to the S_5 cleavage observed in the Oonah Formation.

The distribution of layering orientations (Fig. 3.7a) is consistent with this area being the SE- dipping limb of the E-W trending Duck Creek Syncline. In this framework, the macroscopic B_5 folds in the Whyte Schists are parasitic on this main fold system.

3.5 REGIONAL STRUCTURE AND CORRELATIONS TO THE GRANVILLE HARBOUR AREA

Proterozoic deformation

Multiphase folding affecting the Oonah Formation and Arthur Lineament in addition to low grade metamorphism in the Arthur Lineament has been attributed to the Penguin Orogeny (Williams, 1978). Adams **et al.**,(1985) in summary quotes the Penguin Orogeny to be a Proterozoic Event occurring between 750 and 700 Ma ago.

According to Brown (1980), the Oonah Formation is characterized by the presence of refolded isoclinal folds which contain an early axial surface and are cut by a later crenulation cleavage. Such folds are considered to have formed during the Penguin Orogeny. Refolded isoclinal folds are typical of D_2 deformation in the Oonah Formation at Granville Harbour (Fig. 3.2a), and have been reported from Late Proterozoic sediments in the Strahan area (table 3.1; Baillie and Corbett, 1985). Two phases of deformation have also been attributed to the Penguin Orogeny in the Mount Bischoff and Mount Cleveland area (table 3.1; Williams, 1982; Collins, 1983). In conclusion, D_1 and D_2 deformations in the Granville Harbour area are attributed to the Penguin Orogeny. The highest grade of metamorphism in the Oonah Formation (chlorite-albite zone of the greenschist facies, see Chapter 4) accompanied D_2 deformation and is also attributed to the Penguin Orogeny.

In the Whyte Schists of the Savage River area, Coleman (1975) reports isoclinal NE- trending upright folds (table 3.1). These folds correlate with tight and reclined SSW plunging D_2 folds in the Whyte Schists as previously discussed. Both fold systems may correlate with the D_2 deformation event in the Oonah Formation and are therefore also attributed to the Penguin Orogeny.

AREA	HOST	OROGENY /EVENT	COMMENTS	CORRELATED EVENT	REFERENCE
Strahan Quadrangle	Bell Shale	Tabb. F1 F2	folds plunging 30-90 -->NW. shallow WNW. or ESE. plunging	D4 D5	Baillie and Williams (1975)
	Late Proterozoic Sequences	D1 D2 D3 D4	large scale isoclinal folds steeply dipping, W-NW. trending large symmetrical open folds moderate SW. plunging. upright, N-NNE. trending open and rounded folds, hinges plotting on a plane 050/40 NW.	D1 or D2 (?)	Baillie and Corbett (1985)
Mt. Bischoff Mt. Cleveland	Precambrian Sequences Cambrian Sequences	Penguin Tabb. F1 F2	two phases producing overturned recumbent- reclined folds upright NE. or SW. plunging folds upright SE. or NW. plunging folds	D1 or D2 (?) D4	Williams (1982) Collins (1983)
Rosebery Henty Area	Cambro-Ordovician Sequences	Late Cambrian-Early Ordovician movements Tabb. F1 F2	fault dominated, local or weak cleavage development on similar trends to Devonian deformation E-W shortening of the Dundas Trough, broad open folds. NW.- NNW. trending folds & faults	D3	Corbett and Lees (inprep.) Williams (1978)
Zeehan Quadrangle	Pre-Carboniferous Sequences	Tabb.	dominately SE. trending, reversals of plunge due to E- NE. trending crossfolding, eg. Heemskirk Anticlinorium, Huskinson Syncline Little Henty Syncline.	D4 and D5	Blissett (1962)
Savage River	Whyte Schist	Penguin F1 Tabb. F2 F3	upright, isoclinal, NE. trending folds. broad open NE. trending upright folds. crosscutting faults at acute angles to the F2 foliation.	D2 D4 D5 (?)	Coleman (1975)

Table 3.1 Brief summary of the structure in the Pre- Carboniferous sequences of central western Tasmania. Note that Tabb. refers to the Tabberabberan Orogeny and that the correlated event is that deformation event event in the Granville Harbour area which correlates best on style and general orientation.

Late Cambrian to Early Devonian deformation

Evidence for deformation and uplift during the Cambro-Ordovician in Western Tasmania is provided by:

(i) the presence of clasts of Darwin Granite and of penetratively cleaved volcanics in the base of the Tyndall Group correlates,

(ii) influx of detritus to form the Owen Conglomerate, and

(iii) unconformities of the Jukesian Movement in the Late Cambrian and the Haulage Unconformity in the Early Ordovician (Corbett, 1979, 1985)

The isotopic data of Adams **et al.**,(1985) is suggestive of a widespread thermal event capable of resetting Rb-Sr and K-Ar isotope systems during this period.

The D_3 deformation event of the Granville Harbour area correlates with this Cambro-Ordovician tectono-thermal event. The evidence for this correlation includes the influx of detrital siliciclastic material to form the Zeehan Conglomerate and an angular unconformity between the Zeehan Conglomerate and the underlying Early Cambrian(?) Duck Creek Sequence. Blissett (1962) correlated this unconformity with the Tyennan Unconformity, however, he did not recognize the significance of the Duck Creek Sequence. In light of this new information this unconformity and associated deformation correlates with the Jukesian Movement of Carey and Banks (1954).

Devonian deformation

Between the Early to late-Middle Devonian, a period of deformation (the Tabberabberan Orogeny) affected all Early Palaeozoic rocks in Tasmania and to a lesser extent, rocks of the Rocky Cape and Tyennan regions (Williams **et al.**, 1975; Williams, 1978).

In western Tasmania, two phases of Tabberabberan folding have been recorded. In the Early Devonian Bell Shale correlate of the Strahan area, Baillie and Williams (1975) record the relative sequence of Devonian folding to be :

(i) folds plunging 30-90^{o} NW

(ii) shallow WNW or ESE plunging folds.

Both phases produced a near-vertical primary axial surface cleavage, the second phase also producing a crenulation cleavage in localized areas. The style, orientation and relative timing of these two Tabberabberan folding events correlate respectively with B_4 and B_5 fold systems of the Granville Harbour area. The only difference between the two areas is that B_4 folds in the Granville Harbour area have shallower plunges and that reversals of

plunge of both B_4 and B_5 fold hinges are more common than has been recorded from the Strahan area.

D_4 and D_5 deformation structures also correlate with Tabberabberan structures reported by Blissett (1962). However, no sequence of deformation is given. Only tentative correlations can be made to Tabberabberan structures reported from other areas of Western Tasmania (table 3.1).

CHAPTER 4

IGNEOUS PETROLOGY AND METAMORPHISM

4.1 IGNEOUS PETROLOGY

Minor igneous rocks of spilite and metabasite composition are associated with the Whyte Schist, Oonah Formation and Duck Creek Sequence. Spilites from the Whyte Schists are dominated by albite and chlorite (e.g. 68243, 68244). In outcrop they appear as discordant bodies which cannot be followed along strike. Spry (1964) and Coleman (1975) interpreted these features to be intrusive igneous in origin. However, due to strong deformation, this cannot be considered conclusive.

The stable assemblages in metabasites from the Oonah Formation are albite, actinolite, biotite, epidote and Ti-rich magnetite (e.g. 68245, 68246). Albite in both samples forms subhedral laths that are strongly twinned and have a cloudy appearance due to high inclusion contents produced by albitization. Epidote generally forms fine grained, subhedral, stumpy prismatic grains with low, second order birefringence typical of Fe-poor epidote. Many of the magnetite rhombs exhibit strong cross-hatched ilmenite exsolution twins.

The texture of the metabasites from the Oonah Formation is idiomorphic to decussate, dominated by interlocking albite grains. Both samples are drill core intersections. Their spatial relationship to the enclosing sediments is indeterminate. Unlike similar rocks from the Whyte Schists, these metabasites contain amphibole and do not appear to be extensively spilitized.

The metabasite from the Duck Creek Sequence (68247) is mineralogically, texturally and chemically distinct from those in the Oonah Formation or Whyte Schist. In thin section the rock has a relict "subophitic" texture with fine grained brown to black material pseudomorphing feldspar(?) laths. The dominant mineral in this rock is pale green, weakly pleochroic Fe-poor actinolite. In outcrop this unit occurs as a discrete, 2 m wide body that is everywhere conformable with bedding. This suggests the unit to be a flow, however, due to strong deformation, a sill type origin cannot be excluded.

4.2 GEOCHEMISTRY OF THE METAVOLCANICS

Five samples of metabasite and spilite have been analyzed from the Whyte Schists (68243, 68244), Oonah Formation (68245, 68246) and from the Duck Creek Sequence (68247) in an attempt to define the parentage of these rocks and to allow comparisons with other Tasmanian volcanics. Immobile

UTG'D SAMPLE NUMBER	682245		68246		68244		68243		68247	
MAJOR ELEMENTS	A	B	A	B	A	B	A	B	A	B
SiO2	45.98	48.18	50.32	51.76	45.12	48.90	49.16	52.15	49.38	51.87
TiO2	1.51	1.58	2.06	2.12	2.38	2.58	2.58	2.74	0.38	0.40
Al2O3	13.34	13.98	13.54	13.93	15.79	17.11	16.58	17.59	14.59	15.33
Fe2O3	22.94		16.53		18.06		16.19		10.24	
FeO*		21.64		15.30		17.61		15.46		9.66
MnO	0.16	0.17	0.21	0.22	0.23	0.25	0.14	0.15	0.16	0.17
MgO	6.25	6.55	5.03	5.17	6.71	7.27	5.98	6.34	11.33	11.90
CaO	2.68	2.81	4.23	4.35	1.20	1.30	0.55	0.58	7.75	8.14
Na2O	2.68	2.81	5.62	5.78	4.20	4.55	4.27	4.55	2.23	2.34
K2O	2.00	2.10	1.05	1.08	0.06	0.07	0.07	0.07	0.10	0.11
P2O5	0.18	0.19	0.29	0.30	0.33	0.36	0.37	0.39	0.08	0.08
ign.	2.26		1.02		5.45		4.12		4.20	
total	99.98	100.00	99.99	100.00	99.53	100.00	100.03	100.00	100.42	100.00
TRACE ELEMENTS										
Nb	5.6		10.1		10.9		12.4		5.6	
Zr	111.4		134.5		158.7		178.2		52.5	
Y	38.3		40.0		21.8		28.0		20.2	
Sr	64.6		77.5		41.6		18.2		111.0	
Rb	148.5		71.7		2.9		3.2		4.0	
Ni	98.2		45.0		48.5		63.2		245.9	
Cr	103.0		63.1		75.0		73.7		865.9	
V	282.5		346.5		435.7		404.1		206.7	

Table 4.1 Major and trace element XRF. analysis of metabasites from the Oonah Formation (68245; 68246), Whyte Schist (68244; 68243) and the Duck Creek Sequence (68247) Note that FeO* = (0.9 X Fe2O3), columns A and B refer to uncorrected and corrected to 100% molecular percentages respectively.

elements, Ti, Zr, Y, Nb, Sr, Cr and P_2O_5 are useful in the identification of these ancient magma types. Pearce (1975) considers Ti, Zr, Y, Nb, and Cr to be chemically immobile during weathering and metamorphism below amphibole facies. Sr may be mobile during albitization and extreme weathering.

The tholeiitic character of metabasites from Granville Harbour is indicated by significant iron enrichment on FeO*-FeO*/MgO discrimination diagrams (Fig. 4.1A). This assignment is further supported by the Y/Nb ratios of all the samples which range between 2.0 and 6.8; Pearce and Cann (1973) suggest Y/Nb ratios greater than 1 are typical of tholeiitic parentage while ratios less than 1 are typical of calc-alkaline magmas. Based on Ti/Zr ratios and on the range in values of both major and minor elements, the analyses are further subdivided into metabasites and spilites from the Whyte Schist and Oonah Formation (Ti/Zr = 85-97) and a second type consisting of the metabasite from the Duck Creek Sequence (Ti/Zr = 45). Ti/Zr ratios for chondrite are reported at 110 (Sun, 1982).

Metabasites from the Whyte Schist and Oonah Formation

This group comprises high titanium, high iron, strongly fractionated tholeiites. TiO_2 and FeO^* are in the range of 1.5-2.6% and 15-22% respectively (table 4.1). In Ti-Zr, Ti-Zr/P_2O_5 and Ti-Cr discrimination diagrams (Figs. 4.1A,B&C), these rocks consistently plot in the ocean floor basalt fields. Extensive fractionation of samples 68243, 68244 and 68246 is indicated by low Ni and Cr contents (mean values of 52 ppm and 71 ppm respectively, table 4.1) and accompanying high V and FeO^* contents (mean values of 395 ppm and 16% respectively). Sample 68245 is unusual in that while moderately high Ni (98 ppm) and Cr (103 ppm) and low V (283 ppm) suggest it to be the most primitive of this group, it also has the highest FeO^* content (22%) indicating the highest degrees of fractionation. The high iron content must therefore be attributed strong Fe- metasomatism. Disseminated anhedral magnetite in 68245 and 68246 supports this interpretation.

Alteration affecting these samples is shown in figures 4.2A & B. In the Na_2O+K_2O versus SiO_2 discrimination diagram of figure 4.2B, most analyses plot in the alkalic field due to sodium and potassium enrichment associated with spilitization. Strong K_2O enrichment in the Oonah Formation metabasites is indicated by the trend towards the K_2O apex in figure 4.2A. Pearce (1975) noted similar trends of K_2O enrichment, as shown by K_2O-TiO_2-P_2O_5 discrimination diagrams, to be the result of hydrothermal alteration, metamorphism or weathering. Since both samples were obtained from within 15m of a skarn horizon, potassium enrichment is likely to be associated with

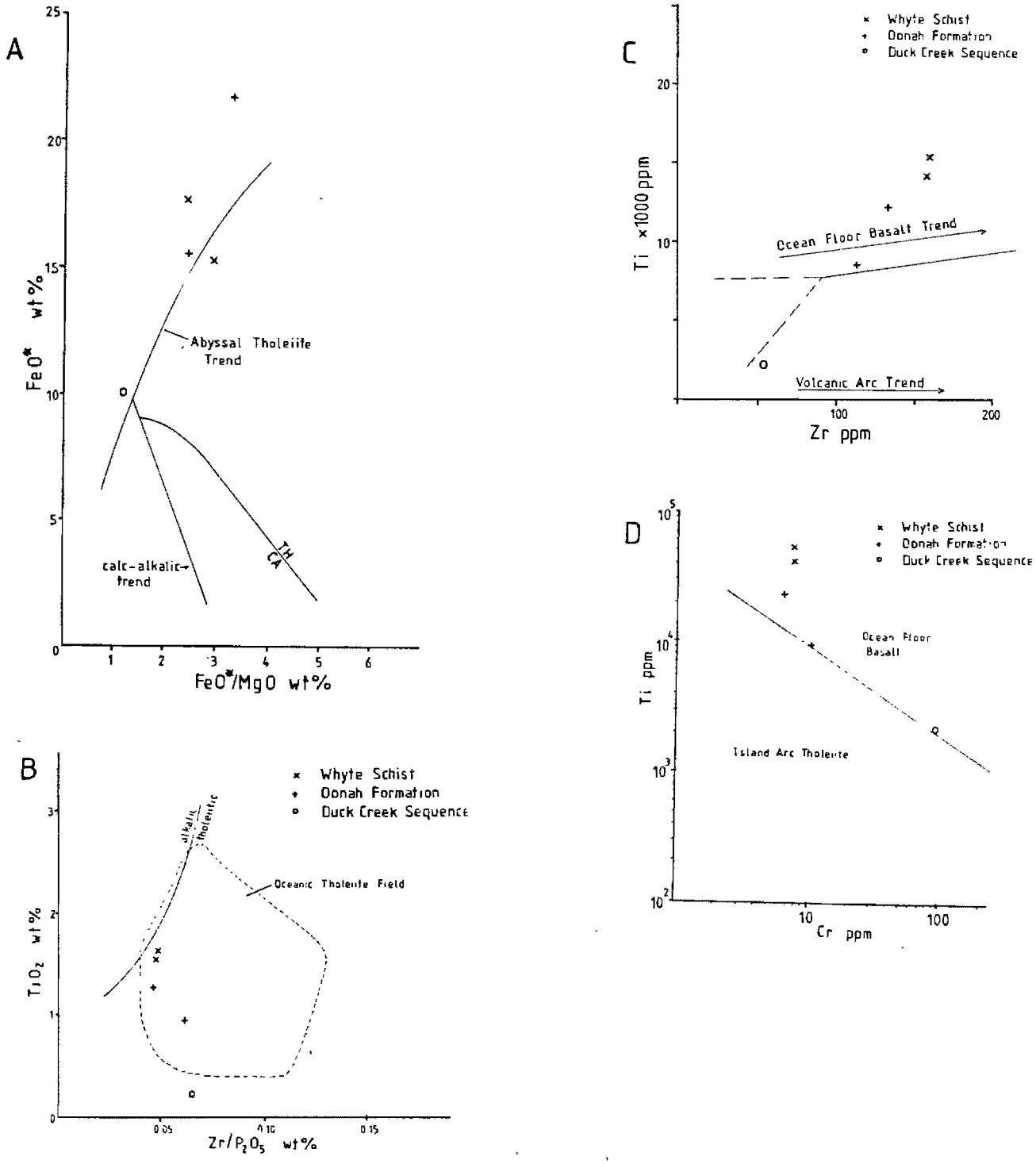

Fig. 4.1 Major and trace element binary discrimination diagrams plotted for metabasites in the Granville Harbour area. (A) FeO* versus FeO*/MgO diagram with typical tholeiite trend. TH = tholeiite, CA = calcalkaline. All trends from Miyashiro (1975). (B) Zr versus Zr/P_2O_5 diagram defining alkalic and tholeiite fields. Enclosed area defines field of oceanic tholeiites (after Winchester and Floyd, 1976). (C) Ti versus Zr plot for ocean floor basalts and volcanic arc basalts [after Pearce and Cann (1973), modified by Garcia (1978)]. (D) Ti versus Cr diagram for ocean floor basalts and island arc tholeiites (after Pearce, 1975).

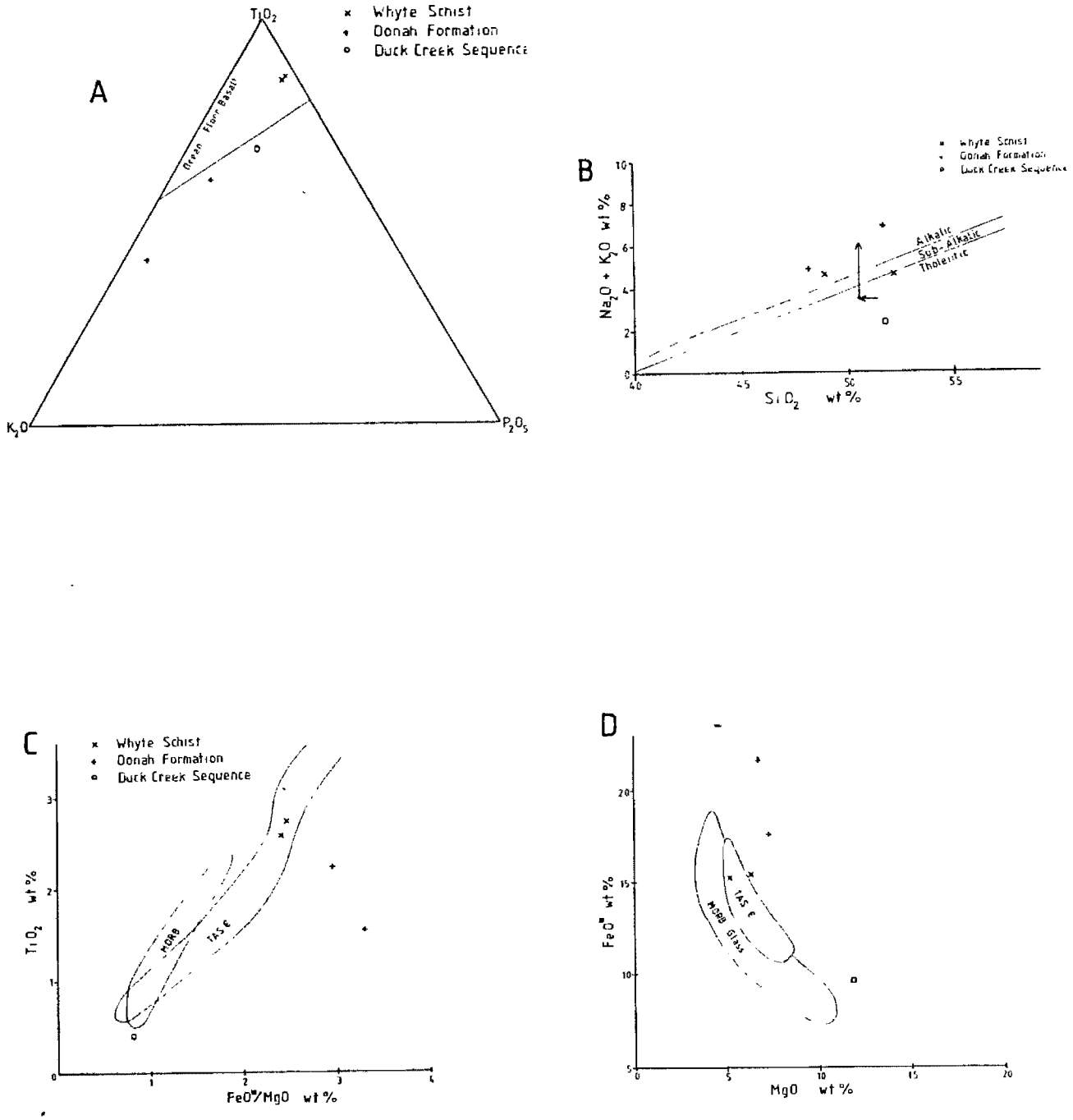

Fig. 4.2 Discrimination diagrams for metabasites in the Granville Harbour area. (A) K_2O-TiO_2-P_2O_5 ternary diagram (after Pearce and Cann, 1973). Oonah Formation samples show strong K_2O enrichment due to skarn alteration. (B) Na_2O+K_2O versus SiO_2 diagram. Alkalic-tholeiite line from MacDonald and Kasura (1964), sub-alkalic alkaline line from Irvine and Barager (1971). Arrows show direction of spilitic degradation of basalt (from Coleman, 1977). (C & D) TiO_2 versus FeO*/MgO diagram and FeO* versus MgO diagram showing fields of Tasmanian Cambrian (TAS€C) in relation to MORB (fields from A.J. Crawford, pers. comm.).

skarn formation. Similar conclusions may be drawn for the strong iron enrichment associated with these rocks.

In comparison to other Tasmanian volcanics, samples from the Whyte Schist and Oonah Formation are similar to the Crimson Creek type, Cambrian tholeiites that occur as flows and intrusives in the Dundas and Smithton Troughs. Similarities in Ti/Zr ratios confirm this correlation (A.J. Crawford, pers. comm.). Volcanics with similar major and minor element chemistry have been recorded from the Deep Creek and Henrys Volcanics at Cleveland by Collins (1983). On TiO_2-FeO*/MgO and FeO*-MgO diagrams of figure 4.2C & D, the samples from the Whyte Schist consistently plot in the Tasmanian Cambrian (Crimson Creek type tholeiite) field. Both Oonah Formation samples plot on the high FeO* side of this field due to strong Fe-enrichment.

Metabasite from the Duck Creek Sequence

The metabasite from the Duck Creek Sequence is characterized by very low TiO_2, FeO and V contents with high Cr and Ni. When plotted on the binary Ti-Zr diagram of Pearce and Cann (1973), figure 4.1C, this sample plots in the volcanic arc basalt field. However, Garcia (1978) points out that rocks with >200 ppm Cr but <4800 ppm Ti cannot be effectively assigned to a particular eruption setting from this diagram. Sample 68247 with 866 ppm Cr and 2280 ppm Ti falls into this category. In other discrimination diagrams (Figs. 4.2B & D), sample 68247 plots in the tholeiite field.

In comparison to other Tasmanian tholeiites, the sample from the Duck Creek Sequence is similar to low titanium basalts in the Heazlewood River and Serpentine Hill Complexes (e.g. Rubenach, 1973; Creenaume, 1980). These low titanium basalts and associated ultramafic intrusives are generally stratigraphically located at the top of the Crimson Creek Formation (eg. Blissett, 1962).

4.3 REGIONAL METAMORPHISM

Whyte Schist

The dominant metamorphic assemblage in the pelitic Whyte Schist includes quartz-chlorite-albite-muscovite and occasional biotite. Such mineral assemblages are consistent with the chlorite zone of the greenschist facies. Samples 68222 and 68220 contain remanent rounded clastic grains of quartz 0.1 to 0.2 mm in diameter.

Oonah Formation

The metamorphic assemblages in rocks least affected by contact metamorphism are again consistent with the chlorite zone of the greenschist facies. Muscovite in 68223, sampled from DDH GC3, defines a strong

crenulation cleavage and is axial planar to tight microfolds. This crenulation cleavage subparallels compositional layering and is consistent in style and orientation with D_2 deformation. Albite in this sample is porphyroblastic with a discontinuous internal foliation, S_i, defined by inclusion trains of magnetite and quartz (Fig. 4.3). S_i typically defines a sigmoidal pattern which is concordant with the external crenulation cleavage, S_2, and has a constant sense of rotation. Albite growth and greenschist facies metamorphism is thus interpreted to be syn-D_2 deformation. Minor reversals in the sense of rotation of S_i towards the outer edges of some porphyroblasts indicates minor late-stage, post-D_2 albite growth.

Quartz in the low grade regionally metamorphosed samples is fine grained and has strong undulose extinctions. This feature and the poor development of a granoblastic texture is typical of negligible contact metamorphism.

4.4 CONTACT METAMORPHISM

Contact metamorphism, associated with the intrusion of the Devonian Heemskirk Granite, has resulted in the re-equilibration of regional metamorphic assemblages in the Oonah Formation up to 3.3 km away from the nearest exposed granite contact. In the highest grades of contact metamorphism, quartz develops a strong and distinctive granoblastic texture (Fig. 4.4). The degree of development of this texture may be considered indicative of the degree of annealing.

Albite-epidote hornfels facies

Contact metamorphic rocks from this facies are defined by the development of albite, epidote, actinolite and minor biotite in the matrix of pelitic rocks (Turner, 1981). At Granville Harbour, this grade of hornfels, grades into and replaces regional metamorphic assemblages making absolute distinctions difficult.

Typical contact metamorphic assemblages are:

quartz-chlorite-biotite-epidote (68225, 68230)
quartz-muscovite-biotite-carbonate (68224)
quartz-chlorite-muscovite-biotite-albite (68228)
quartz-muscovite-biotite-tourmaline (68226)
quartz-biotite-epidote-actinolite (68227).

In all assemblages, the phyllosilicates chlorite and muscovite, define a relict foliation while quartz exhibits weak annealing. Epidote forms stumpy birefringent grains that clearly overprint the foliation defined by chlorite. The form of biotite in these samples is variable. In 68245,

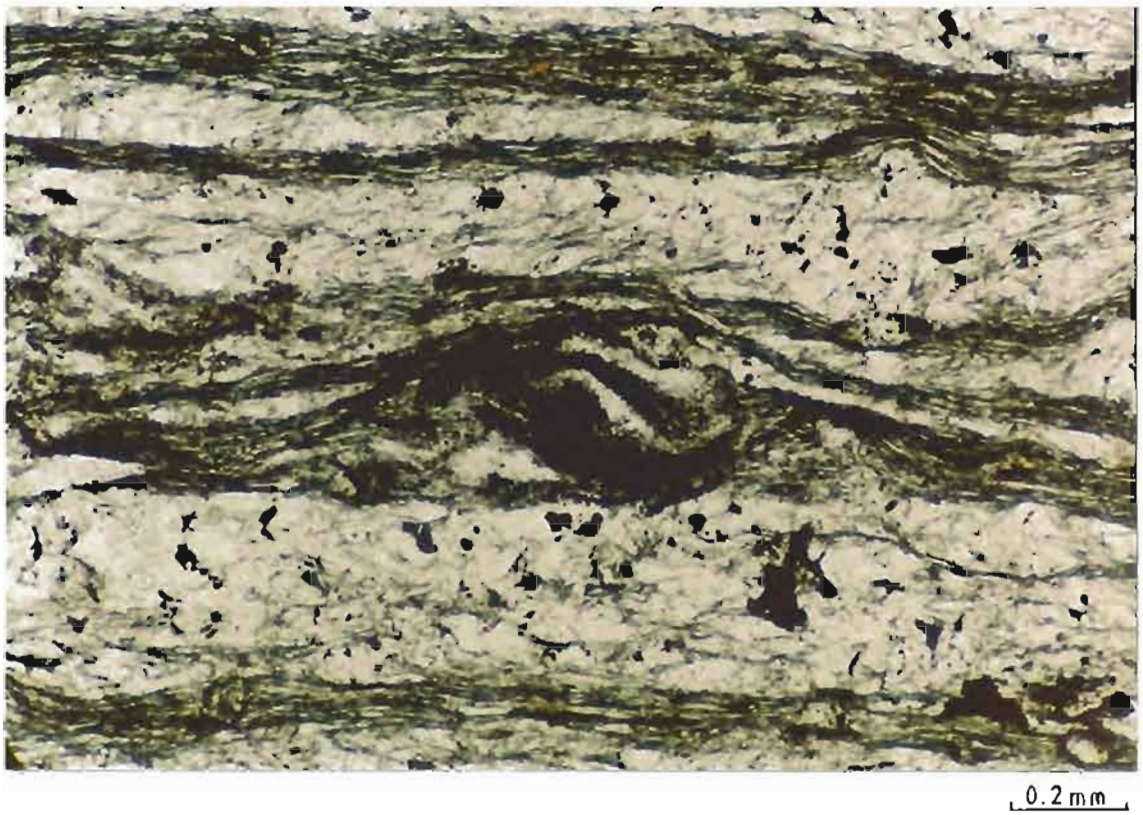

Fig. 4.3 Quartz-muscovite-albite-epidote-magnetite schist. Muscovite defines a crenulation cleavage consistent in orientation and style to the second phase cleavage. Albite porphyroblast (centre) has sigmoidal intrusion train defined by magnetite. Plane light photomicrograph.

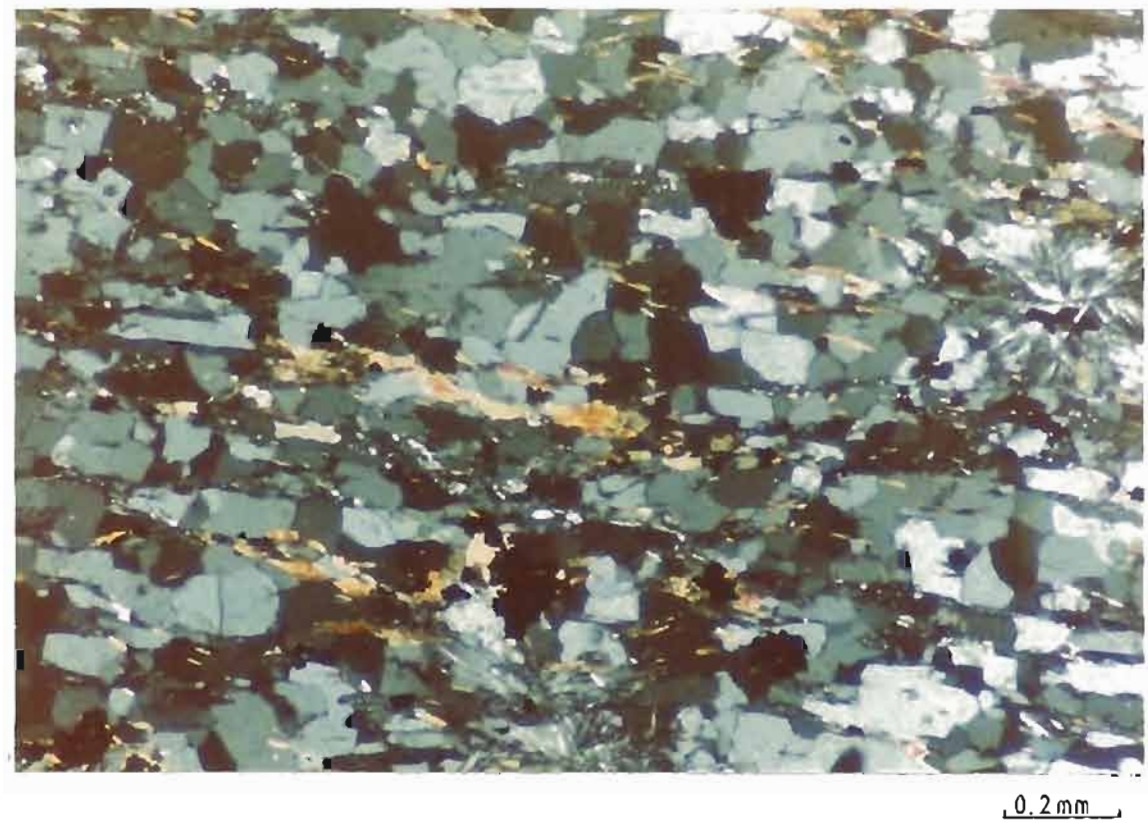

Fig. 4.4 Highly annealed granoblastic quartz-biotite-sillimanite hornfels typical of the hornblende hornfels facies. Sillimanite in this sample forms radiating clusters of fine grained, low birefringent , acicular grains. Polarized light photomicrograph.

68228 and 68230 it is fine grained, anhedral, weakly pleochroic in browns and appears in some areas to be replacing chlorite. In comparison, biotite in 68226 is strongly pleochroic in browns, and forms subhedral to euhedral,randomly orientated, bladed grains. This sample is suggested to be intermediate to the next stage of thermal metamorphism. Minor (<2%) tourmaline in this rock indicates infiltration of boron-rich granitic fluids.

Hornblende-hornfels facies

Stable assemblages in this facies are quartz-biotite-muscovite with andalusite or sillimanite and/or cordierite in pelites and calcite-diopside-tremolite or calcite-diopside-grossular in calcic sediments (Turner, 1981).

Typical assemblages consistent with this facies of thermal metamorphism at Granville Harbour are:

quartz-biotite-tremolite-actinolite (68235, 68231, 68232)

quartz-ferroactinolite (68233)

quartz-biotite-cordierite-tourmaline-tremolite (68236, 68239)

quartz-biotite-tourmaline-pyrite (68234)

quartz-biotite-sillimanite (68240)

quartz-Mn garnet-pyrrhotite-cordierite-muscovite-biotite (68241).

The most distinguishing feature of this grade of metamorphism is the development of biotite in preference to chlorite. In most samples it occurs as strongly pleochroic red-brown euhedral blades and in some cases pseudomorphs early phyllosilicates. In 68234, mimetic crystallization of biotite results in the preservation of two relict cleavages while in 68239, mimetic crystallization of biotite and cordierite preserves relict microfolds and foliations Cordierite forms in preference to biotite in the low potassium zones.

The growth of sillimanite in these samples is minor but when present occurs as fine radiating clusters of acicular crystals. The cores of these clusters are often altered to chlorite. In the calcic- sediments, amphiboles, tremolite and actinolite have developed in preference to other silicates (e.g. 68231, 68232).

The highest grade of metamorphism is observed from 68241, sampled from DDH GC3 at a depth of 338.8 m. This is a medium grained (0.5-1 mm), weakly banded granular rock with a mineral assemblage of Mn-garnet, cordierite, biotite, muscovite and pyrrhotite. The garnets are strongly fractured and replaced by magnetite while the cordierite is crowded with biotite inclusions. If in equilibrium, this mineral assemblage indicates temperatures of 600^{o}C at 2 kb (Hirschberg and Winkler, 1968). The

occurrence of sillimanite in these samples indicates a minimum metamorphic temperatures of 650°C (Holdaway, 1971).

The Contact Aureole

Due to sporadic sampling, the exact nature of the contact aureole may only be tentatively defined. On the coastal section, albite-epidote hornfels facies assemblages are observed throughout the Oonah Formation as far north as the fault contact with the Duck Creek Sequence (Fig. 3.1). This is approximately 3.3 km from the nearest exposed granite at Granville Harbour. The observed hornfels assemblages are transitional to the lower greenschist facies regional metamorphic assemblages making the limit of the contact aureole only a tentatively defined boundary. The transition to the hornblende hornfels facies occurs to the south of the Stingray Bay where calcite in basic phyllites is replaced by tremolite and actinolite. At Granville Harbour, samples are strongly annealed and have mineral assemblages consistent with moderate grades of hornblende hornfels facies metamorphism.

A complete spectrum of metamorphic grades is observed from drill core sections. In DDH GC3, the top 120 m show no effects of thermal metamorphism and contain assemblages consistent with lower greenschist facies of regional metamorphism. At a depth of 338.8 m (e.g. 68241) the highest grades of thermal metamorphism are observed by the development of Mn-garnet cordierite, biotite and muscovite.

CHAPTER 5

MINERALIZATION, MINERALOGY AND PETROLOGY

The area of mineralization under study is situated directly north of Granville Harbour in an area referred to by the CRA/Geopeko Joint Venture partners as the Gourlays Creek Prospect. Based on magnetic anomaly interpretations (Fig. 3.1) and on drill core intersections (Fig. 5.1), two contrasting styles of mineralization are defined:

(i) infiltration metasomatic exoskarn with a typical calcic skarn mineralogy, and

(ii) massive and banded magnetite-pyrite-(quartz) and massive barite-magnetite-pyrite.

The skarn forms the upper and most eastern mineralized horizon of figures 5.1 and 3.1 while the magnetite-pyrite-barite-rich mineralization forms the lower and most western horizon. Each style is henceforth referred to as the upper and lower mineralized horizons respectively, characteristics of each are summarized in table 5.1.

The relative distribution of these two contrasting forms of mineralized horizon is reflected in the down-hole projections of Fe, Cu and Sn concentrations as shown in figures 5.2 and 5.3. From these diagrams it is noted that most of the Sn (3500 ppm) is concentrated in the upper skarn horizon of DDH GCA. Only minor Sn is found in the lower mineralized horizon. Cu is concentrated in the lower mineralized horizon reaching concentrations of 4600 ppm. As, Pb, Zn and W are rarely above background levels for these two drill holes and have not been plotted on figures 5.2 and 5.3. No geochemical data for DDH GC3 are available.

The host to the mineralization at Gourlays Creek is a sequence of interbedded siltstones, quartzites, shales, calcsilicates and carbonate all dipping to the east at approximately 50^{o}. The degree of deformation observed in phyllites from the top of DDH GCA (Fig. 5.5) is consistent with D_1 and D_2 deformation as observed in the Oonah Formation from the coastal section. The relative stratigraphic position of the mineralized horizons within the Oonah Formation cannot be ascertained with confidence. The axis of the aeromagnetic anomaly (Fig. 3.1), which generally parallels bedding, suggests the mineralized horizons to correlate with the most northern exposures of the Oonah Formation along the coastal section. The only carbonates mapped in this area are minor dolomitic units within the Duck Creek Sequence. However, since the skarns indicate a lime- rich protolith and deformation of the host sequence is typical of D_1 and D_2 deformation in

	Upper mineralized horizon	Lower mineralized horizon
Mineralogy: Early prograde	clinopyroxene garnet	magnetite barite pyrite siderite quartz
Late retrograde	actinolite pyrite calcite pyrrhotite quartz magnetite epidote chalcopyrite axinite	
Alteration	Calcsilicate (mainly tremolite) in the surrounding sediments	Banded pyrite confined to the footwall (Fig. 5.1), minor chlorite alteration
Metal concentrations: max. Sn max. Cu max. Fe Pb, Zn, W	 less than 3500 ppm less than 3300 ppm less than 25% weakly anomalous, generally background levels or slightly above	 less than 1300 ppm less than 4600 ppm less than 50% weakly anomalous, generally background levels or slight above
Form	Massive calcsilicate-rich stratabound	Massive and banded magnetite and pyrite dominant, stratabound and stratiform
Style of Mineralization	Calcic Cu-Fe skarn, similar to calcic Cu-Fe skarns of Einaudi **et al.** (1981).	Sediment-hosted, exhalative banded iron formation (?), sulphide and oxide facies.

Table 5.1 Characteristics of the upper (skarn) mineralized horizon and the lower (banded and massive magnetite-pyrite-quartz-barite) horizon. The upper and lower mineralized horizons refer to the relative position of these two distinct mineralization types in drill core. Note that the prograde-retrograde terminology refers only to the skarn horizons.

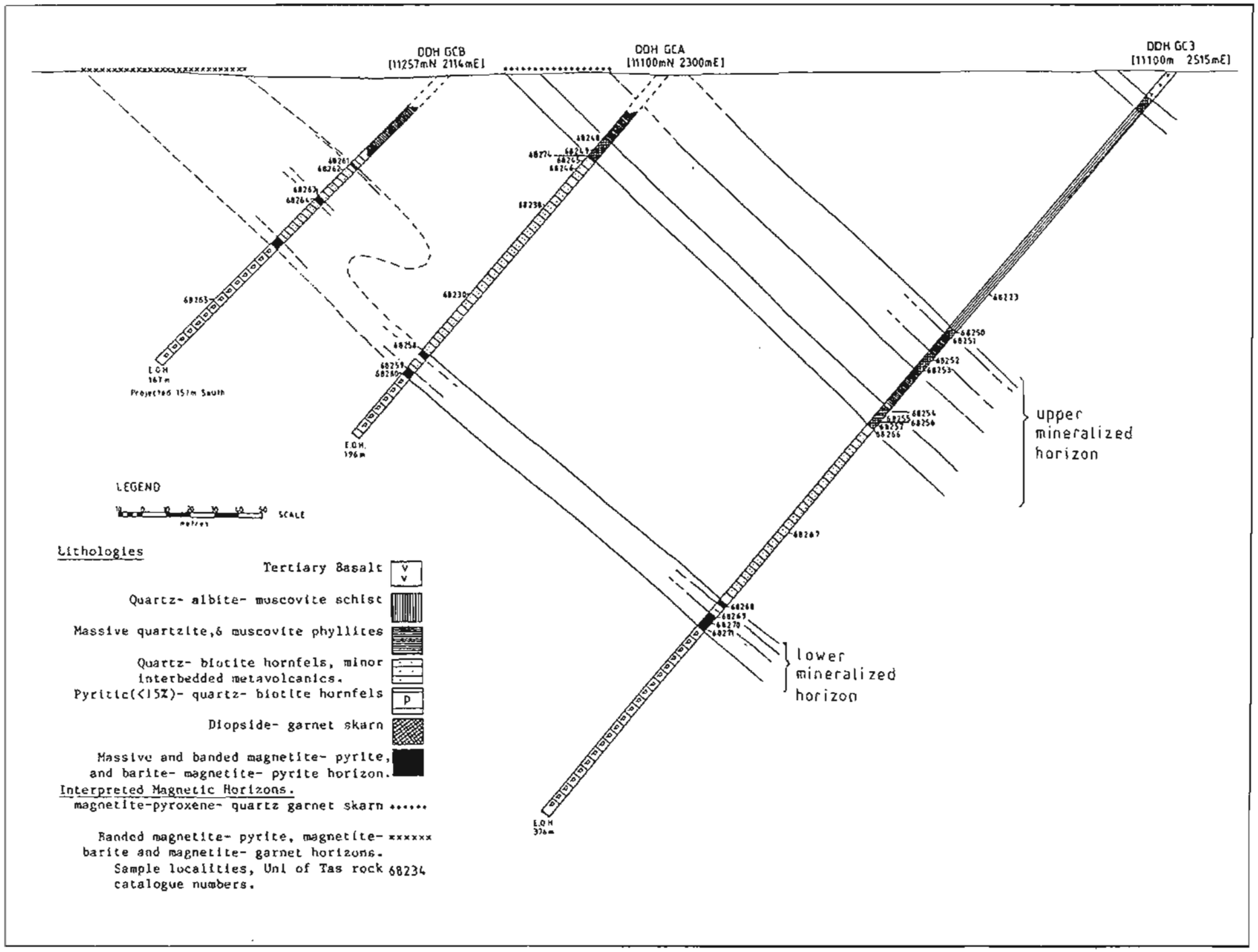

Fig 5.1 Interpreted drill hole crossection for the Gourlays Creek Prospect. Note that DDH GCB has been projected 157m south along strike. Interpreted magnetic horizons from Kendall (1984)

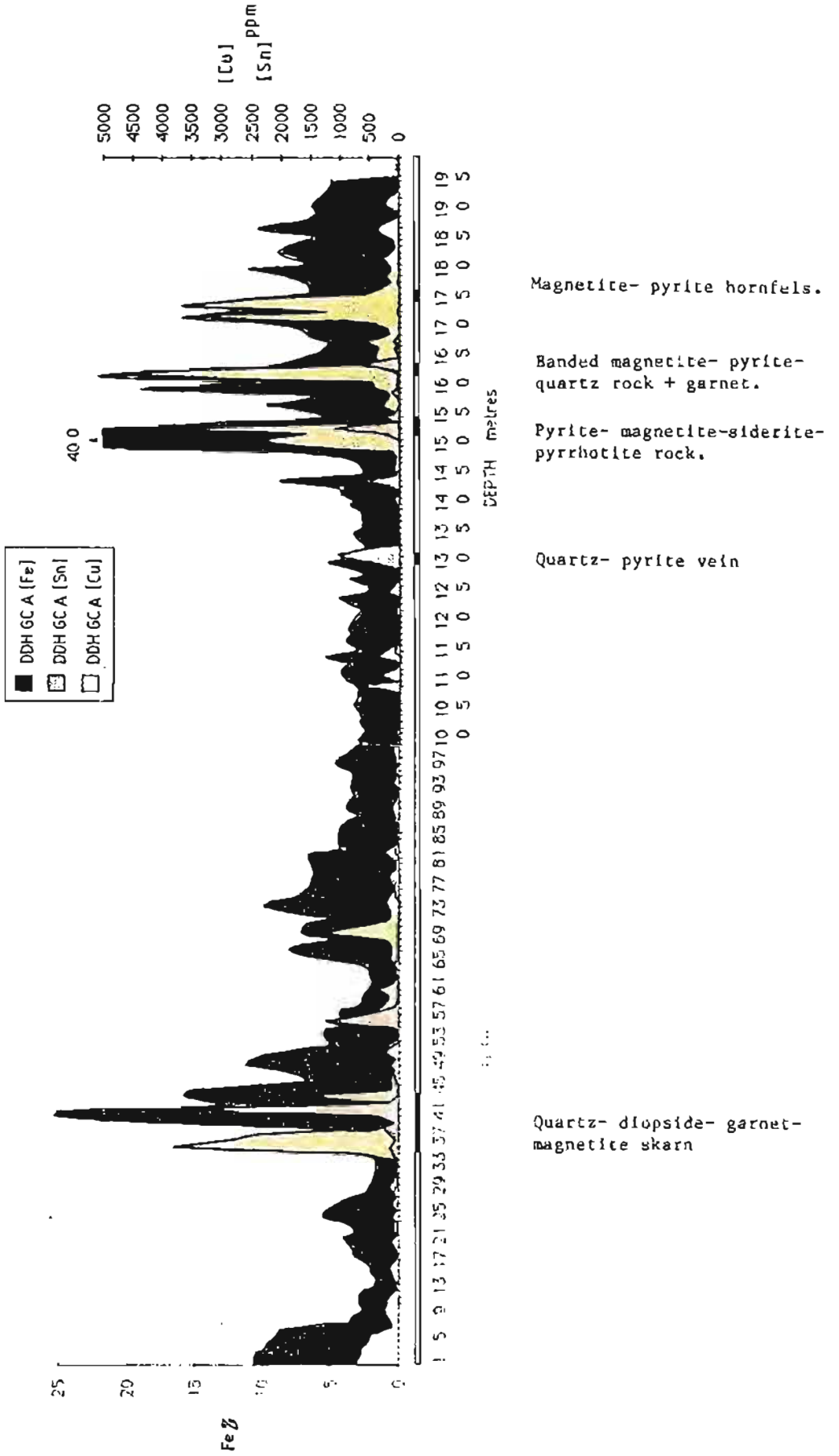

Fig 5.2 Down hole projections of Fe, Cu and Sn concentrations as a function of depth in DDH GCA. All analytical data from Kendall (1984)

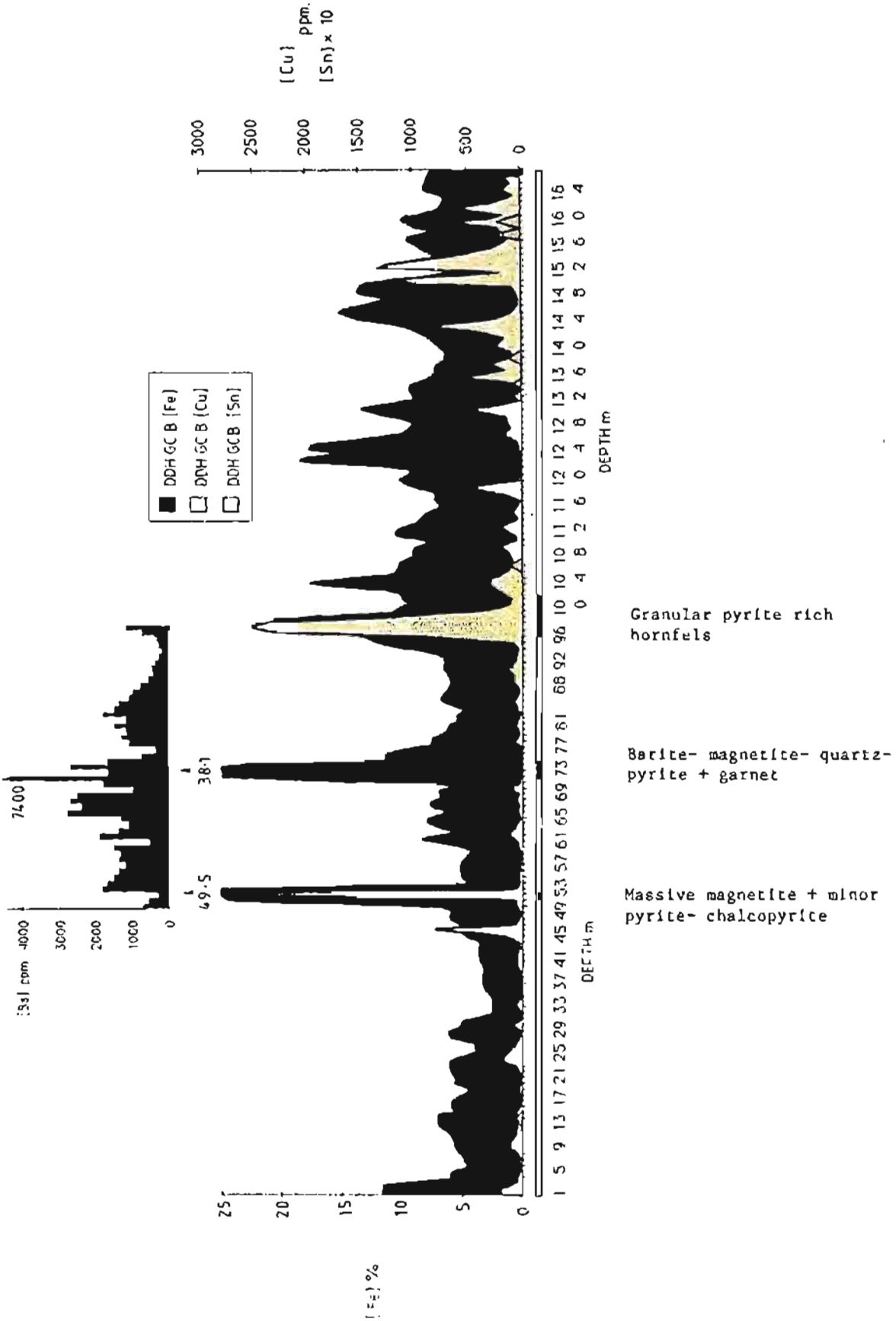

Fig 5.3 Down hole projections of Fe, Cu and Sn concentrations as a function of depth in DDH GCB. Concentrations of barite are superimposed on this projection for the depths of 50 to 100 metres. All analytical data from Kendall (1984).

the Oonah formation, the Duck Creek Sequence is an unlikely host for the mineralization.

The only evidence of surface mineralization in the grid area is minor outcrops of massive and banded magnetite-(hematite)-pyrite-quartz and of calcsilicate rocks (Fig 5.1). Minor tourmalinization and greisenization in the vicinity of the Devonian Heemskirk Granite, which outcrops in the southern part of the grid area, are evidence for metasomatic fluids moving out from the granite. Due to the poor outcrops of the mineralized horizons, the following interpretation of the mineralization is based on intersections from diamond drill holes DDH GCA, DDH GCB and DDH GC3. The aerial distribution of these three holes with respect to the mineralized horizons is shown in figure 3.1. An interpreted schematic cross section of the drill core is represented in figure 5.1 while summary drill core logs are presented in appendix A.2.

5.1 SKARNS

A skarn by definition consists of coarse grained Ca-Fe-Mg-Mn silicates formed by replacement of carbonate-bearing rocks during regional or contact metamorphism and metasomatism (Einaudi **et al.**, 1981). The Gourlays Creek skarn (i.e. the upper mineralized horizon) is a stratabound unit up to 12 m thick. In DDH GC3, three distinct intersections of skarns are observed. The lower intersection is correlated with the skarn intersection in DDH GCA (Fig. 5.1).

The Gourlays Creek skarns consist of a prograde mineral assemblage dominated by clinopyroxene and garnet. This mineralogy is typical of calcic skarns where the protolith carbonate is a limestone. Retrograde minerals in the Gourlays Creek skarns include tremolite-actinolite, chlorite, calcite, quartz, magnetite, pyrite and pyrrhotite. Most of the magnetite appears to be concentrated in the footwall of the lowest skarn intersection of DDH GC3, where it is associated with quartz hornfels. This magnetite may represent primary, pre-skarn mineralization. On this basis it is estimated that less than 20% Fe-oxides and sulphides are genetically associated with skarn formation. Einaudi **et al.**,(1981) report up to 10% Fe-oxides and 2-15% sulphides from similar clinopyroxene-garnet skarns. In all cases, opaques are associated with retrograde assemblages and reflect higher oxidation and sulphidization states and lower temperatures than earlier mineralization.

No evidence of bimetasomatic zonation has been found in the Gourlays Creek skarns reflecting the lack of major chemical or permeability gradients. Minor evidence of metasomatic infiltration is observed in figure 5.6 where calcium- and magnesium-rich fluids are observed to have moved

Fig. 5.4 Banded hematite-quartz rock (68273) with coarse grained, subhedral pyrite grains in both quartz and hematite layers. Sample from surface outcrop.

Fig 5.5

Fig 5.6

Fig. 5.5 Quartz sericite phyllite from the top of DDH GCA. The strong deformation reflected by this sample is typical of D_2, D_4 and D_5 deformations in the Oonah Formation.

Fig. 5.6. Bimetasomatic infiltration, movement of iron- and magnesium- rich fluids up microfractures and along carbonate- rich bands has resulted in the deposition of tremolite- actinolite.

along microfractures and to replace fine carbonate-rich layers. Similar distributions of hornblende is observed in 68238. The occurrence of axinite in the skarn rocks (e.g. 68254, 68257) suggests a granitic origin of the metasomatic fluids.

Metasomatic zonations have not been identified from the Gourlays Creek skarn although this is likely to reflect the limited number of holes intersecting the skarn horizon (i.e. two) rather than the absence of zoning. Typical metasomatic zoning for calcic skarns as described by Einaudi and Burt (1982) is garnet --> pyroxene --> (wollastonite) --> marble. In this scheme the pyroxene-rich pyroxene-garnet skarns of Gourlays Creek belong to a zone typical of intermediate distance from the granite source.

The common skarn assemblages from Gourlays Creek are:-

(i) pyroxene-garnet (e.g. 68248, 68251, 68252, 68253, 68256)

(ii) pyroxene-magnetite-quartz (e.g. 68249, 68250, 68274)

(iii) pyroxene-chlorite (e.g. 68254)

(iv) pyroxene-epidote-actinolite (e.g. 68255)

(v) hornblende-calcite-axinite (e.g. 68257)

Clinopyroxene-garnet Skarn

Pyroxene-garnet skarn, representative of prograde mineralization, forms the largest proportion of skarn mineralization at Gourlays Creek. In hand specimen the rocks are massive pale yellow-green in colour with garnets being recognized as watery reddish-brown grains or polygranular masses. Pyroxene may form up to 60% of the bulk mineralogy while garnet which is usually subordinate to pyroxene, may form up to 50%. Multiple generations of pyroxene growth is recognized by subtle variations in colour and grainsize (Fig. 5.14).

Retrograde alteration of the skarn has resulted in the progressive replacement of garnet and especially of pyroxene by quartz, calcite, actinolite, sulphides and magnetite. Sulphides and Fe-oxides form as fine grained disseminations and replacements and rarely exceed 20% of the bulk mineralogy. Pyrrhotite is the dominant sulphide followed by chalcopyrite and then pyrite. In 68256, pyrrhotite is observed to replace diopside or occurs in vughs and cross cutting veinlets (Fig. 5.17A).

Sample 68248 represents a contact between calcareous siltstone and limestone. The siltstone has been replaced by tremolite-chlorite-magnetite hornfels and the limestone by pyroxene-garnet-calcite skarn. No evidence of bimetasomatic reactions is observed along this contact.

Pyroxene-magnetite-quartz skarn

In 68250, fine grained anhedral magnetite is associated with pyroxene quartz and serpentine. The occurrence of serpentine suggests the protolith

of this sample to be a dolomitic unit. In other samples (e.g. 68249, 68274), most of the magnetite is suggested to be pre-skarn and primary in origin. Evidence for this is observed in 68274 where pyroxene skarn invades the quartz-magnetite zone through a series of fractures and veinlets thus indicating pyroxene to be post magnetite deposition. In almost all skarns, the opposite paragenesis has been observed (e.g. Einaudi **et al.**, 1981). In 68249, magnetite is strongly associated with quartz hornfels and pseudomorphs the secular lath form of hematite. The hematite-to-magnetite transformation is, according to Ramdohr (1969), typical of contact metamorphism.

Pyroxene-chlorite skarn

Sample 68254 exhibits almost complete retrograde alteration of pyroxene skarn to chlorite and serpentine (?). The intensity of alteration increases towards an axinite-filled vein suggesting most of the alteration fluids to have penetrated the skarn from this vein. Minor fine grained disseminated magnetite is associated with this rock.

Pyroxene-epidote-actinolite skarn

Epidote in 68255 forms up to 60% of the bulk mineralogy and occurs as granular subidioblastic grains. The exact origin of epidote in this sample is unknown. Two possibilities are (i) replacement of aluminous sediments, or (ii) retrograde alteration of pyroxene skarn. Déchomets (1985) has reported the formation of epidote skarn from a mica schist protolith.

In other samples (e.g. 68251), epidote occurs in veins that penetrate both garnet and pyroxene suggesting a retrograde origin. In 68255, minor actinolite also replaces pyroxene.

Hornblende-calcite skarn

This rock represents the highest grades of retrograde alteration in that no remanent prograde minerals or their associated textures are preserved. In 68257, the sequence of alteration is given as hornblende, calcite, axinite, and finally quartz. In hand specimen, laths of hornblende are enclosed by coarse grained calcite. Axinite and quartz are present as vugh fill.

In summary, the Gourlays Creek skarns are characterized by a prograde assemblage of pyroxene and garnet which on alteration forms actinolite-chlorite-epidote-hornblende-calcite-quartz and serpentine(?). Pyrrhotite, chalcopyrite, pyrite and magnetite are also deposited during retrograde alteration although most of the magnetite appears to be pre-skarn and primary in origin. Similar retrograde replacements and mineralogies have been reported from ten polymetallic garnet-pyroxene skarns from southwestern

Type	Calcic Fe	Magnesian Fe	Calcic Cu	Calcic Sn	Magnesian Sn
Relative abundance (number of examples listed in text)	Abundant (20)	Abundant (8)	Abundant (43)	Rare (14)	Rare (14)
Size: largest known (million tons ore)	Sarbai, U.S.S.R., 725 m.t., 47% Fe	Sherogesh, U.S.S.R., 234 m.t. 35% Fe	Twin Buttes, Ariz., 500 m.t., 0.8% Cu	Moina, Tasmania 30 m.t., 0.15% Sn	?
Typical size	5–200 m.t.	5–100 m.t.	1–100 m.t.	0.1–3 m.t.	1 m.t.
Typical grade	40% Fe	40% Fe	2% Cu u.g., 1% Cu o.p.		
Metal association (minor metals)	Fe (Cu, Co, Au)	Fe (Cu, Zn)	Cu, Mo (W, Zn)	Sn, F (Be, W)	Sn, F (Be, B)
Tectonic setting	Oceanic island arc; rifted continental margins	Continental margin; synorogenic	Continental margin; syn-orogenic to late orogenic	Continental margin; late orogenic to postorogenic	Continental margin; late orogenic to postorogenic
Associated igneous rocks					
Intrusive rock composition	Gabbro to syenite, mostly diorite, some with diabase	Granodiorite to granite	Granodiorite to quartz monzonite; rarely monzonite	Granite	Granite
Co-genetic volcanics	Common: basalt, andesite	Absent	Common: andesite	Mostly absent	Mostly absent
Intrusive texture	Medium to fine grained; equigranular	Medium to fine grained; equigranular	Medium grained to aphanitic; porphyritic	Coarse to fine grained; equigranular to porphyritic	Coarse to fine grained; equigranular to porphyritic
Intrusive morphology	Large to small stocks, dikes	Small stocks, dikes, sills	Stocks, dikes	Stocks, batholiths	Stocks, batholiths
Intrusive alteration	Na-silicates, extensive endoskarn	Minor endoskarn; propylitic	K-silicate, sericitic, local endoskarn	Greisen	Greisen
Mineralogy:					
Prograde	Grandite, salite, ferrosalite, epidote, magnetite	Forsterite, calcite, spinel, diopside, magnetite	Andraditic garnet, salitic pyroxene, local wollastonite	Malayaite, danburite, datolite, grandite, idocrase	Spinel, fassaite, forsterite, phlogopite, magnetite, humite, ludwigite, paigeite
Retrograde	Amphibole, chlorite (ilvaite)	Amphibole, humite serpentine, pholgopite	Actinolite, chlorite, montmorillonoids	Amphibole, mica, chlorite, tourmaline, fluorite	Cassiterite, fluoborite, magnetite, micas, fluorite
Ore	Magnetite (chalcopyrite, cobaltite, pyrrhotite)	Magnetite (pyrite, chalcopyrite, sphalerite, pyrrhotite)	Chalcopyrite, bornite, pyrite, hematite, magnetite	Cassiterite, arsenopyrite, stannite, pyrrhotite	Cassiterite, minor arsenopyrite, pyrrhotite, stannite, sphalerite

Table 5.2 Comparison of major skarn types that have similarites to mineralization at Gourlays Creek. Note that calcic W, Zn-Pb and Mo skarns have not been included. Modified after Einaudi et al. (1981, table 1).

United States of America, Japan and Italy (Burton **et al.**, 1982) and in Fe-Cu skarns from Japan (Uchida and Iiyama, 1982).

5.2 MASSIVE and BANDED MAGNETITE-PYRITE-QUARTZ-BARITE MINERALIZATION

Two important features of this lower mineralized horizon are its stratabound and often stratiform nature, and the predominance of magnetite and pyrite with only minor associated calcsilicate minerals. The only possible skarn analogue to these deposits are the Fe skarns of Einaudi **et al.**,(1981). From table 5.2, calcic-Fe skarns are generally associated with gabbros and diorites in volcano-sedimentary sequences while magnesium-Fe skarns have Mg-rich prograde and retrograde mineralogies (e.g. forsterite, calcite, spinel, diopside, magnetite, amphibole, humite, serpentinite and phlogopite). Such igneous rock associations and mineralogies contradict what has been observed at Gourlays Creek where skarns are associated with the Devonian Heemskirk Granite. Minor calcsilicate minerals associated with this lower horizon are dominantly calcic (e.g. clinopyroxene and andradite garnet). The St Dizier skarn located 10 km ESE has a mineralogy dominated by magnetite-pyrrhotite and Mg-rich minerals (Purvis, 1978) and may correlate with a mixed magnesium Sn-Fe skarn. This mineralogy is unlike that observed for the lower mineralized horizon at Gourlays Creek.

Many features of this lower magnetite-pyrite horizon are suggestive of a primary, syngenetic origin. Evidence supporting this conclusion is briefly summarized below.

(1) The statiform nature and high sulphide contents of this horizon is unlike any known skarn mineralization but is typical of syngenetic deposits. The strong quartz-magnetite-pyrite banding is typical of recrystallized banded material representative of banded iron formations.

(2) The strain suffered by quartz appears inhomogeneous with respect to magnetite and pyrite. In the quartz-rich bands, quartz is highly elongate with length-to-breadth ratios of up to 4:1 and with strong undulose extinctions. In comparison, quartz from the sulphide-oxide layers is weakly strained occurring as subhedral polygonal grains. Alternatively, quartz forms pressure-type shadows around magnetite and pyrite grains. Such evidence indicates magnetite and pyrite to be at least pre-deformation. The skarns in comparison are post-deformation.

(3) Moderate annealing of massive magnetite and pyrite (Fig's 7A & B) indicates moderate degrees of textural equilibrium and grades of metamorphism. In comparison with rocks from Balcooma, (Queensland),

A

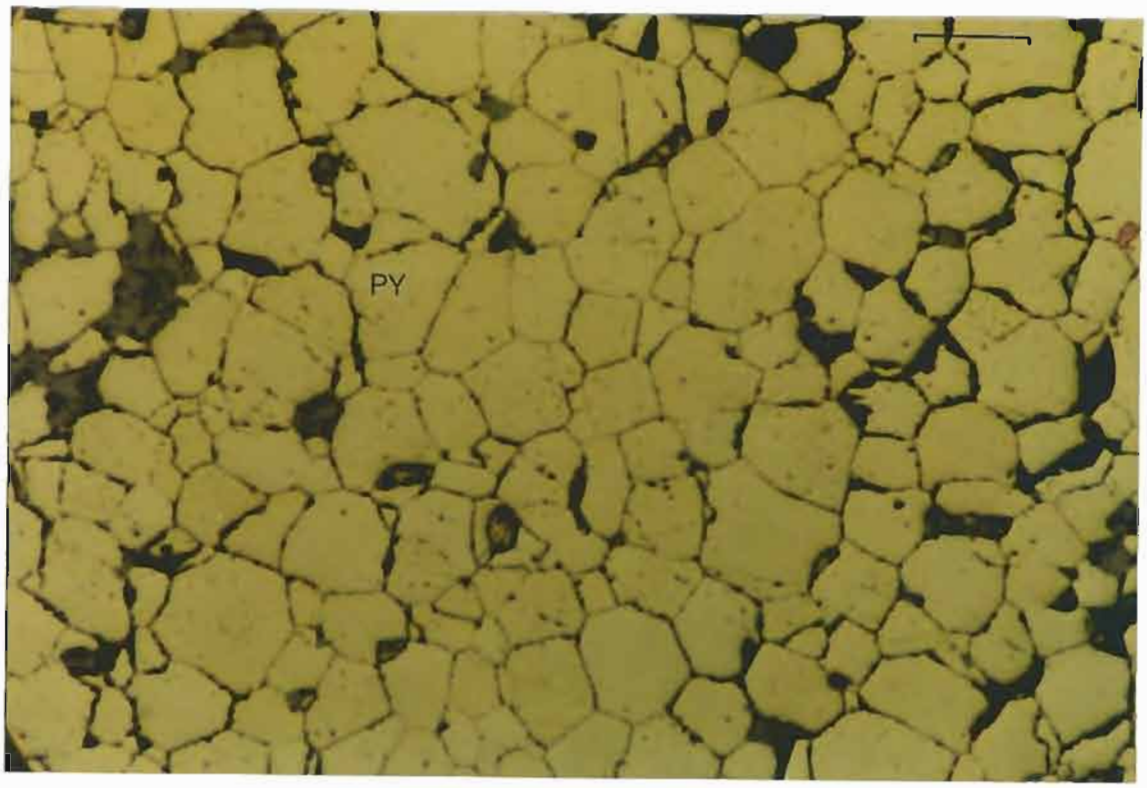

B

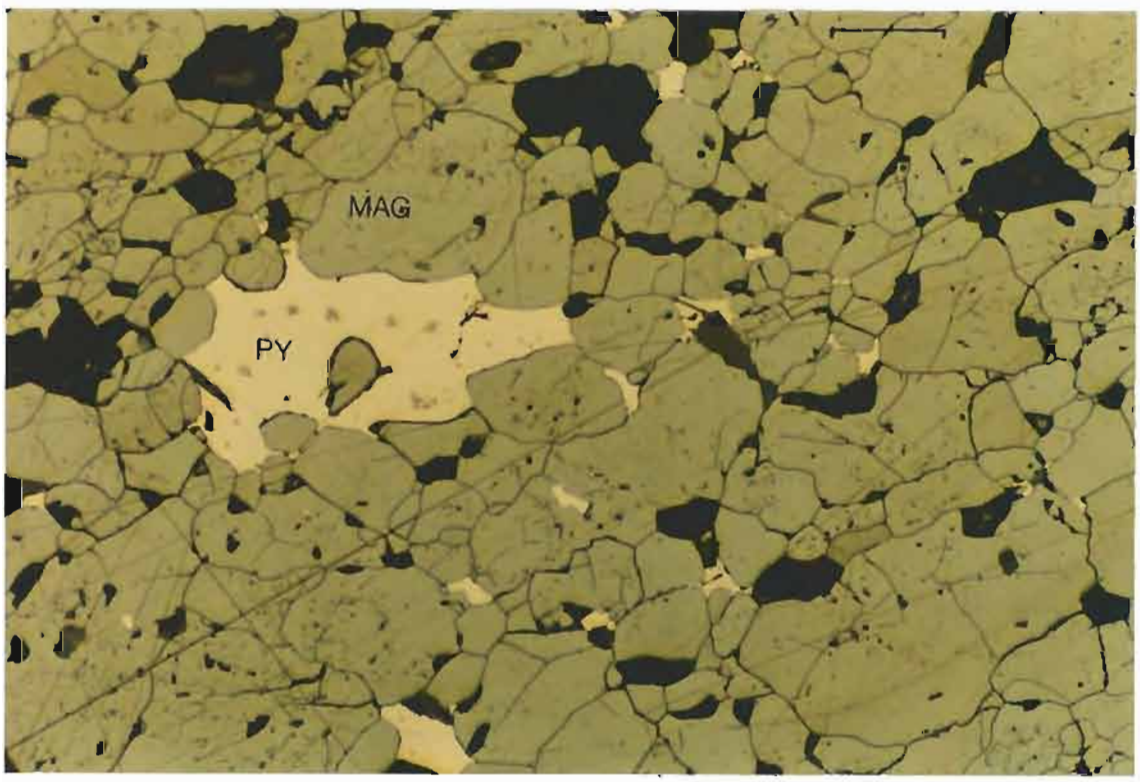

Fig. 5.7 Photomicrographs of moderately well annealed massive pyrite (PY) and massive magnetite (MAG). Note the minor interstitial magnetite and chalcopyrite in A and interstitial pyrrhotite (PO) in B. Both sections have been etched with HI for 1 minute. Black marks observed on each slide result from removal of the polished surface. The bar scale equals 0.2 mm.

and Savage River, similar annealing textures are observed. Both these later deposits have been metamorphosed to lower amphibolite facies.

(4) An association of barite in DDH GCA suggests this deposit to be exhalative in origin. To the author's knowledge, barite has not been reported from any other skarn.

(5) The presence of a weak lineation at a high angle to layering in the banded magnetite-pyrite rocks (e.g. Fig. 5.8) may represent an early cleavage. This lineation is typically defined by fine granular pyrite which forms veinlets or thin bands that cut across the layering.

In summary this lower mineralized horizon (Fig. 5.1) is unlike known skarn deposits but has many features indicating it to be a primary banded iron formation of chemical origin.

The common mineralogies of this lower mineralized horizon are:

(i) banded magnetite-pyrite-(quartz) (e.g. 68259, 68260, 68266, 68268, 68270, 68271)

(ii) massive magnetite and massive pyrite (e.g. 68269, 68261, 68258, 68264)

(iii) banded granular pyrite-rich hornfels (e.g. 68272, 68262, 68265)

(iv) massive barite-magnetite-quartz-garnet (e.g. 68263)

(v) massive and brecciated siderite.

Banded magnetite-pyrite-(quartz)

This mineral assemblage forms the bulk of the lower mineralized horizon and may be further subdivided into quartz-rich and pyrite-rich assemblages. In the former, the average proportions of magnetite, quartz and pyrite are 50%, 40% and <10% respectively. Pyrrhotite in the form of late-stage veinlets and replacements of magnetite may comprise up to 30% of the bulk mineralogy (e.g. 68266). Chalcopyrite has a similar distribution to that of pyrrhotite but rarely forms more than 5% of the bulk mineralogy.

In 68259 and 68260, minor garnet and pyroxene is noted to overprint and cut across magnetite zones in a series of microfractures and veinlets indicating these minerals to be post-magnetite deposition. In thin section, chalcopyrite and pyrrhotite poikilotopically enclose calcsilicate minerals (e.g. Fig. 5.17B) suggesting the deposition of chalcopyrite and pyrrhotite to be associated with late-stage skarn alteration.

A typical banded magnetite-pyrite rock is represented by sample 68268 and by figure 5.8. Magnetite and pyrite are the only minerals in this rock and occur in subequal proportions. Moderately strong annealed granular textures are common and layering appears to be stratiform.

Fig. 5.8 Banded magnetite pyrite rock (68268) from the lower mineralized horizon. Note the lineation in magnetite-rich layers marked by small veinlets of pyrite at a high angle to layering (i.e. bottom right hand corner to top left hand corner).

Fig. 5.9 A pyrite-rich intersection of the lower mineralized horizon in DDH GC3. The footwall is in the lower right hand corner and the hangingwall in the upper left hand corner. Zoning from the footwall upwards is: disrupted quartz veining, massive clastic (brecciated) pyrite, massive fine grained pyrite, banded magnetite pyrite, and finally, banded pyrite hornfels.

Massive magnetite and massive pyrite

Massive pyrite is observed from the lower mineralized horizon from all three drill holes while massive magnetite is confined to the upper intersection of DDH GCB.

A typical pyrite-rich intersection is shown in figure 5.9. The footwall is characterized by vein quartz followed by clastic (brecciated) massive pyrite. This zone grades into fine grained massive pyrite into banded magnetite-pyrite and finally into banded pyritic hornfels in the hangingwall. Such zoning supports a primary exhalative-type origin for this mineralized horizon.

Massive pyrite rocks include 68264 and 68269, both contain >70% pyrite with accessory quartz. Pyrite has a grainsize varying from 0.1 to 2 mm and has a well annealed, granoblastic texture. An unusual form of massive pyrite is represented by sample 68258. This sample has a distinct sponge-like appearance in hand specimen and an equally distinct texture in thin section (Fig. 5.13). Corroded relict magnetite (<20%) indicates this rock to have formed by the near complete replacement of magnetite.

The only massive magnetite rocks associated with this horizon are represented by a 2 m thick unit in the uppermost mineralized intersection of DDH GCB. Minor pyrite, chalcopyrite, tremolite and calcite are associated with this rock (e.g. 68261). The footwall of this unit is characterized by banded magnetite-pyrite.

Banded pyrite-rich hornfels

This style of mineralization is gradational to the massive pyrite rocks and is common in the hangingwall of many of the massive and banded magnetite-pyrite horizons (e.g. Fig. 5.9) and also in the pyritic hornfels that underly the lower mineralized horizon of figure 5.1. In this latter case, pyrite occurs in granular bands 0.5 mm to 0.5 m thick or as disseminations whose distribution and orientation appear to be controlled by a cleavage that subparallels layering. The host rocks to these pyritic intersections, quartz-biotite-chlorite hornfels, are considered to be a likely alteration zone associated with the deposition of the lower mineralized horizon.

Massive barite-magnetite-quartz-garnet

A 12 m thick unit of this assemblage is present in the middle intersection of DDH GCB. A typical hand specimen texture of this rock is shown in figure 5.10. In thin section (Fig. 5.11), andradite garnet forms in the interstices of barite and appears to be post-barite deposition. In comparison, barite and magnetite appear to be in textural equilibrium.

Fig. 5.10 Disrupted magnetite-barite-quartz-garnet (68263) from the middle intersection of the lower mineralized horizon of DDH GCB. The dirty yellow brown mineral is andradite garnet and the white zones are a mixture of barite and quartz.

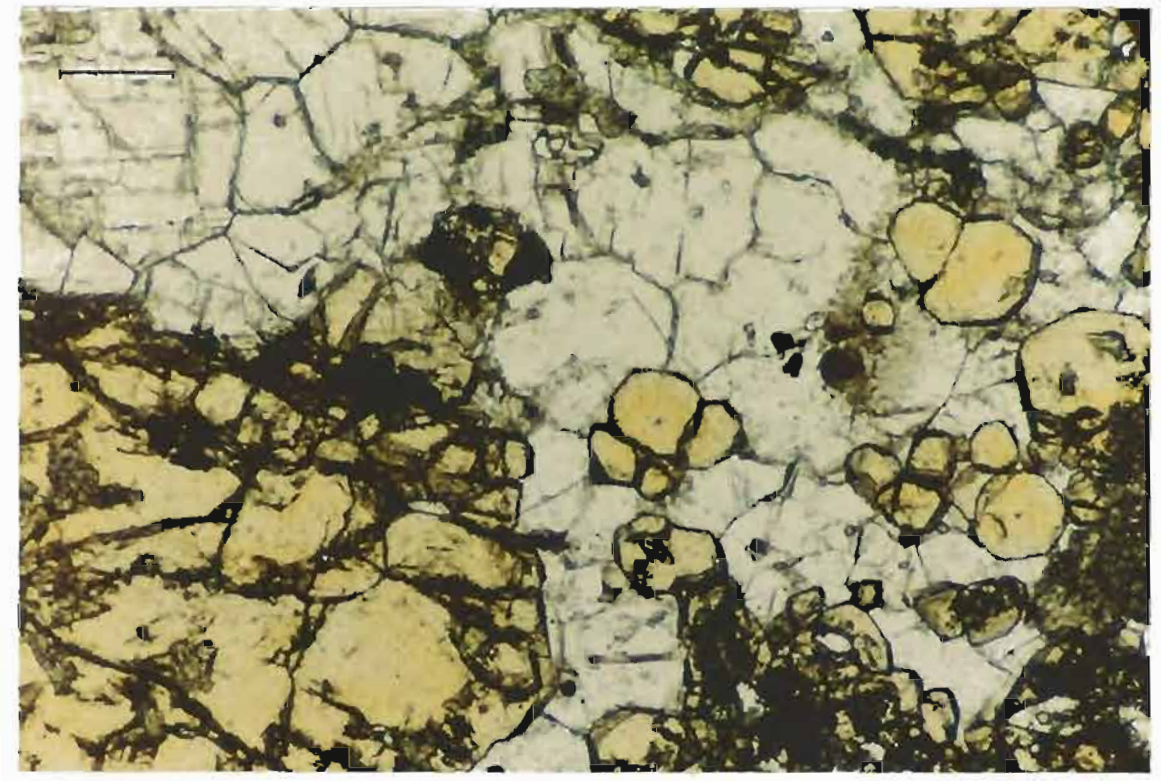

Fig. 5.11 Photomicrograph of barite (white), andradite garnet (yellow) rock (68263). Scale bar equals 0.2 mm.

Fig. 5.12 Brecciated and massive siderite-pyrite rock from the upper intersection of the lower mineralized horizon in DDH GCA. Note the distinct massive siderite-pyrite intersection. The pyrite in these samples formed by the replacement of magnetite.

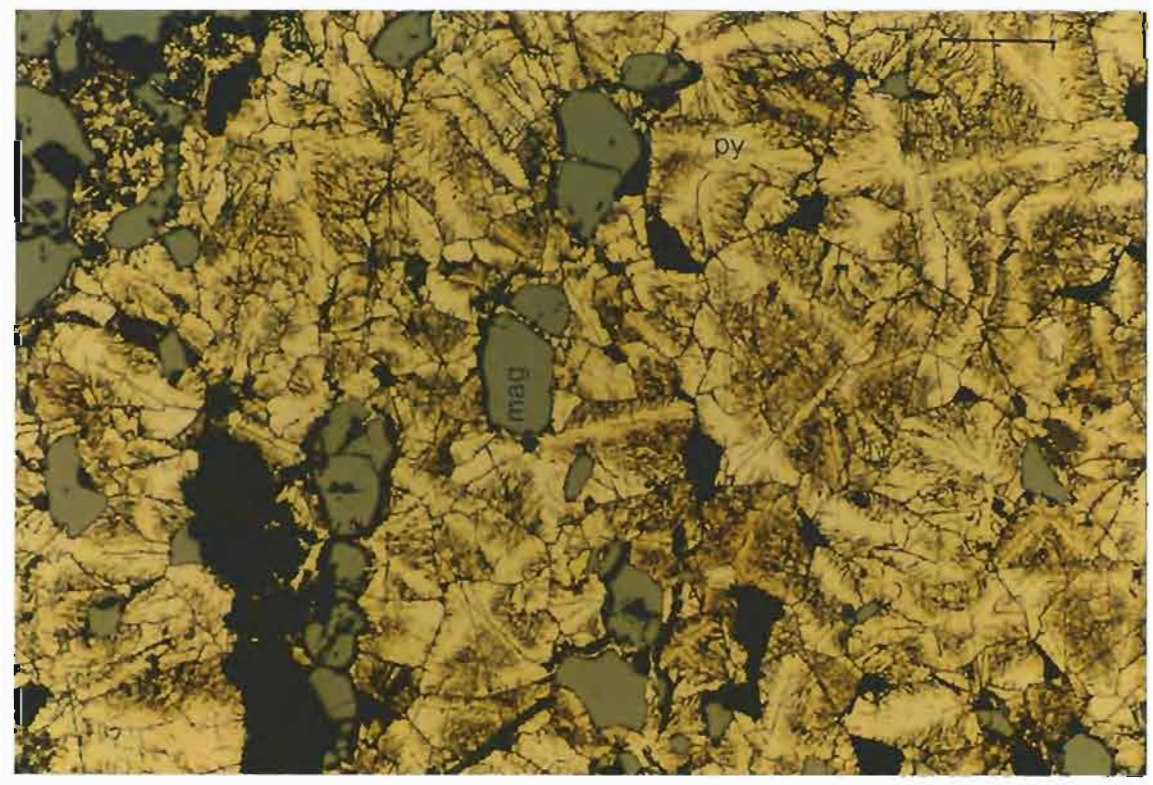

Fig. 5.13 Unusually textured (moon-landscape) pyrite (py) replacing magnetite (mag) from the middle intersection of the lower mineralized horizon. Bar scale equals 0.2 mm.

Massive and brecciated siderite

Massive and brecciated siderite overlies the spongy pyrite of specimen 68258 and forms the hangingwall of this intersection. Minor siderite veins are noted to cut through the spongy pyrite unit suggesting siderite deposition to be post-pyrite replacement of magnetite. The cause of brecciation is unknown. Photographs of the massive and brecciated siderite are shown in figure 5.12.

5.3 MINERALOGY AND ORE PETROLOGY

The mineralogy and petrology of the major minerals associated with mineralization are summarized below. Calcsilicate skarn minerals are discussed first, followed by sulphide and Fe-oxides. It must be noted that this is not a comprehensive account of all the mineralogies and that only the common minerals are discussed. Representative microprobe analyses of most of these minerals are given in appendix A.5.

Clinopyroxene

Clinopyroxene is the most common mineral in the Gourlays Creek skarns. Formation of clinopyroxene and closely associated garnet is attributed to prograde skarn alteration.

In thin section clinopyroxene forms distinct pale yellow-green subidioblastic grains and has a decussate texture (Fig. 5.14B). Clinopyroxene also forms euhedral tabular grains (<0.5 mm in length), growing into calcite, pyrrhotite and quartz-filled vughs and veins. Such crystal forms indicate open space growth of clinopyroxene and pre-calcite, pyrrhotite and quartz deposition. Multi- generations of pyroxene growth are indicated by subtle variations in colour and in grain size. In figure 5.14A, fine grained clinopyroxene corrodes and replaces coarse grained clinopyroxene.

Electron microprobe analysis of clinopyroxenes show that in addition to the major components (Ca, Fe, Al and Si), Mn is the only other major element present in detectable concentrations. A triangular plot of the compositions (Fig. 5.15D) shows the clinopyroxenes to be essentially a solid solution between hedenbergite (Hd) and diopside (Di) with a johannsenite (Jo) component of less than 5%. The compositions vary from Di (66%), Hd (30%), Jo (4%) to Di (18%), Hd (78%), Jo (4%). This range in compositions is intermediate between those recorded for Fe and Cu skarns as shown in figure 5.15A. In comparision to other Tasmanian Sn-(W) bearing skarns (Fig 5.15C), a similar range in compositions is observed

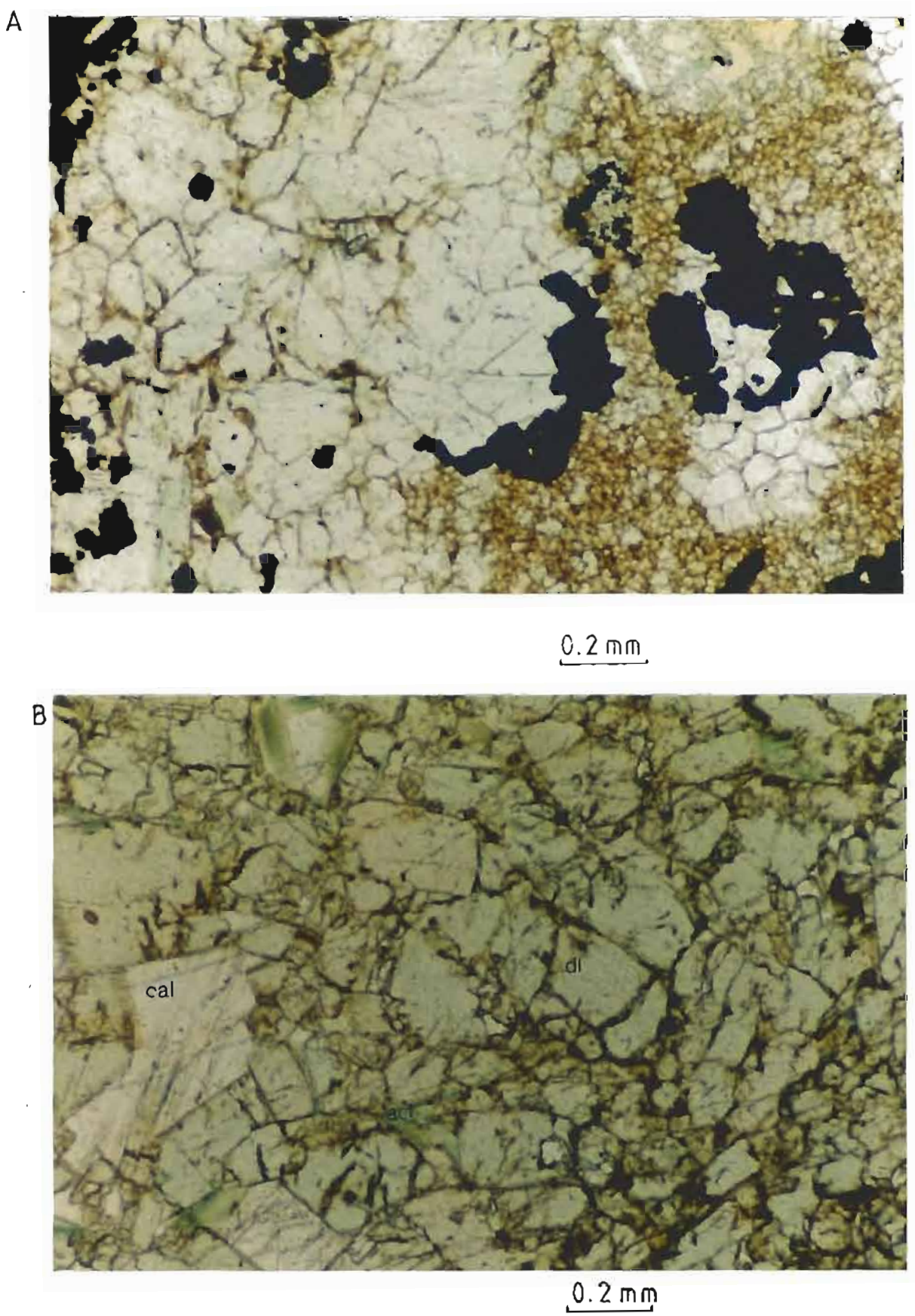

Fig. 5.14 Transmitted plane light photomicrographs of massive clinopyroxene skarn. (A) multi-generations of pyroxene defined by the bimodal grain size. The fine grained clinopyroxene appears to corrode and replace the course grained clinopyroxene. Opaques, pyrrhotite and chalcopyrite, are late-stage replacement; (B) medium coarse grained, decussate clinopyroxene (di) exhibiting retrograde replacement by actinolite (act) and calcite (cal).

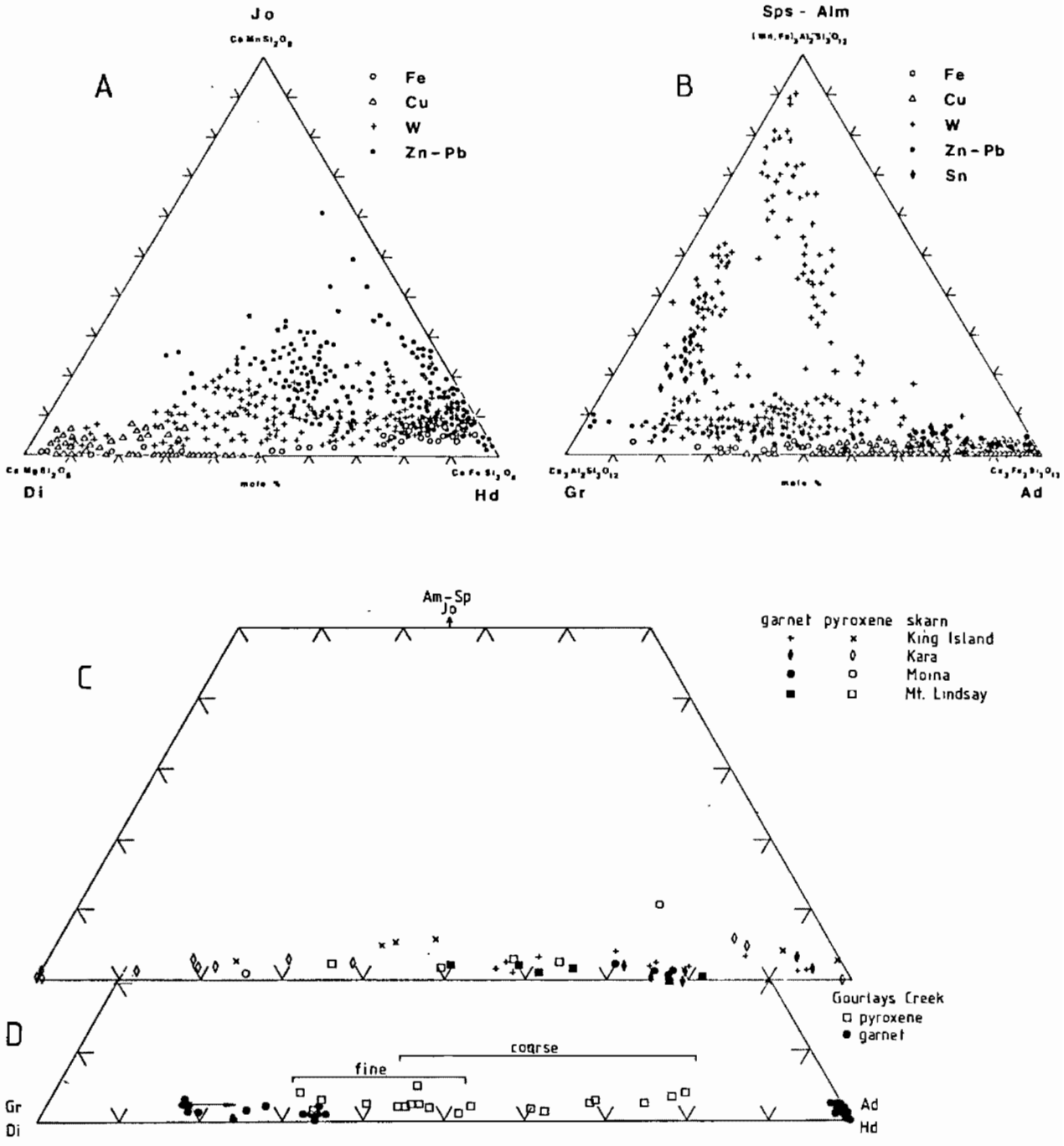

Fig. 5.15 Plots of pyroxene and garnet compositions as defined by microprobe analysis. (A and B) compositions of pyroxenes and garnets respectively from calcic skarns classified in terms of their major ore metals (from Einaudi and Burt, 1982); (C) compositions of clinopyroxenes and garnets from King Island and Kara W- skarns; Moina and Mt. Lindsay Sn-wrigglite skarns. Data from representative microprobe analysis of Kwak and Tan (1981), Barrett (unpubl.), Kwak and Askin (1981), Kwak (1983), Eadington and Kinealy (1983). (D) composition of pyroxenes, and garnets, from the Gourlays Creek skarn. Fine and coarse refer to the range in composition of fine and coarse grained clinopyroxenes, the arrow defines the direction of change in composition of grandite garnets during growth. Abbreviations are: Di = diopside ($CaMgSi_2O_6$), Hd = hedenbergite ($CaFeSi_2O_6$) and Jo = johannsenite [$Ca(MnFe)Si_2O_6$] for the pyroxenes and Gr = grossular ($Ca_3Al_2Si_3O_{12}$), Ad = andradite ($Ca_3Fe_2Si_3O_{12}$) and Sp-Alm = spessartine-almandine [$(MnFe_3)Al_2Si_3O_{12}$] for the garnets.

Retrograde alteration of diopside involves alteration to actinolite and epidote and replacement by minor sulphides and oxides. Minor retrograde alteration is shown in figs 5.14A and B.

Garnet

Garnets of two distinct forms are associated with clinopyroxene in many of the skarns with nearly pure andradite and grossular-rich compositions being indicated by microprobe analysis (Fig. 5.15D). Both garnet types contain less than 4% almandine-spessartine components.

Andradite garnets (Fig's 5.16A, 5.11) are pale greenish yellow to moderate yellow in colour and isotropic to very weakly anisotropic. In the pyroxene skarns, andradites are generally xenoblastic and are often corroded and replaced by pyroxene.

Grossular-rich grandite garnets are in comparison subhedral to euhedral with hexagonal outlines and are weakly anisotropic with low birefringence. Distinct zoning is noted under polarized light (Fig. 5.16B). Microprobe analysis of these garnets (Fig. 5.15D) indicates a range in composition of Gr (81%), Ad (15%), Am-Sp (4%) to Gr (64%), Ad (35%), Am-Sp (1%) with the andradite-rich grandite compositions being typical of the outer margins of individual grains. Such zoning suggests the system to be progressively depleted in Al and enriched in Fe during grandite garnet formation.

From the garnet compositions defined by Einaudi and Burt (1982) (Fig. 5.15B), pure andradite garnets are common to Cu-bearing skarns while grossular-rich grandite garnets are typical of Cu- and Fe-bearing skarns. In comparison, garnets from Sn-bearing skarns tend to have significant spesartine and almandine components. This is in contrast to other Tasmanian Sn-(W) skarns (Fig 5.15C) where garnet compositions are similar to those observed at Gourlays Creek (ie. andadite- grossular solid solutions with no significant spesartine- almandine component). This, in addition to the pyroxene analyses, suggests that for the Tasmanian skarns, garnet- pyroxene compositions alone may not be used to define the different skarn types of Einaudi and Burt (1982).

Tremolite-actinolite

Tremolite is a common mineral associated with the contact hornfels adjacent to the skarn horizons (e.g. 68248) and also in outcropping calcsilicate rocks. Weakly green pleochroic actinolite is also a common replacement of clinopyroxene.

Epidote

Epidote forms both as a replacement of clinopyroxene- garnet skarn and as a contact metamorphic mineral in the host rocks. The typical form of epidote in the skarns is subhedral stumpy grains with weak yellow-green

A

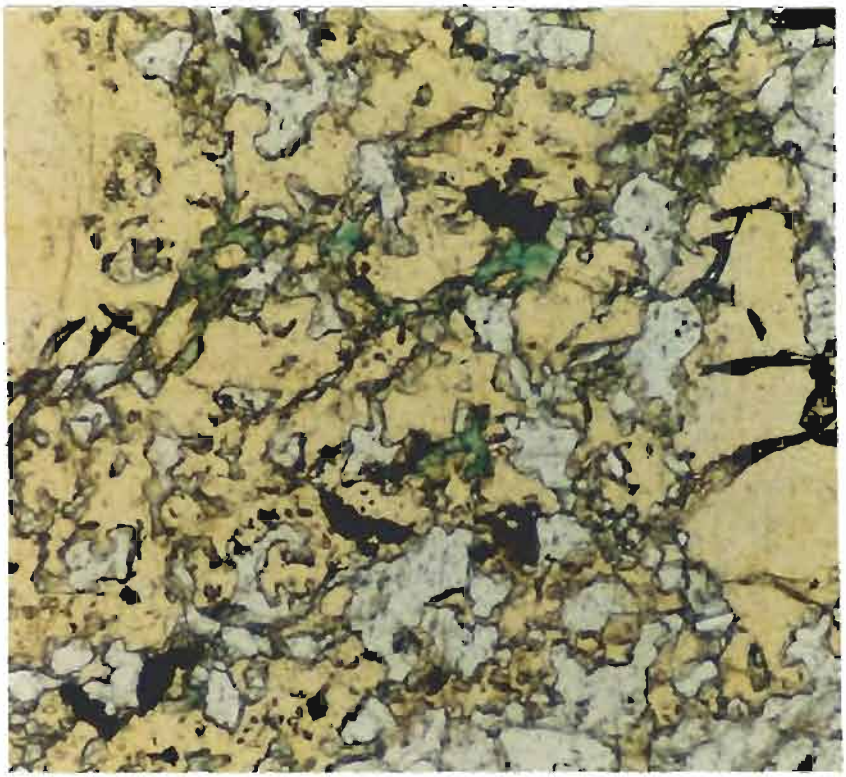

0.2 mm

B

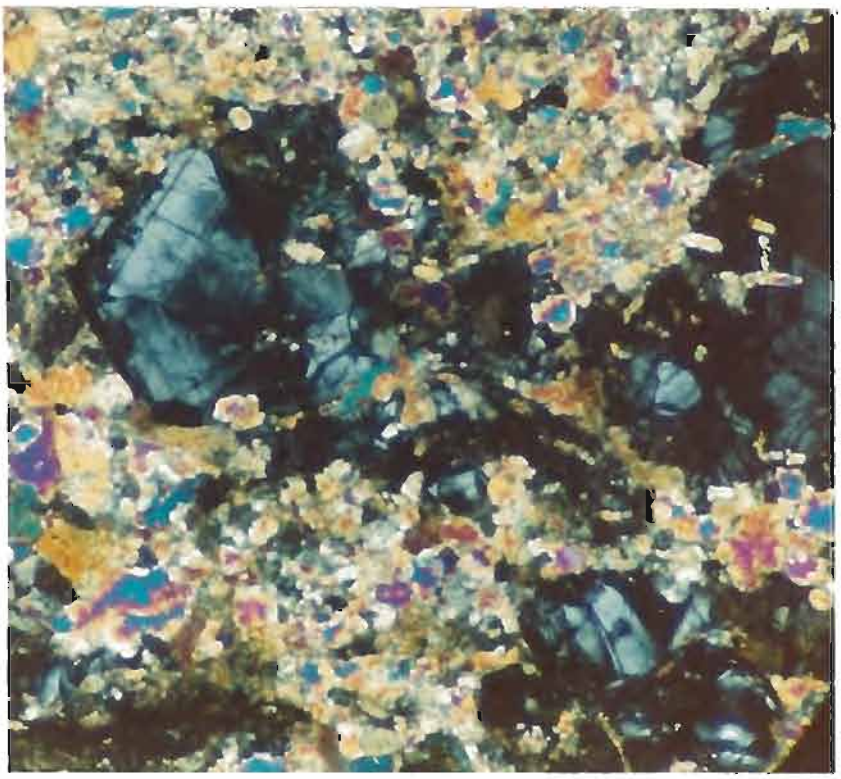

0.2 mm

Fig. 5.16 Transmitted light photomicrographs of garnet-clinopyroxene skarn. (A) Xenoblastic yellow andraditic garnet showing strong replacement by diopside (white), actinolite (green) and minor opaques (N.B. plane light photomicrograph); (B) subhedral, hexagonal, weakly anisotropic grandite garnet (grey-black) showing partial replacement by clinopyroxene (N.B. crossed nicols photomicrograph).

pleochroism. Microprobe analysis (appendix A.5) shows epidote to be Fe-rich as opposed to Al-rich clinozoisite.

Hornblende

Hornblende in association with calcite, axinite and quartz forms a minor skarn type (e.g. 68257). In these skarns, hornblende forms medium-coarse (0.5-1 mm) subhedral bladed grains and felted or decussate textures. Calcite, axinite and quartz all form interstitially to hornblende.

Calcite-quartz-axinite

These three minerals form late-stage replacements and vugh fill in the skarn horizons. The mean ratio of CaO:FeO:MnO in axinite as defined by microprobe analysis (appendix A.5) is 0.66:0.22:0.11. The deposition of these three minerals represents the last stages of retrograde skarn alteration.

Magnetite

Magnetite is associated with both the upper and lower mineralized horizons. In the skarns, magnetite forms a minor component typically replacing clinopyroxene or garnet. It is likely that most of the magnetite associated with quartz in the footwall of the skarn horizon is primary in origin (refer to section 5.1).

In the lower mineralized horizon, magnetite exhibits variable grain size distribution (0.05-1 mm) and moderate degrees of annealing. Granoblastic textures are well developed in the massive magnetite rocks (Fig. 5.7B). Minor magnetite has a lath-like form similar to that of secular hematite suggesting some of the magnetite to be pseudomorphing hematite. Hematite-to-magnetite transformations are common to thermal metamorphism (Ramdohr, 1969).

Pyrite

Pyrite has a similar spatial distribution to that of magnetite being common to the lower mineralized horizon. Moderately well annealed granoblastic textures and sulphur isotope evidence (chapter 7), strongly suggest most of the pyrite to be primary in origin. An unusual form of pyrite in 68258 (Fig. 5.13) is shown to be the result of replacement of magnetite.

Barite

Barite forms subhedral equant grains and is generally associated with magnetite and quartz. Based on textural relationships and sulphur isotope data (chapter 7), a primary syngenetic origin is suggested. The strong banding common to the magnetite- pyrite- quartz assemblages is not retained in the barite rich rocks due to the contrasting competancies between barite and magnetite.

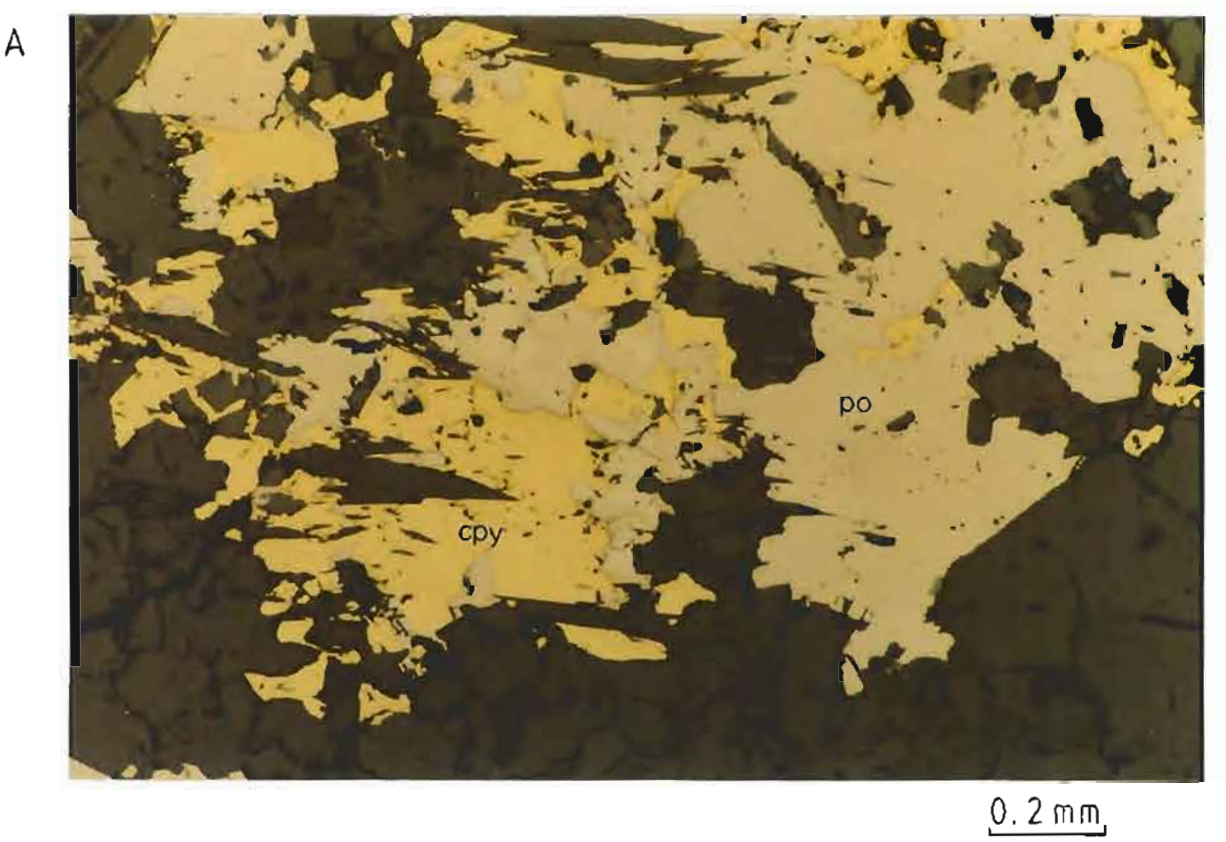

Fig. 5.17 Reflected light photomicrographs showing typical distributions of pyrrhotite and chalcopyrite. (A) pyrrhotite (po) and chalcopyrite (cpy) occurring as vug fill within clinopyroxene (deep grey) skarn; (B) pyrrhotite and chalcopyrite rimming corroded pyrite (py) and replacing magnetite (mag) in the lower magnetite-pyrite-quartz-barite horizon. Acicular inclusions of actinolite (blue-green), and of diopside in other sections, suggest that pyrrhotite and chalcopyrite deposition in this lower horizon is a skarn overprint associated with similar mineralization in the upper skarn horizon (i.e. as in fig. 5.17A).

Pyrrhotite and chalcopyrite

Pyrrhotite and chalcopyrite form as veinlets, disseminations or vugh fill in the skarn horizon (Fig. 5.17A). In the massive and banded magnetite- pyrite- quartz- barite horizon, pyrrhotite and chalcopyrite rim pyrite and replace magnetite. Poikilotopic inclusions of actinolite (Fig. 5.17B) and of minor diopside suggest these two minerals to be deposited later than actinolite-diopside deposition. The distribution of pyrrhotite and chalcopyrite in the skarn horizon suggests deposition to be associated with late-stage, retrograde skarn formation.

CHAPTER 6
FLUID INCLUSIONS

A fluid inclusion study has been undertaken to determine the temperature and composition of skarn-associated hydrothermal fluids. Over 150 inclusions were analyzed on a Chaixmeca heating/freezing stage. Details of experimental technique, calibration of the heating/freezing stage and accuracies of the stage are given in appendix A.3.

Heating measurements are reported directly as homogenization temperature T_H and freezing measurements are reported in weight % equivalent NaCl. Conversion of freezing temperature T_M to salinity is by the use of salt depression freezing equations for the system H_2O-NaCl (Appendix A3; Potter **et al.**, 1978). Based on fluid inclusion studies, pressures of homogenization P_H and trapping P_T are estimated.

The theory and assumptions involved in fluid inclusion studies and the criteria for differentiating primary, secondary and pseudosecondary inclusions have been discussed at length by Roedder (1979, 1984). In this study, inclusions of all three origins are studied.

6.1 NATURE OF THE INCLUSIONS

The only minerals from the Gourlays Creek Prospect suitable for fluid inclusion studies are garnet and quartz. The dominant form of inclusions in all samples are two-phase aqueous inclusions of low to moderate salinity. Inclusions saturated in NaCl or KCl have not been observed. Rare gas-rich inclusions with vapour bubbles occupying up to 70% of the inclusion volume which homogenize to the vapour phase have been observed in both vein quartz and garnets. These inclusions are indicative of localized boiling, or necking down and leakage of fluids from the inclusion. Microscopic work could not confirm or deny this latter possibility. No evidence of CO_2 in the form of clathrate or solid CO_2 was observed in any of the inclusions during freezing experiments.

The cavity shapes of the fluid inclusions are extremely variable. Primary inclusions tend to be faceted subhedral or have negative crystal shapes. In quartz, primary inclusions are equant to slightly elongate and have vapour bubbles occupying 30-40% of the total volume. In garnet, primary inclusions either have negative crystal shapes or occur as moderately elongate, faceted inclusions with curviplanar boundaries and rounded terminations. Vapour bubbles occupy up to 50% of the total inclusion volume.

By comparison, secondary inclusions tend to be very small (less than 10 microns), faceted ovoid and have vapour bubble volumes of 10-30%. Most secondary inclusions form along planar fractures and are common to drusy vein quartz. A broad distribution of homogenization temperatures is observed for secondary inclusions (Fig. 6.1).

6.2 GARNET-HOSTED INCLUSIONS

Fluid inclusions in andradite garnets from the pyroxene-garnet skarn horizon (e.g. 68251, 68249, 68256, 68248) are sporadic and of poor quality due to strong alteration of the garnets. Garnets however form during prograde skarn alteration and are therefore likely to record the peak of thermal alteration. Most primary inclusions in garnet do not show signs of homogenizing at 500°C, the limit of the Chaixmeca heating stage. Homogenization temperatures are thus above 500°C (Fig. 6.1). Secondary inclusions in garnet exhibit a broad range of homogenization temperatures from 420-310°C with the modal population at 350-360°C.

6.3 QUARTZ-HOSTED INCLUSIONS

Two types of quartz have been studied for fluid inclusions:

(i) vein quartz associated with pyrite-arsenopyrite and chalcopyrite (e.g. 68267), and

(ii) late stage retrograde skarn, vuggy quartz (e.g. 68248).

The quartz vein of 68267 was sampled stratigraphically below the skarn horizon (Fig. 5.1), and is considered a likely feeder to this mineralized horizon. The quartz occurs as medium to coarse grained druses of prismatic crystals on the vein walls. Individual crystals measure 1-3 mm in length and often poikilitically enclose acicular actinolite grains. Sulphides generally form isolated pods in the quartzose vein mass and are post drusy quartz growth.

Quartz of this form is highly fractured and inclusions dominantly secondary in origin. Randomly orientated microfractures which control the distribution of the secondary inclusions are generally confined to individual grains and do not continue into adjacent grains. Under high magnification, fine opaque (sulphide) solid inclusions are observed along these fractures. On this basis the secondary inclusions in type (i) vein quartz are considered to be cogenetic with pyrite-arsenopyrite-chalcopyrite mineralization in the vein. They are also likely to be representative of retrograde pyrite-chalcopyrite mineralization in the skarn.

Homogenization temperature distribution of secondary inclusions in vein quartz has a similar range to that of secondary inclusions in

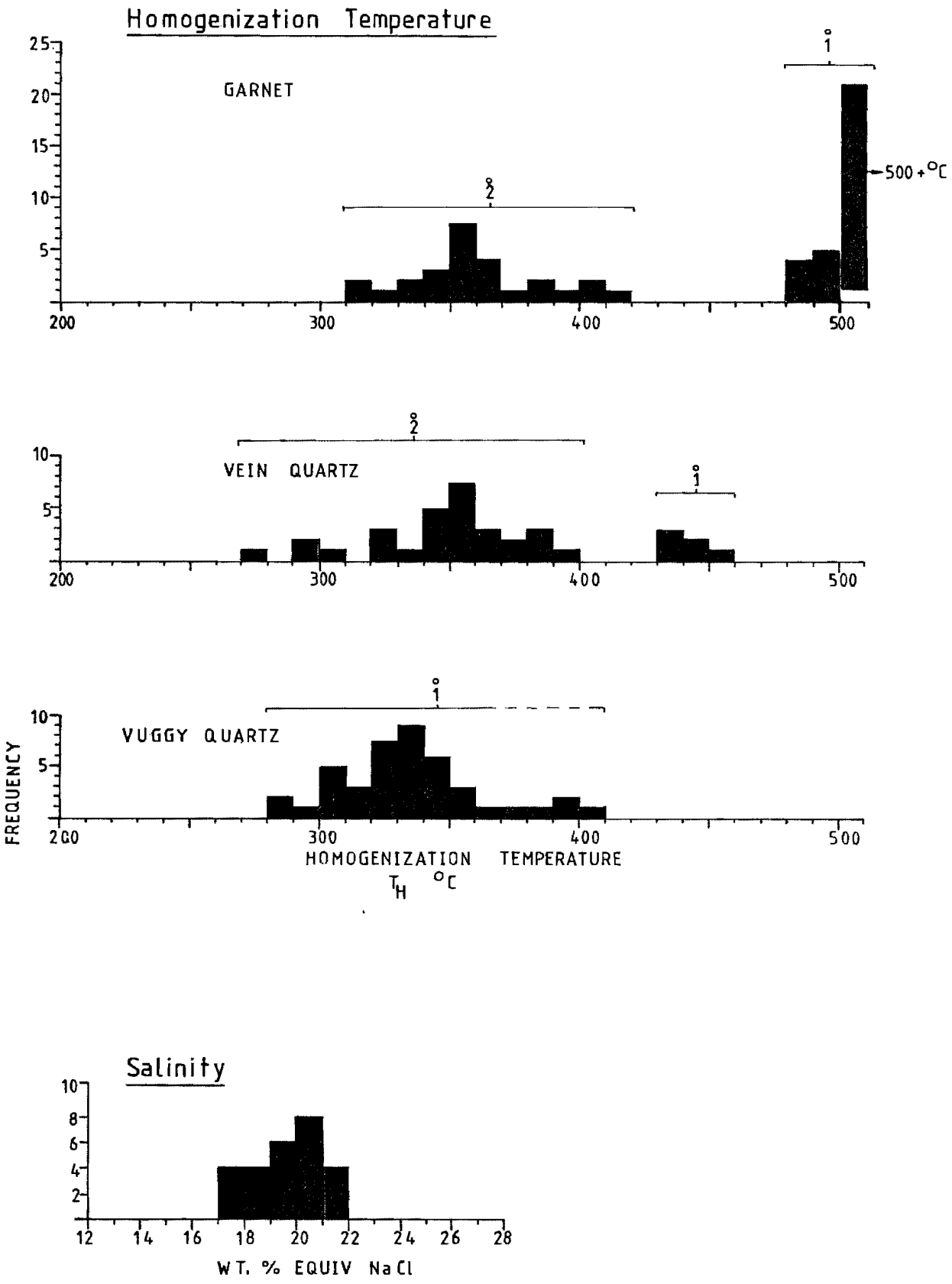

Fig 6.1 Homogenization temperatures for garnet and quartz from the Gourlays Creek Prospect. $^{0}_{1}$ and $^{0}_{2}$ refer to primary and secondary inclusions respectively, note that primary inclusions in garnet mostly have homogenization temperatures above 500 °C. Salinity data in bottom figure is from secondary inclusions in vein quartz.

garnet. Values range between 400-320°C and have a modal population of 350-360°C. This wide range of values may reflect a broad range in filling temperatures or be due to changes in the inclusion (e.g. leakage, necking down) after trapping. However, no obvious evidence of the latter has been observed. The similar range of values for secondary inclusions in both garnet and vein quartz suggests that their formation is related.

Only inclusions considered to be of primary origin were measured from type (ii) vuggy quartz. The distribution of homogenization temperatures (Fig. 6.1) ranges from 410-280°C with the modal population at 330-340°C. Poikilitic inclusions of sulphides and pyrrhotite-chalcopyrite intergrowths suggest vugh quartz to be deposited late to post-sulphide mineralization in the garnet-pyroxene skarns. These inclusions are thus representative of the final stages of skarn alteration.

6.4 FLUID COMPOSITION

Complete absence of daughter crystal phases in all the fluid inclusions indicates the aqueous inclusion fluid to be undersaturated in NaCl (i.e. <26.0 wt% equiv. NaCl, Roedder, 1984). The lack of evidence for CO_2 even after careful observation at low temperatures indicates the skarn-associated fluids to have had low mole fractions of CO_2.

A quantitative estimate of the overall composition of the aqueous solution may be deduced from phase changes induced in fluid inclusions at low temperatures (Roedder, 1984). Of the samples investigated, only the secondary inclusions in 68267 proved to be of sufficient quality and quantity to allow freezing point depression determinations. These inclusions are among the most important for such work since they are considered to be associated with sulphide deposition.

Freezing point depressions of -14.0 to -20.0°C were recorded for the secondary inclusions in vein quartz giving salinities of 17-22 wt% equiv. NaCl (appendix A3, Potter **et al.**, 1978). The mean salinity is given at 20-21 wt% equiv. NaCl (Fig. 6.1).

6.5 GEOBAROMETRY

Geological Considerations

An estimate of pressure may be obtained by calculating the maximum thickness of overburden above the fluid inclusion-bearing phases at the time of deposition.

Since intrusion of the late Devonian granitoids followed folding in the Tabberabberan Orogeny (Solomon, 1981), an estimate of the overburden

thickness is easily calculated from the current configuration of overlying lithologies along the coastal section, e.g.

Duck Creek Sequence	420 m
Mount Zeehan Conglomerate |	
Gordon Limestone |	950 m
Eldon Group |	
	1370 m

The mineralized horizons are suggested to correlate in stratigraphic position with the upper part of the Oonah Formation as observed on the coastal section (eg Fig 2.1 and 2.2). Hence overburden due to this lithology is considered minor. The amount of overburden removed by erosion following uplift during the Tabberabberan Orogeny but preceding skarn formation also cannot be taken into account. Fortunately both these uncertainties have opposite effects on the overburden thickness thus reducing their combined effect.

From an estimated overburden thickness of 1370 m, a lithostatic load of 35.0 MPa (ρ_{crust} = 2.7 g cm^{-3}) and a hydrostatic load of 12.9 MPa (ρ_{H_2O} = 1.0 g cm^{-3}) is calculated. The upper limit of trapping pressure for inclusions, may be derived from the level of emplacement of the late Devonian granitoids which according to Solomon (1981), appear to have been emplaced at relatively shallow depths at confining pressures below 200 MPa.

Fluid Inclusion Data

The confining pressure at the time of inclusion formation may be estimated from the nature and composition of the fluid inclusions (eg Roedder, 1984).

Assuming the fluid inclusions to be derived from a homogeneous fluid and boiling to be negligible to absent, then the inclusions must form at a pressure and temperature above the solvus of the hydrothermal fluid. For the secondary inclusions in 68267 with salinities in the order of 20 wt% equiv. NaCl and homogenization temperatures of 360°C, the position of the solvus corresponds to a pressure of 18 MPa or a hydrostatic column of 1350 m (appendix A.3, extrapolated from Haas 1971). Extrapolation of similar data summarized in appendix A.3, (Roedder and Bodnar ,1980), of a 25 wt% NaCl solution with homogenization temperatures of 360°C gives the position of the solvus at 15.6 MPa.

The above values represent pressures of homogenization (i.e. P_H). If the previously defined vapour-rich inclusions are due to boiling and not changes to the inclusion since trapping, then the inclusions must form on or near the solvus and the homogenization pressure P_H will equal the

pressure at trapping P_T. In summary, geobarometry studies give an estimated pressure of trapping between 15.6 and 35.0 MPa. Minor evidence of boiling suggests trapping pressures to be towards the lower end of this range.

Pressure-Salinity Corrections

For inclusions derived from homogenous fluids in the absence of boiling, a pressure-salinity correction is esential to estimate the temperature of trapping T_T from the temperature of homogenization T_H. For confining pressures of 35.0 MPa, homogenization temperatures of 360^{o}C and salinities of 20 wt% equiv. NaCl, pressure corrections of +22^{o}C are required (appendix A.3, Potter, 1977)

If the inclusion fluids in 68267 formed near the solvus, no pressure correction is required and trapping temperature T_T equals the homogenization temperature T_H.

6.6 CORRELATIONS WITH OTHER SKARNS AND MASSIVE SULPHIDE-CASSITERITE DEPOSITS.

Most skarn deposits are high temperature (400-650^{o}C) intermediate salinity (10-45 wt% equiv. NaCl) with relatively low CO_2 contents (X_{CO_2} less than 0.1). Boiling is generally observed only in the upper parts of skarn systems (Einaudi et al., 1981).

One of the best studied skarns in terms of fluid inclusions is the King Island scheelite skarn. From garnets, Tan and Kwak (1979) report homogenization temperatures of 300-800^{o}C and salinities of 24-55 wt% equiv. NaCl while scheelite records homogenization temperatures of 100-400^{o}C and high salinities. Interstitial calcite and quartz have homogenization temperatures as low as 180^{0}C and salinities of less than 3 wt% equiv. NaCl (Kwak and Tan, 1981). The skarn at Gourlays Creek records a similar history with early high-temperature garnets and late low-temperature quartz deposition.

In the calcic Sn-W-F wrigglite skarn at Moina, vein quartz considered to be cogenetic with skarn formation records an average homogenization temperature of 331^{o}C (Kwak and Askins, 1981). Gas-rich and saline-rich (30-40 wt% equiv. NaCl) fluid inclusions that occur together suggest the fluid inclusions were trapped from a boiling solution. Liquid CO_2 has been recorded as a common constituent.

Fluid inclusions from massive sulphide-cassiterite deposits (e.g. Renison, Cleveland and Mount Bischoff) indicate moderate pressures (75-200 MPa) and homogenization temperatures (100-600^{o}C), with salinities in the order of 10 wt% equiv. NaCl for the early stages of mineralization and up to 30 wt% equiv. in the late stages (Groves and Solomon, 1969; Patterson **et al.**, 1981; Collins, 1983). CO_2-bearing inclusions have been recorded from the Cleveland deposit. Of significance is the relatively low pressures recorded by inclusions at Gourlays Creek (e.g. 68267) as compared to those for the massive sulphide-cassiterite bodies. These low pressures are unusual in that the massive sulphide-cassiterite deposits are considered to be a distal analogue of the skarn-forming geothermal system.

CHAPTER 7

SULPHUR ISOTOPE STUDIES

A sulphur isotope study was undertaken to determine the isotopic composition of the mineralizing fluid and to ascertain the chemistry of ore deposition. Details of sample preparation and analytical techniques are given in appendix A.4 while the $\delta^{34}S$ values of analyzed sulphide and sulphate minerals are listed in table 7.1 and summarized in figure 7.1. All results are reported in per mil deviation from the standard Canõn Diablo Triolite (C.D.T.).

To aid in analysis of sulphur isotope values, the analyzed samples have been divided into three groups based on textural features both in hand specimen and thin section. **Group I** sulphides are a group of primary sulphides hosted in black quartz-albite-muscovite schist in the top 120 m of DDH GC3. **Group II** sulphides are associated with retrograde skarn alteration. Temperatures for groupII sulphide deposition, (as indicated by fluid inclusion studies of vein pyrite-arsenopyrite-chalcopyrite in 68256), are in the order of 360°C. The **group III** sulphides are associated with the lower banded magnetite-pyrite-quartz horizon or occur in the pyritic hornfels below this horizon. A primary origin is suggested by mineralogical, textural and paragenetic studies. Pyrite and barite are the only sulphur-bearing phases in group III compared to pyrite, pyrrhotite and chalcopyrite in groups I and II.

Group I

The $\delta^{34}S$ values of group I sulphides range from -1.9 to +7.4 ‰ (eg. Fig. 7.1, table 7.1). The minimum $\delta^{34}S$ value (-1.9 ‰) which correlates with the value of maximum population, and the skewed distribution towards positive values, is typical of low temperature ($T < 50°C$), bacterial reduction of seawater sulphate in a system closed to sulphate, i.e. shallow marine and brackish environments (**sensu** Ohmoto and Rye, 1979). According to Ohmoto and Rye (1979), the contemporaneous seawater may be assumed to have a $\delta^{34}S$ value of 25 ‰ higher than the $\delta^{34}S$ minimum value of bacterial reduced sulphides, giving a $\delta^{34}S$ of Precambrian seawater for Gourlays Creek at +23 ‰. This value is within the limits of late Precambrian $\delta^{34}S$ seawater values reported by Holser and Kaplan (1966).

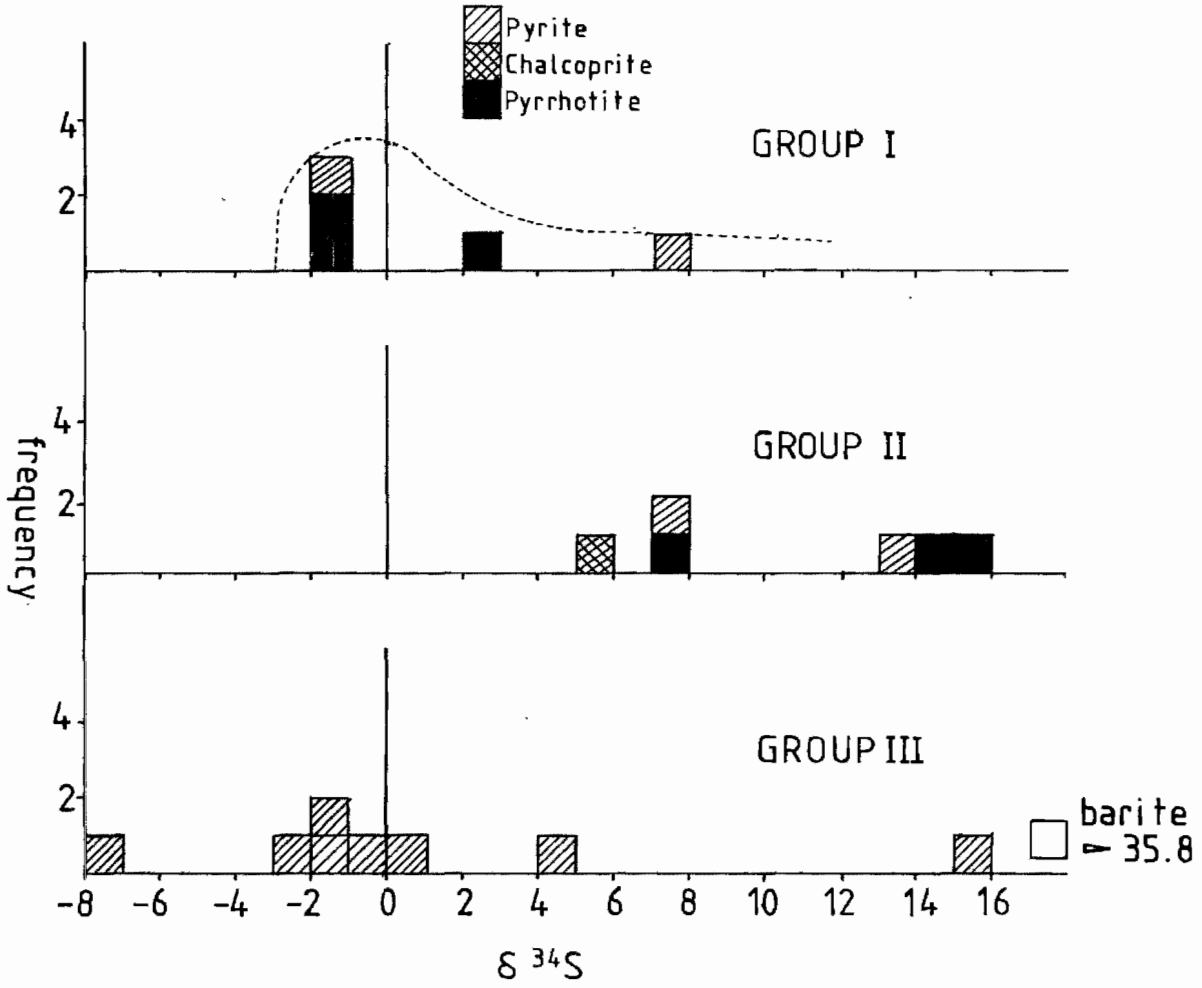

Fig 7.1 Distribution of $\delta^{34}S$ values of sulphur bearing minerals from Gourlays Creek. Groupings as refered to in text; group I= disseminated sedimentary sulphides, group II= skarn associated sulphides, and group III= banded magnetite- pyrite and massive pyrite associated pyrite and barite. The area inscribed by the dashed line in group I represents the distribution of bacterial reduced, shallow to brackish water sedimentary sulphides of Ohmoto and Rye (1979).

UTG'D No.	S phase	$\delta^{34}S$	DDH/depth metres	Description
Group I				
68223	po	-1.8	GC3/86.1m	primary pyrrotite as prismatic crystals
"	po	-2.0	GC3/91.7	with distinct quartz pressure shadows in
"	py	-1.2		quartz albite muscovite schist, primary
"	po	+2.6	GC3/103.8	pyrite as anhedral qrains or tabular
"	py	+7.4		flakes along the cleavage plane.
Group II				
68272	cpy	+5.3	GC3/394.1	replacing pyrite in quartz- pyrite hornfels
68267	py	+7.2	GC3/254.2	open space fill in quartz- pyrite arsenopyrite vein.
68256	po	+7.6	GC3/190.4	vug fill in diopside- garnet skarn.
68259	py	+13.5	GCA/162.4	fracture fill and fine grained bands in quartz- magnetite- pyrite rock.
68271	po	+14.4	GC3/301.7	replacing magnetite.
68266	po	+15.2	GC3/193.6	fracture fill in massive magnetite- pyrite- pyrrhotite rock.
Group III				
(i)				
68268	py	+4.1	GC3/289.0	strongly annealed, banded magnetite- pyrite
68269	py	-1.9	GC3/296.2	massive magnetite pyrite rock.
68270	py	-0.1	GC3/289.9	pyrite- magnetite- chalcopyrite quartz hornfels.
68272	py	+0.9	GC3/394.1	course grained pyrite rimmed by quartz.
68263	$BaSO_4$	+35.8	GCB/71.8	barite- magnetite pyrite rock with minor skarn overprint.
(ii)				
68262	py	-7.6	GCB/50.0	strongly annealed massive granular pyrite
68264	py	-1.6	GCB/72.8	
"	py	-2.1		
68273	py	+15.5	surface	euhedral pyrite cubes in banded quartz- hematite- pyrite rock.

Table 7.1 $\delta^{34}S_{CDT}$ values for sulphide and sulphate bearing minerals from the Gourlays Creek prospect. Abbreviations are; po= pyrrhotite, py= pyrite, cpy= chalcopyrite. All sample numbers refer to the Uni. of Tas. rock catalogue.

Group II

The $\delta^{34}S$ values of skarn associated pyrrhotites fall in the range of +7.6 to +15.2 ‰(Fig 7.1 group II). From figure 7.2, low to slightly positive (0 to +8 ‰) fractionation factors are expected for the pyrrhotite stability field suggesting the source fluid to have a $\delta^{34}S$ value, in the range of +7 to +15 ‰ .

Pyrites shown to be of skarn origin (e.g. 68256, 68259) have $\delta^{34}S$ values that may be explained in terms of isotopic fraction of the previously defined source fluids. The relatively low $\delta^{34}S$ values of pyrite and chalcopyrite in 68267 and 68272 (ie. +7.2 ‰ and +5.3 ‰ respectively), indicate moderately negative fractionation factors and also, from figure 7.2, moderately high fO_2 and/or pH's. Such arguments suggest chalcopyrite is not in equilibrium with pyrrhotite assuming the source fluid to have a homogeneous $\delta^{34}S$ value. Relatively high $\delta^{34}S$ values for skarn associated pyrite in 68259 (+13.5 ‰) suggest low fraction factors and from figure 7.2, low fO_2 and/or pH's of deposition.

Group III

The $\delta^{34}S$ values of group III sulphides range from -7.6 to +15.5 ‰. The magnetite-associated sulphides (group III (i), table 7.1) have $\delta^{34}S$ values that fall within the range of bacterial reduced sulphides (ie. -1.9 to +7.4 ‰) while sulphides of group III (ii) are more widely distributed.

A possible model to explain the variation in $\delta^{34}S$ values of these sulphur bearing minerals is summarized by Ohmoto and Rye (1979) who suggest that inorganic reduction of seawater sulphate may occur through simple redox reactions, e.g.

$$SO_4^{2-} + 8Fe^{2+}_{(silicates)} + 10H^+ \langle===\rangle H_2S + 8Fe^{3+} + 4H_2O.$$

Such reactions have been reported from the Atlantis II Deep of the Red Sea Geothermal Deposits (Shanks and Bischoff, 1983) where carbon has acted as the reducing agent in place of ferric iron. At temperatures above 250°C, isotopic equilibrium is attained thus allowing the use of stability and isotope fractionation diagrams.

Isotopic data from Gourlays Creek supporting this model include the range in $\delta^{34}S$ values of group III (i) (table 7.1) magnetite-associated pyrites which given a fraction factor of -20 ‰ for magnetite-pyrite stable (eg. Fig. 7.2b), a source fluid with a $\delta^{34}S$ value of +20 to +25 ‰ is indicated. This range of values is typical of Precambrian seawater. Barite ($\delta^{34}S$ = 34.8 ‰) can be derived from a similar source fluid at 250°C

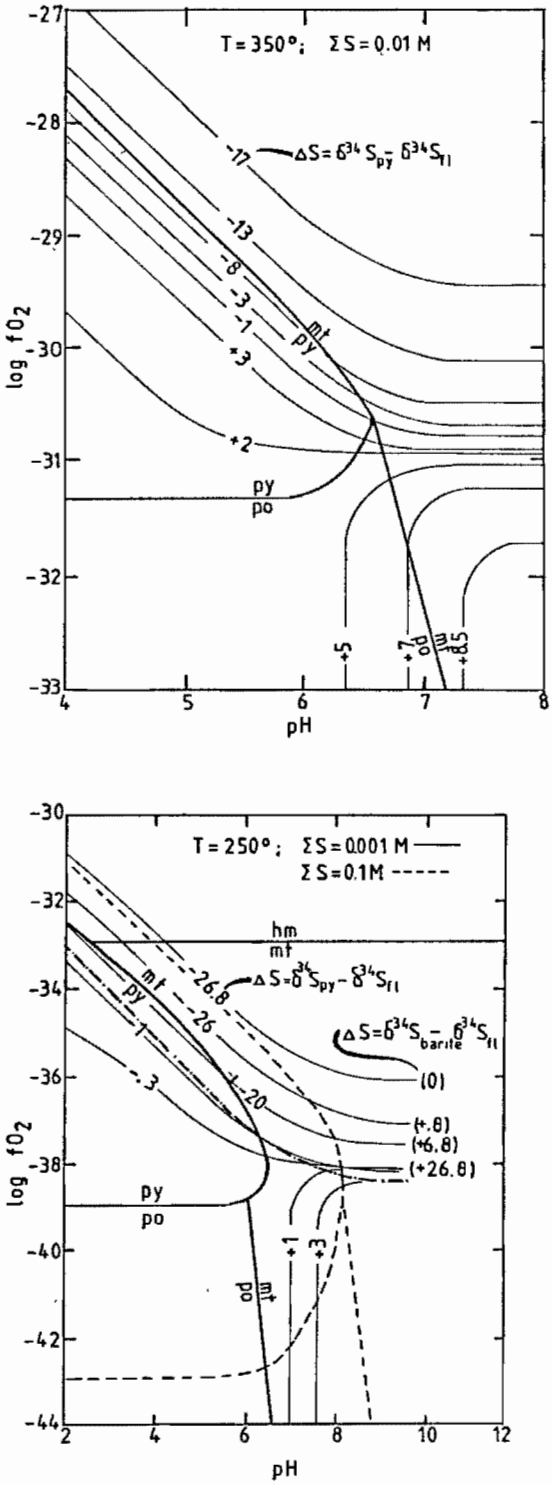

Fig 7.2 Composite diagrams showing the pH-fO_2 relationship between the stability fields of hydrothermal minerals and sulphur isotopic composition of sulphide and sulphate minerals at 350° C and 250° C respectively. Heavy solid lines: mineral stability boundaries among pyrite (py), pyrrhotite (po), magnetite (mt) and hematite (hem). Dash and dot line, fig 7.2b: barite soluble/ insoluble boundary at $a_{Ba^{2+}} \cdot a_{\Sigma S^{2-}} = 10^{-4}$. Thin lines: $\delta^{34}S$ contours for pyrite under a condition of $\delta^{34}S_{\Sigma S^{2-}} = 0$ per mil. The same contours can be applied to other sulphides, eg. subtract 0.8 at 350° C or 1.1 at 250° C for pyrrhotite and add 18.0 for barite at 350° C, [for appropiate calculations refer to appendix A4]. Modified after Rye and Ohmoto,(1974), figures 6 & 8.

with fractionation factors in the order of +10 ‰ being typical of the barite-magnetite stability field at 250°C (eg. Fig. 7.2b).

The main evidence mitigating inorganic reduction with isotopic equilibrium is the relative distribution of group III $\delta^{34}S$ values. From figure 7.2 a & b, a decrease in oxygen fugacity is accompanied by an increase in the fractionation factor. Thus on passing from hematite-pyrite to magnetite-pyrite to pyrite only stablities, dramatic increases in $\delta^{34}S$ values of the pyrites are expected. Analysis of group III pyrites from Gourlays Creek shows the opposite trend to be operative with hematite-associated pyrite giving the highest $\delta^{34}S$ value at +15.5 ‰ (eg. 68273) and massive pyrite the lowest at -7.6 ‰ (eg. 68262). If inorganic reduction resulted in the deposition of pyrite during sedimentation, then isotopic equilibrium cannot be maintained between SO_4^{2-} and H_2S. According to Ohmoto and Rye (1979), isotopic disequilibrium is typical in the reduction of sulphate at temperatures below 250°C.

A skarn-type origin for the lower mineralized horizon is considered unlikely based on sulphur isotope studies. Firstly the occurrence of barite with a $\delta^{34}S$ value equal to +35.8 ‰ indicates a source fluid of at least +9 ‰ since the maximum fractionation factor obtainable for barite is 26.8 ‰ (eg. Fig. 7.2b). Dissolution of group I sedimentary sulphides (-2.0 to +7.4 ‰) or magmatic sulphur (-3 to +7 ‰, Ohmoto and Rye, 1979) is unlikely to produce fluids with a $\delta^{34}S$ value of +9 ‰. In addition, dissolution of sedimentary nor magmatic sulphur could produce the indicated isotope compositions of the source fluids of the group III (i) pyrites (ie δ^{34}= +20 to +25 ‰).

In the Archean, volcanogenic, siderite pyrite rich Helen Formation of Canada, Goodwin et. al.,(1985) reports a range of $\delta^{34}S$ for pyrite of +19 to -11.6‰ with values from the oxide facies being uniformally close to zero. A similar distribution of values is typical for group III sulphides at Gourlays Creek. Goodwin et. al.,(1985) suggests this range in values to be characteristic of low temperature, biogenic reduction of seawater sulphate.

In conclusion, sulphur isotope studies support a two-stage mineralization process with a deposition of banded magnetite-pyrite-quartz horizons by sedimentary exhalations in the Precambrian followed later in the Devonian by pyrrhotite- chalcopyrite- pyrite deposition during skarn overprinting. During the sedimentary exhalative stage, deposition of the lower magnetite-pyrite-quartz, magnetite-pyrite-barite and massive pyrite horizons occurred from a source fluid with a $\delta^{34}S$ value in the range of +20 to +25 ‰. Such $\delta^{34}S$ values are typical of Precambrian seawater. To fully

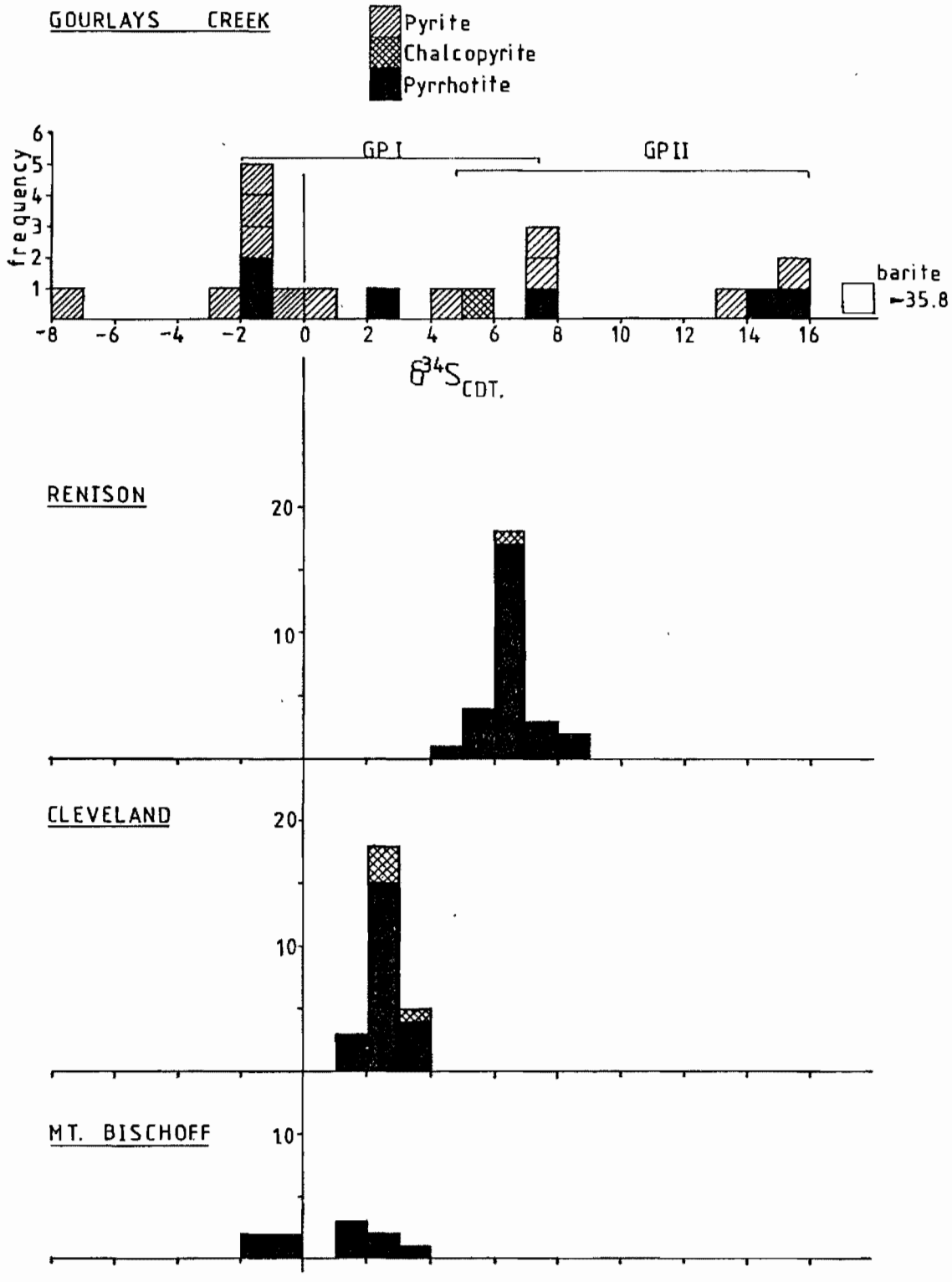

Fig 7.3 Sulphur isotope compositions of sulphur bearing minerals from the Gourlays Creek Prospect. Groups I and II are refered to in the text. Data from Renison, Cleveland and Mt. Bischoff summarized by Collins, (1983), fig 7.3 .

explain the range of values, isotopic disequilibrium is considered likely. This phenomenon is typical for deposition temperatures of less than 250°C (Ohmoto and Rye, 1979).

Pyrrhotite, pyrite and chalcopyrite were the dominant sulphur-bearing minerals deposited during the skarn stage of mineralization. Group II sulphides indicate a source fluid with a $\delta^{34}S$ signature in the range of +7 to +15 ‰. Such high $\delta^{34}S$ values indicate an inhomogeneous source fluid consisting of a mixture of the following:

(i) dissolution of barite associated with the sedimentary exhalative mineralization,

(ii) dissolution of sedimentary sulphide and/or magmatic sulphur.

In comparison to the sulphide- cassiterite deposition of western Tasmania, $\delta^{34}S$ values from Gourlays Creek are more widely dispersed than those from Renison, Cleveland or Mount Bischoff mines (eg. Fig. 7.3). This wider distribution reflects the more complex mineralization process and the mixed source of sulphur at Gourlays Creek. A magmatic sulphide source is considered likely for the sulphide-cassiterite deposits (e.g. Rafter and Solomon, 1967). Coleman (1974) reports $\delta^{34}S$ values of five pyritic samples from Savage River to range from +7.7 to +11.1 ‰. These values are quite different from those of Gourlays Creek group III samples, however, this is not unusual considering the contrasting modes of origin (i.e. volcanogenic exhalative at Savage River as opposed to probable sedimentary exhalative with isotopic disequilibrium at Gourlays Creek).

Pyrites from fresh Heemskirk Granite and from sorrounding Precambrian sediments are reported to have mean $\delta^{34}S$ values of +1.8 and +19‰ respectively, (Hajitaheri and Solomon, 1984). Greisen zones gave $\delta^{34}S$ values in the range of +3.7 to +12.8 ‰, while cassiterite-polymetallic sulphide deposits near the margin of the Heemskirk Granite (e.g. Sweeneys and Globe Mines) possess $\delta^{34}S$ values in the range of +9.7 to +15 ‰. Like the values from Gourlays Creek, these values indicate little or no input of magmatic sulphur. Hajitaheri and Solomon (1984) conclude that most of the mineralization associated with Heemskirk Granite formed during magmatic-hydrothermal activity and that the source of sulphur in many of these deposits was through dissolution of sedimentary pyrites.

CHAPTER 8

SUMMARY AND CONCLUSIONS

8.1 GENERAL

The stratigraphy of Granville Harbour is dominated by a sedimentary sequence ranging in age from Late Proterozoic to Devonian. The main lithology in the area, consisting of interlayered quartzites, schists, phyllites and hornfels, is correlated with the Oonah Formation. Faulted against the most northern exposures of the Oonah Formation is 415 m of interbedded schist, phyllite, quartzite and dolomite. These sediments have been termed the Duck Creek Sequence and are considered to be lithostratigraphic correlates of the Early Cambrian Crimson Creek Formation. Blissett (1962) and Williams (1976) have erroneously correlated these sediments with the Whyte Schist which outcrops in the north of the field area.

The Duck Creek Sequence is unconformably overlain by sediments of the Mt Zeehan Conglomerate, Gordon Limestone and Eldon Group. The youngest outcropping formation of the Eldon Group, the Florence Quartzite, occupies the core of the Duck Creek Syncline and is faulted against the Whyte Schist in the north of the field area. Adjacent to this fault are 120 m of strongly sheared micritic limestone. An Early to Middle Devonian age of a coral sampled from this lithology indicates it to be part of the Florence Quartzite. Blissett (1962) previously correlated this unit with the Ordovician Gordon Limestone.

Minor spilite and metabasite volcanics of ocean floor tholeiite affinities are associated with the Whyte Schist, Oonah Formation and the Duck Creek Sequence. Based on their chemistry, samples from both the Whyte Schist and Oonah Formation correlate with Crimson Creek tholeiite basalts while the metabasite from the Duck Creek Sequence correlate with the Cambrian ophiolite basalts.

Five phases of deformation are recognized in the Granville Harbour area. Two phases are correlated with the Late Proterozoic Penguin Orogeny, one with the Late Cambrian Jukesian Movement and two with the Early to late-Middle Devonian Tabberabberan Orogeny. Deformation events associated with the Penguin Orogeny are restricted in occurrence to the Whyte Schist and Oonah Formation. The first phase is recognized by a strong spaced cleavage in coarse grained psammite units, while the second produced fold closures in both the primary layering and the first phase cleavage. The style of the former folds is tight to isoclinal, angular and recumbent to plunging inclined. The latter folds are open, rounded and plunging inclined. A moderately strong schistosity forms axial planar to the second phase folds

and is generally observed to be subparallel to layering throughout most of the Proterozoic sediments. The highest degree of metamorphism, the chlorite zone of the greenschist facies, accompanied the second phase of deformation.

The development of a Jukesian correlated unconformity which separates the Duck Creek Sequence and the Mt Zeehan Conglomerate is attributed to D_3 deformation. This unconformity represents a minimum contact angle of 30^{o}. A moderately strong slaty cleavage in the Duck Creek Sequence is also attributed to D_3 deformation. This cleavage subparallels, but is significantly stronger than, the S_5 cleavage as observed in other lithologies.

The Tabberabberan D_4 and D_5 deformation events produced open, concentric and horizontal to plunging normal folds. The mean orientation of axial planes to these folds are NW-SE and E-W respectively. The relative sequence of deformation has been defined by overprinting relationships. Both fold generations have produced regional antiforms and synforms in the area.

8.2 MINERALIZATION

Two distinct styles of mineralization occur in the Gourlays Creek Prospect:

(i) stratiform and stratabound, massive and banded magnetite-pyrite-(quartz) and magnetite-barite mineralization; and

(ii) pyroxene-garnet skarn.

The former style of mineralization is distinctly stratiform and is unlike any known skarn mineralization. From this study it is suggested to be a metamorphosed equivalent of a banded iron formation of essentially chemical origin. The banded magnetite-quartz and massive pyrite horizons are the oxide and sulphide facies, respectively, of this syngenetic deposit. A possible analogue is the (Recent) Red Sea metalliferous sediments (e.g. Bignell, 1975; Shanks and Bischoff, 1980; Pottorf and Barnes, 1983).

The similarities between the Gourlays Creek magnetite-pyrite horizon and the Red Sea metalliferous sediments include the dominance of magnetite and pyrite, the stratiform nature, and the abundant pyrite as granular bands and disseminations concentrated in the footwall of this horizon. The Red Sea metalliferous-type deposits are also considered to have footwall vein and disseminated pyrite (Gunblach and Marchig, 1982). The main differences are the absence of volcanics and negligible Cu-Zn mineralization associated with this horizon. The general spatial association of volcanics is considered to have little control on this style of deposit (Bignell, 1975). Negligible Cu-Zn mineralization may simply reflect low temperatures, low

oxygen fugacities and high pH's of the Gourlays Creek metalliferous sediments (i.e. chemical conditions unfavourable for Cu-Zn transportation in the hydrothermal fluids).

Sulphur isotope studies support the proposed sediment-hosted exhalative-type origin for this horizon. The $\delta^{34}S$ values range from -7.6 to +15.5% for pyrite and +35.8% for barite. Two possible models explain this range of pyrite values: (1) inorganic reduction of Precambrian seawater ($\delta^{34}S$ = +20 to +25%) with isotope disequilibrium ; and (2) biogenic reduction of seawater sulphate in a system closed to sulphate. In the analogous Red Sea metalliferous sediments, both inorganic and biogenic reduction are considered to be operative (Shanks and Bischoff, 1980).

The host to this stratiform magnetite-pyrite-rich horizon is the Late Precambriam Oonah Formation. The syngenetic, chemical exhalative, banded iron formation is thus also Precambrian in age and represents the only recognized deposit of this type in Tasmania. The Savage River magnetite deposit, located approximately 35 km NNW, is similar but is considered to have a volcanogenic exhalative origin (Coleman, 1975).

A second period of mineralization accompanied the intrusion of the Heemskirk Granite in the Late Devonian. The Gourlays Creek skarn, defined as a calcic, metasomatic infiltration, exoskarn, formed by replacement of calcic sediments of the Oonah Formation. These calcic sediments may represent the carbonate facies of the banded iron formation.

Two stages of skarn formation are defined:

(i) prograde alteration resulting in the development of clinopyroxene-garnet skarn; and

(ii) retrograde alteration of the clinopyroxene skarn resulting in the deposition of actinolite, hornblende, calcite, quartz, epidote, axinite, magnetite, pyrrhotite, chalcopyrite and minor pyrite.

The prograde stage of alteration is considered to be essentially isochemical. The garnets and clinopyroxenes are composed of grossular-andradite and diopside-hedenbergite solid solutions respectively. Most garnets are nearly pure andradite in composition, however, minor grossular-rich garnets occur in some horizons. In the carbonate-poor sediments, tremolite-(epidote) hornfels has developed in place of the pyroxene garnet skarns.

Infiltration metasomatism characterizes the retrograde stage of alteration. Amphiboles and epidote replace the prograde mineral assemblage while influx of calcium and silica-rich fluids resulted in deposition of quartz and calcite as vein and vugh fill. The occurrence of axinite supports a granitic source for these fluids. Deposition of sulphides also

accompanied this stage of mineralization. The bulk of the magnetite, which forms a major component in some of the skarns, is considered to be primary in origin. However, minor magnetite is also observed replacing the skarn mineralogy and as vugh fill indicating at least some magnetite deposition accompanied skarn alteration.

In the lower exhalative banded iron formation horizon, skarn alteration is recognized by minor deposition of calcsilicate minerals (i.e. garnet, clinopyroxene, epidote), replacement of magnetite and pyrite by pyrrhotite, and deposition of chalcopyrite in microveinlets and in vughs. No cassiterite was observed in either type of mineralized horizon. Similarly, microprobe analysis of garnets, clinopyroxene, actinolite, epidote and axinite did not detect any tin. A geochemical association between Cu and Sn suggests Sn deposition to be associated with retrograde skarn alteration and chalcopyrite deposition.

Sulphur isotope studies of skarn associated sulphides indicate a source fluid with a $\delta^{34}S$ value of between +7 to +15‰ . These high values indicate an inhomogeneous source of sulphur consisting of a mixture of the following:

(i) dissolute barite associated with the primary exhalative banded iron formation; and

(ii) dissolute sedimentary sulphides and/or magmatic sulphur.

Fluid inclusion data indicate homogenization temperatures for garnet above 500°C and for late-stage retrograde vugh quartz in the order of 330-340°C. Temperatures for sulphide deposition during retrograde skarn alteration, as inferred from secondary inclusions hosted in vein quartz, are in the order of 350-360°C. The salinity of fluids forming these secondary inclusions is 20-21 wt% equiv. NaCl. Pressure of trapping, estimated from overburden thicknesses and fluid inclusion data, is in the range of 13-35 MPa.

REFERENCES

Adams, C.J., Black, L.P., Corbett, K.D. and Green, G.R. (1985), Reconnaissance isotope studies on the tectonothermal history of Early Palaeozoic and Late Proterozoic sequences in western Tasmania. **Aust. J. Earth Sci.** 32: 7-36.

Barrett, D.E. (1980), Geology, mineralogy and conditions of formation of the Kara scheelite skarn. Unpubl. Honours thesis, Univ. of Tasm.: 194pp.

Baillie, P.W. and Corbett, K.D. (1985), Strahan, Geological Atlas 1:50,000 Series sheet 57. **Geol. Surv. Explan. Rept**: 76 pp.

Baillie, P.W. and Williams, P.R. (1975), Sedimentary and structural features of the Bell Shale Correlate (Early Devonian), Strahan Quadrangle, western Tasmania. **Pap. Proc. Roy. Soc. Tasm.** 109: 1-15. Q93.R64 32

Beattie, R.D. (1978), A compilation and interpretation of aeromagnetic data from Bass Strait and Tasmania. **CSIRO Min. Res. Lab. Investigation Report** 124.

Bignell, R.D. (1975), Timing, distribution and origin of submarine mineralization in the Red Sea. **Inst. Min. Metall. Trans.** 84B; 1-6.

Blissett, A.H. (1962), Zeehan, 1 mile geol. map series K55-5-50. **Rep. Geol. Surv. Tasm:** 274pp.

Brown, A.V. (1980), Some aspects of the geology of the Mt Lindsay-Dundas areas, western Tasmania. Unpubl. Rept., Dept of Mines Tasm. 1980/42.

Burton, J.C., Taylor, L.A. and Chou, I-M. (1982), The fO_2 and fS_2-T stability relations of hedenbergite and of hedenbergite-johannsenite solid solutions. **Econ. Geol.** 77: 764-784.

Carey, S.W. and Banks, M.R. (1954), Lower Palaeozoic unconformities in Tasmania. **Pap. Proc. Roy. Soc. Tasm.** 88: 245-269.

Coleman, R.G. (1977), **Ophiolites.** Springer-Verlag, Berlin-Heidelberg: 229 pp.

Coleman, R.J. (1975), The Savage River magnetite deposits. **In** C.L. Knight, Economic Geology of Australia and Papua New Guinea, I, Metals. **Aust. Inst. Min. Metall., Mon.** 5: 598-604.

Collins, P.L.F. (1983), Geology and mineralisation at the Cleveland Mines, western Tasmania. Unpubl. Ph.D. thesis, Univ. of Tasm.

Corbett, K.D. (1979), Stratigraphy, correlation and evolution of the Mt Read Volcanics in the Queenstown, Jukes-Darwin and Mt Sedgwick area. **Bull. Geol. Surv. Tasm.** 58: 74pp.

Corbett, K.D. and Brown, A.V. (1976), Queenstown, Geological atlas 1:250,000 series. Sheet SK-55/5. **Explan. Rept Geol. Surv. Tasm:** 19pp.

Corbett, K.D. and Lees, T.C. (1985), Revised stratigraphy and tectonics of the Cambrian arc and forearc sequences and a probable accretionary complex in the Rosebery-Lyell area, western Tasmania. Submitted to **Aust., J. Earth Sci.**, Oct, 1985.

Creenaune, P. (1980), The volcanics of the Heazlewood River Complex. Unpubl. Honours thesis, Univ. of Tasm.

Crook, K.A.W. (1979), Tectonic implications of some field relations of the Adelaidean Cooee Dolerite, Tasmania. **J. Geol. Soc. Aust.** 26: 353-361.

Déchomets, R. (1985), Sur l'origine de la pyrite et des skarns du gisement, en contexte evaporitique, de Niccioleta (Toscane, Italie). **Mineralium Deposita** 20: 201-210. (english abstract)

Eadington, P.J. and Kinealy, K. (1983), Some aspects of the hydrothermal reactions of tin during skarn formation. **Jour. Geol. Soc. Aust.** 30: 461-471.

Einaudi, M.T. and Burt, D.M. (1982), A special issue devoted to skarn deposits. Introduction - Terminology, classification and compositions of Skarn Deposits. **Econ. Geol.** 77: 745-754.

Einaudi, M.T., Meinert, L.D. and Newberry, R.J. (1981), **Skarn Deposits.** Economic Geology 75th Anniv. Volume: 317-391.

Garcia, M.O. (1978), Criteria for the identification of ancient volcanic arcs. **Earth Science Reviews**, 14: 147-165.

Gee, R.D. (1967), The tectonic evolution of the Rocky Cape Geanticline in northwestern Tasmania. Unpubl. Ph.D. thesis, Univ. of Tasm.

Gee, R.D. (1977), Burnie, Geological Atlas 1 mile series, zone 7, sheet 28. **Explan Rept Geol. Surv. Tasm:** 80pp.

Goodwin, A.M., Thode, H.G., Chou, C.L., and Karkhansis, S.N., (1984), Chemostratigraphy and origin of the late Archean siderite- pyrite rich Helen Iron Formation, Michipicoten Belt, Canada. **Can. J. Earth Sci.** 22: 72-84.

Groves, D.I., Martin, E.L., Murchie, H. and Wellington, H.K. (1972), A century of tin mining at Mt Bischoff, 1871-1971. **Bull. Geol. Surv. Tasm.** 55: 7-116.

Groves, D.I. and Solomon, M. (1969), Fluid inclusion studies at Mt Bischoff, Tasmania. **Trans. Inst. Min. Metall.**, 78: B1-B11.

Gundlach, H. and Marchig, V. (1982), Ocean floor "metalliferous sediments" - two possibilities for genesis. **In** Amstutz et al. (Eds): Ore Genesis; the State of the Art. Spec. Publ. 2, Society for Geology Applied to Mineral Deposits: 200-211.

Hajitaheri, J. and Solomon, M. (1984), Sulphur isotopes in the Zeehan District, Western Tasmania. Geoscience in the development of natural resources. Abstracts of the 7th Aust. Geol. Conv., Sydney, 1984. Geol. Soc. Aust. 46-50

Haas, J.L. (1971), The effect of salinity on the maximum thermal gradient of a hydrothermal system at hydrostatic pressure. **Econ. Geol.** 66: 940-946.

Hirschberg, A. and Winkler, H.G.F. (1968), Stabilitats beziehungen zwischen chlorit, cordierit und almandin bei der metamorphose. **Cont. Mineral. Petrol.** 18: 17-42. (english abstract).

Holdaway, M.J. (1971), Stability of andalusite and the aluminium silica phase diagram. **Am. J. Sci.** 271: 97-131.

Holser, W.T. and Kaplan, I.R. (1966), Isotope geochemistry of sedimentary sulphates. **Chemical Geology** 1: 93-135.

Irvine, T.N. and Barager, W.R.A. (1971), A guide to the chemical classification of common volcanic rocks. **Can J. Earth Sci.** 8: 523-548.

Kendall, C. (1984), Annual progress report, E.L. 1/77, Rocky Cape-Gourlays Creek Prospect. C.R.A./Geopeko Joint Venture. Unpubl.

Klominsky, J. (1972), The Heemskirk granite Massif, western Tasmania. Unpubl. Ph.D. thesis, Univ. of Tasm.

Kwak, T.A.P. (1983), The geology and geochemistry of the zoned Sn-W-F-Be skarns at Mt Lindsay, Tasmania, Australia. **Econ. Geol.** 78: 1440-1464.

Kwak, T.A.P. and Askins, P.W. (1981), Geology and genesis of the F-Sn-W(-Be-Zn) skarn (Wrigglite) at Moina, Tasmania. **Econ. Geol.** 76: 439-468.

Kwak, T.A.P. and Tan, T.H. (1981), The geochemistry of zoning in skarn minerals at King Island (Dolphin) mine. **Econ. Geol.** 76: 468-497.

MacDonald, G.A. and Kasura, T. (1964), Chemical composition of Hawaiian lavas. **J. Petrol.** 5: 82-133.

McDougall, I. and Leggo, P.J. (1965), Isotopic age determinations on granitic rocks from Tasmania. **J. Geol. Soc. Aust.** 12: 295-332.

Miyashiro, A. (1975), Classification, characteristics and origin of ophiolites. **J. Geology** 83: 249-281.

Ohmoto, H. and Rye, R.O. (1979), Isotopes of sulphur and carbon. **In** H.L. Barnes (Ed.), Geochemistry of Hydrothermal Ore Deposits: 509-567.

Patterson, D.J., Ohmoto, H. and Solomon, M. (1981), Geologic setting and genesis of cassiterite-sulphide mineralization at Renison Bell, western Tasmania. **Econ. Geol.** 76: 393-438.

Pearce, J.A. (1975), Basalt geochemistry used to investigate past tectonic environment on Cyprus. **Tectonophysics** 25: 41-67.

Pearce, J.A. and Cann, J.R. (1973), Tectonic setting of basic volcanic rock determined by trace element analysis. **Earth Planet. Sci. Lett.** 19: 290-300.

Perring, R.J. (1983), Annual progress report, E.L. 1/77, Rocky Cape-Gourlays Creek Prospect. C.R.A./Geopeko Joint Venture. Unpubl.

Porter, T.M. (1980, Annual progress report, E.L. 1/77, Rocky Cape-Gourlays Creek Prospect. C.R.A./Geopeko Joint Venture. Unpubl.

Potter, R.W. (1977), Pressure corrections for fluid inclusion homogenization temperatures based on the volumetric properties of the system NaCl-H_2O. **U.S. Geol. Surv. J. Res. 5: 603-607.**

Potter, R.W., Clynne, M.A. and Brown, D.L. (1978), Freezing point depression of aqueous sodium chloride solutions. **Econ. Geol.** 73: 284-285.

Pottorf, R.J. and Barnes, H.L. (1983), MinHralogy, geochemistry and ore genesis of hydrothermal sediments from the Atlantis II Deep, Red Sea. **Econ. Geol. Mon.** 5: 198-223.

Purvis, J.G. (1978), An appraisal of the St Dizier tin deposit, Zeehan, western Tasmania. Unpubl. Rept. No. 9478, CRAE, Melbourne, Burnie.

Rafter, T.A. and Solomon, M. (1967), Sulphur isotope and oxygen isotope studies of Tasmanian ore deposits. **In** The Geology of Western Tasmania - a symposium. Geology Dept, Univ. Tasm., Hobart.

Ramdohr, P. (1969), **The Ore Minerals and their Intergrowths.** Permagon Press. 1174pp.

Roedder, E. (1979), Fluid inclusions as samples of ore fluids. **In** H.L. Barnes (Ed.), Geochemistry of Hydrothermal Ore Deposits. 2nd Ed. Wiley New York: 684-737.

Roedder, E. (1984), Fluid inclusions. In P.H. Ribbe (Ed.), Reviews in Mineralogy, vol. 12. Mineralogical Society of America.

Roedder, E. and Bodnar, R.J. (1980), Geological pressure determinations from fluid inclusion studies. **Ann. Rev. Earth Planet. Sci.** 8: 263-301.

Rubenach, M. (1973), The Tasmania ultramafic-gabbro and ophiolite complexes. Unpubl. Ph.D. thesis, Univ. of Tasm.

Rye, R.O. and Ohmoto, H. (1974), Sulphur and carbon isotopes in ore genesis: a review. **Econ. Geol.** 69: 826-842.

Shanks, W.C. and Bischoff, J.C. (1980), Geochemistry, sulphur isotope composition and accumulation rates of the Red Sea geothermal deposits. **Econ. Geol.** 75: 445-457.

Solomon, M. (1981), An introduction to the geology and metallic ore deposits of Tasmania. **Econ. Geol.** 76: 194-208.

Spry, A.H. (1964), Precambrian rocks of Tasmania. Part IV, the Zeehan-Corinna area. **Pap. Proc. Roy. Soc. Tasm.** 98: 23-48.

Sun, S-S. (1982), Chemical composition of the earth's primitive mantle. **Geochim. Cosmochim. Acta** 46: 179-445.

Tan, T.H. and Kwak, T.A.P. (1979), The measurement of the thermal history around the Grassy Granodiorite, King Island, Tasmania, by use of fluid inclusion data. **J. Geol.** 87: 43-54,

Turner, F.J. (1981), **Metamorphic Petrology; Mineralogical, Field and Tectonic Aspects.** 2nd ed. McGraw-Hill Book Company.

Uchida, E. and Iiyama, J.T. (1982), Physiochemical study of skarn formation in the Shinyama iron-copper ore deposit of the Kamaishi Mine, northeastern Japan. **Econ. Geol.** 77: 809-823.

Williams, S.E. (1976), Structural Map of Pre-Carboniferous Rocks of Tasmania: Base map from Tasmanian 1:500000 Sheet, Mines Dept. of Tasmania.

Williams, E. (1978), Tasman Fold Belt System in Tasmania. **Tectonophysics** 48: 159-205.

Williams, P.R. (1982), Structural geology of the Mt Bischoff Precambrian rocks. Unpubl. Rept Dept Mines Tasm., 1982/11.

Williams, E., Solomon, M. and Green, G.R. (1975), The geological setting of metalliferous ore deposits in Tasmania. **In** C.L Knight (Ed.), Economic Geology of Australia and Papua New Guinea - Metals. **Aust. Inst. Min. Metall. Mon.** 5: 567-581.

Winchester, J.A. and Floyd, P.A. (1976), Geochemical magma type discrimination: application to altered and metamorphosed basic igneous rocks. **Earth Planet. Sci. Lett.** 28: 459-469.

APPENDIX A1

ROCK CATALOGUE

The following samples are referred to in the text and are now stored in the Geology Department, University of Tasmania, Rock Store. The locality terminology are as follows; AMG grid coordinates given in round brackets ( ), Gourlays Creek Prospect grid coordinates given in square brackets [ ], and diamond drill hole samples referred to by the drill hole number and by the depth in metres. Note that all surface sample localities are given to the nearest 10 metres.

The preparation terminology is as follows;

R = Hand Specimen

T = Thin Section

PT = Polished Thin Section

D = X-ray Disc

P = X-ray Pill

PD = Powdered Specimen

No.	Locality	Description	Prepn.
Greenschist Facies Metapelites.			
68220	(537432/33347)	quartz-chlorite-albite metagreywacke	T.R
68221	[10800/1470]	quartz-chlorite-albite metagreywacke	T.R
68222	(537475/33369)	quartz-chlorite metasandstone	T.R
68223	GCB 122.6	Quartz- albite- muscovite schist + pyrrhotite + pyrite	PT.R.
Albite-Epidote Hornfels.			
68224	(537200/33435)	Muscovite-quartz-biotite-carbonate schist	T.R
68225	(537121/33496)	quartz-chlorite-epidote hornfels	T.R
68226	[10000/1720]	quartz-muscovite-biotite-tourmaline hornfels	T.R
68227	[10100/2060]	quartz-biotite-actinolite hornfels	T.R
68228	[11200/2130]	quartz-chlorite-muscovite-biotite albite hornfels	T.R
68229	[11300/2250]	tremolite-actinolite hornfels	T.R
68230	GCA 120.0	quartz-chlorite-actinolite-hornfels	T.R
Hornblende Hornfels			
68231	(537029/33534)	quartz-tremolite hornfels	T.R
68232	(537027/33535)	quartz-tremolite-actinolite hornfels	T.R
68233	(536965/33640)	hornblende-biotite-tourmaline hornfels	T.R
68234	(536919/33626)	quartz-biotite-tourmaline hornfels	T.R
68235	(537055/33634)	banded quartz-biotite/quartz-tremolite hornfels	T.R
68236	(537071/33668)	banded quartz-biotite/quartz-corderiete-tourmaline hornfels	T.R
68237	(537079/33681)	quartz-biotite hornfels	T.R
68238	GCA 66.6	hornblende-chlorite-biotite-quartz carbonate hornfels	T.R
68239	GC3 288.3	quartz-biotite-corderiete hornfels	T.R
68240	GC3 302.3	quartz-corderiete-biotite-sillimanite hornfels	T.R
68241	GC3 338.8	corderiete-Mn-garnet-biotite-K-feldspar-muscovite hornfels	T.R
Metavolcanics			
68242	(537422/33391)	chlorite-quartz metabasite tuff(?)	T.R
68243	(" ")	albite-chlorite metabasite	T.PD.R
68244	(" ")	albite-chlorite metabasite	T.PD.R
68245	GCA 43.5	albite-actinolite-chlorite-quartz metabasite	T.PD.R
68246	GCA 49.1	albite-chlorite metabasite	T.PD.R
68247	(537129/33429)	relict feldspar-actinolite-chlorite metabasite	T.PD.R
Unmetamorphosed Lithologies			
68275	(537259/33418)	dolimitized lime mudstone, Gordon Limestone	T.R
68276	(537407/33398)	lime mudstone, Eldon Group	T.R
68277	(" ")	**Favosites moonbiensis** (3X)	T

No.	Locality	Description	Prep.
Skarns			
68248	GCA 37.9	tremolite(70%)-chlorite(20%)-magnetite(10%) hornfels--> diopside(60%)-garnet(20%)-calcite(10%) skarn	T.R
68249	GCA 39.5	quartz(50%)-magnetite(25%)-garnet(15%)-diopside(10%) skarn + pyrrhotite	T.R
68274	GCA 41.9	diopside skarn--> quartz magnetite rock	T.R
68250	GC3 133.5	diopside(40%)-magnetite(40%)-serpentine(20%) skarn	T.R
68251	GC3 134.7	garnet(50%)-diopside(50%) skarn	T.R
68252	GC3 157.9	diopside(60%)-garnet(35%)-calcite-actinolite skarn	T.R
68253	GC3 159.3	diopside(50%)-garnet(20%)-skarn + pyrrhotite(20%)- chalcopyrite(5%)-pyrite(5%)	T.R
68254	GC3 188.9	diopside(50%)-chlorite(25%)-serpentine(20%)-axinite(5%) skarn	T.R
68255	GC3 189.4	epidote(60%)-actinolite(15%)-diopside(15%)-quartz(10%) skarn	T.R
68256	GC3 190.4	diopside(45%)-garnet(20%)-calcite(10%)-quartz(10%)- actinolite(5%) skarn +pyrrhotite(10%)- chalcopyrite- pyrite	T.R
68257	GC3 193.0	hornblende(50%)-calcite(30%)-quartz(10%)-actinolite(5%) axinite(5%) skarn	T.R

No.	Locality	Description	Prep.
Massive and Banded Magnetite-pyrite-quartz rocks			
68258	GCA 151.4	massive pyrite(70%)-magnetite(20%)-quartz(5%)- chalcopyrite(5%)	PT.R
68259	GCA 162.4	banded magnetite(45%) quartz(35%) pyrite(15%) chalcopyrite(5%).	PT.R
68260	GCA 162.7	banded magnetite(40%)-quartz(30%)-garnet(15%)-pyrite(10%)- chalcopyrite	PT.R
68261	GCB 50.5	massive magnetite(90%) + pyrite-quartz-chalcopyrite	PT.R
68262	GCB 54.8	annealed pyrite(60%) quartz(40%) rock.	PT.R
68263	GCB 71.8	barite(60%)-garnet(10%)-quartz(10%)-magnetite(10%)- pyrite(10%) + chalcopyrite	PT.R
68264	GCB 72.8	granular pyrite(90%) quartz hornfels	PT.R
68265	GCB 124.8	granular pyrite(50%)-chlorite(30%)-biotite(10%) quartz hornfels	PT.R
68266	GC3 193.6	banded-magnetite(30%)-pyrrhotite(30%)-quartz(30%)- garnet(5%) + diopside-tremolite-chalcopyrite	PT
68267	GC3 254.2	quartz-pyrite-chalcopyrite-arsenopyrite vein	PT.R
68268	GC3 289.0	banded granular magnetite(50%) pyrite(50%) rock	R
68269	GC3 291.2	massive pyrite(95%)-magnetite(5%)	PT.R
68270	GC3 298.9	magnetite(50%)-pyrrhotite(35%)-chalcopyrite(15%) + pyrite	PT.R
68271	GC3 301.7	banded quartz(40%)-magnetite(40%)-pyrite(10%)-pyrrhotite(10%) + chalcopyrite	PT.R
68272	GC3 394.1	quartz pyrite(20%) pyrrhotite(20%) chalcopyrite(15%) hornfels.	PT.R
68273	[11400/2130]	banded quartz-hematite + pyrite	PT.R

APPENDIX A2

Three diamond drill holes were sunk in the Gourlays Creek Prospect by the CRA/Geopeko Joint Venture. The collar co-ordinates, orientations, proposed targets and summary logs are given in the following pages. Note that the collar co-ordinates refer to the Gourlays Creek grid, and not to the AMG.

HOLE GCA

Collar co-ordinates		2300 mE, 11100 mN
Azimuth		270° grid
Declination		-50°
Proposed length		150-200 m
Target		1. Strong Sn anomaly of 2000 ppm outlined by bedrock geochem. 2. Chargeable, conductive zone shown by IP. 3. Magnetic anomaly of 5000 nT.
Summary log:	0-34.3 m	Grey-green phyllitic shales
	34-3.39	Pyroxene-hornblende-quartz-calcite skarn with a trace of disseminated chalcopyrite
	39-41	Banded quartz-magnetite rock
	41-44	Pyroxene-quartz-magnetite rock with trace chalcopyrite
	44-50	Amphibolite with disseminated magnetite (possibly metabasic tuff)
	50-150.6	Biotite-actinolite hornfels
	150.6-153.9	Massive pyrite (80%), siderite (15%) and magnetite (5%)
	153.9-160.3	Altered biotite hornfels with quartz veining. Minor pyrite
	160.3-163.5	Banded magnetite-quartz-pyrite rock
	163.5-177.5	Altered pyritic quartzite (2% pyrite)
	177.5-198	Biotite quartzite
	E.O.H.	

HOLE GCB

Collar co-ordinates		2114 mE, 11257 mN
		Collared on diagonal line at line point 1500 NE
Azimuth		244° grid
Declination		-45°
Proposed length		200 m
Target		1. Intense magnetic anomaly co-incident with outcropping magnetite zones. 2. Deep chargeable conductor as shown by IP. 3. Outcropping pyrite-tourmaline quartzite carrying 500-4000 ppm Sn.
Summary log	0-34.9 m	Grey green quartzites and meta-siltstones (heavily oxidised)
	34.9-50.8	Grey phyllites with irregular quartz veins
	50.8-51.8	Massive magnetite
	51.8-52.0	Massive pyrite
	52.0-68.8	Biotite hornfels
	68.8-72.9	Pyrite 50%, magnetite 30%, garnet 2% Barite Quartz rock
	72.9-75.5	Amphibolite with quartz veins
	77.5-96.8	Banded meta-siltstones and schists with quartz veins and sulphide bands parallel to banding
	96.8-97.0	Massive pyrite
	97.0-167.0	Meta-siltstone showing chlorite alteration
	E.O.H.	Pyrite/magnetite bands parallel to banding.

DDH GC3

Collar co-ordinates		2515 mE, 11100 mN
Azimuth		270° grid
Declination		-45°
Depth		150 m
Target		1. Well defined magnetic anomaly. 2. Magnetite zones associated with Vincents Copper Prospect located 15 m south of collar position. 3. Cu, Sn geochem. anomaly.
Summary log	0-16 m	Tertiary basalt
	16-18.5	Calc-silicate horizon
	18.5-56.0	Siltstones, quartzites and shales
	56.0-69.5	Siltstones and black shales
	69.5-133	Siltstones, quartzite and shales with minor sulphides (pyrite and pyrrhotite)
	133-134	Banded quartz magnetite rock
	134-135	Calc-silicate
	135-156	Quartz mica schist
	156-165	Pyroxene garnet pyrite, pyrrhotite rock
	165-184	Micaceous schists
	184-200	Pyroxene garnet rock with pyrrhotite, magnetite, axinite and tourmaline?
	200-217	Quartz mica schists
	217-227	Biotite hornfels (mineralized)
	227-291	Biotite hornfels
	291-306	Massive sulphides and banded sulphides, pyrite, pyrrhotite, chalcopyrite and magnetite
	306-376	Quartzites, biotite hornfels.

APPENDIX A3

FLUID INCLUSION MICROTHERMOMETRY

Fluid inclusions were studied in thin (0.03 or less) doubly polished plates. The plates were initially examined under the microscope for selection of suitable inclusions, and the plates then broken into smaller chips that could be handled in the microthermometric apparatus.

All heating and freezing measurements were made on a Chaixmeca heating/cooling stage mounted on a Leitz petrographic microscope. A thin (170 m thick) glass coverslip was placed over the condenser lens as a means of protecting that lens. During freezing runs a plastic sleeve was placed between the stage and the objective to prevent water vapour from freezing on either the objective lens or on the sample under observation. During heating runs an extra glass coverslip window was placed over the sample and the plastic sleeve was removed. During all runs, a 25X objective of long focal length was used. At temperatures above 100^{o}C, the lens was cooled by the circulation of cold water.

All quantitative observations of phase transitions were performed in the heating cycle. The heating rate during freezing experiments was maintained at 0.5-1^{o}C/min and for heating experiments was regulated at 1-2^{o} C/min. The freezing rate of the apparatus could not be adequately controlled to allow any measurements during freezing.

Calibration of the Microthermometric Apparatus

The heating/freezing stage and temperature readout were calibrated by a combination of melting points of standard compounds and by use of synthetic fluid inclusions of known homogenization temperatures.

Standards used in the calibration are zinc metal (M.P. = 419.8^{o}C), potassium dichromate (398^{o}C), sodium nitrate (306.8^{o}C), adipic acid (220^{o}C), naphalene (80.5^{o}C), dionised water (0^{o}C) and chloroform (-63.5^{o}C). Reagents of high analytical grades were used in all cases. Temperatures established using synthetic inclusions are the average of five runs of each inclusion type. The calibration curve is given in fig. A3.1

Estimated precision of the apparatus base on repeatability of temperatures for known standards is estimated at $\pm$5^{o}C at low temperature (<100^{o}C) and up to $\pm$20^{o}C at temperatures above 400^{o}C.

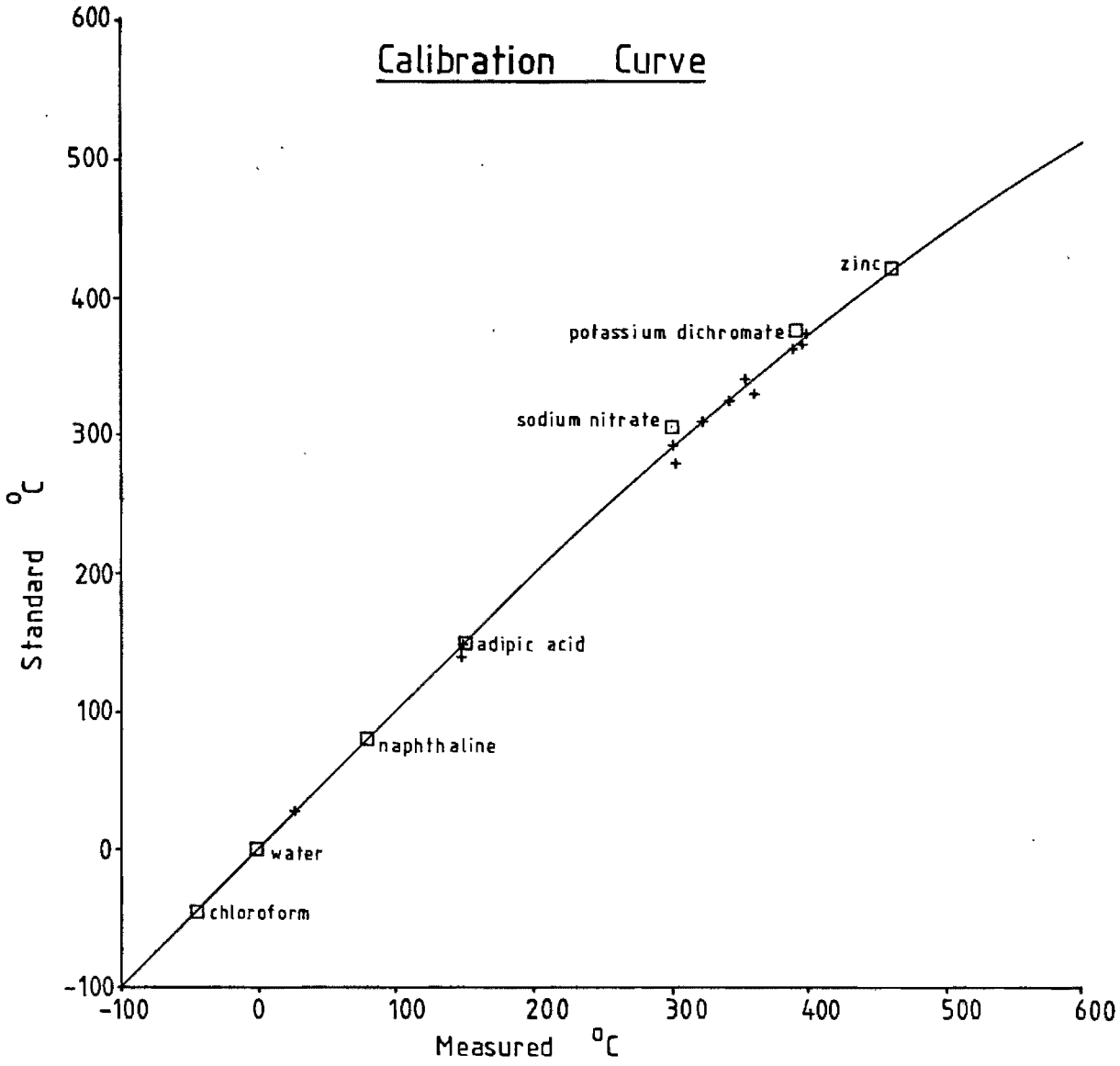

Fig A3.1 Calibration curve for Chaixmeca heating/ freezing stage held by the University of Tasmania. Standards used are as given, crosses refer to the homogenization temperatures of synthetic inclusions for which the homogenization temperatures are reasonably known.

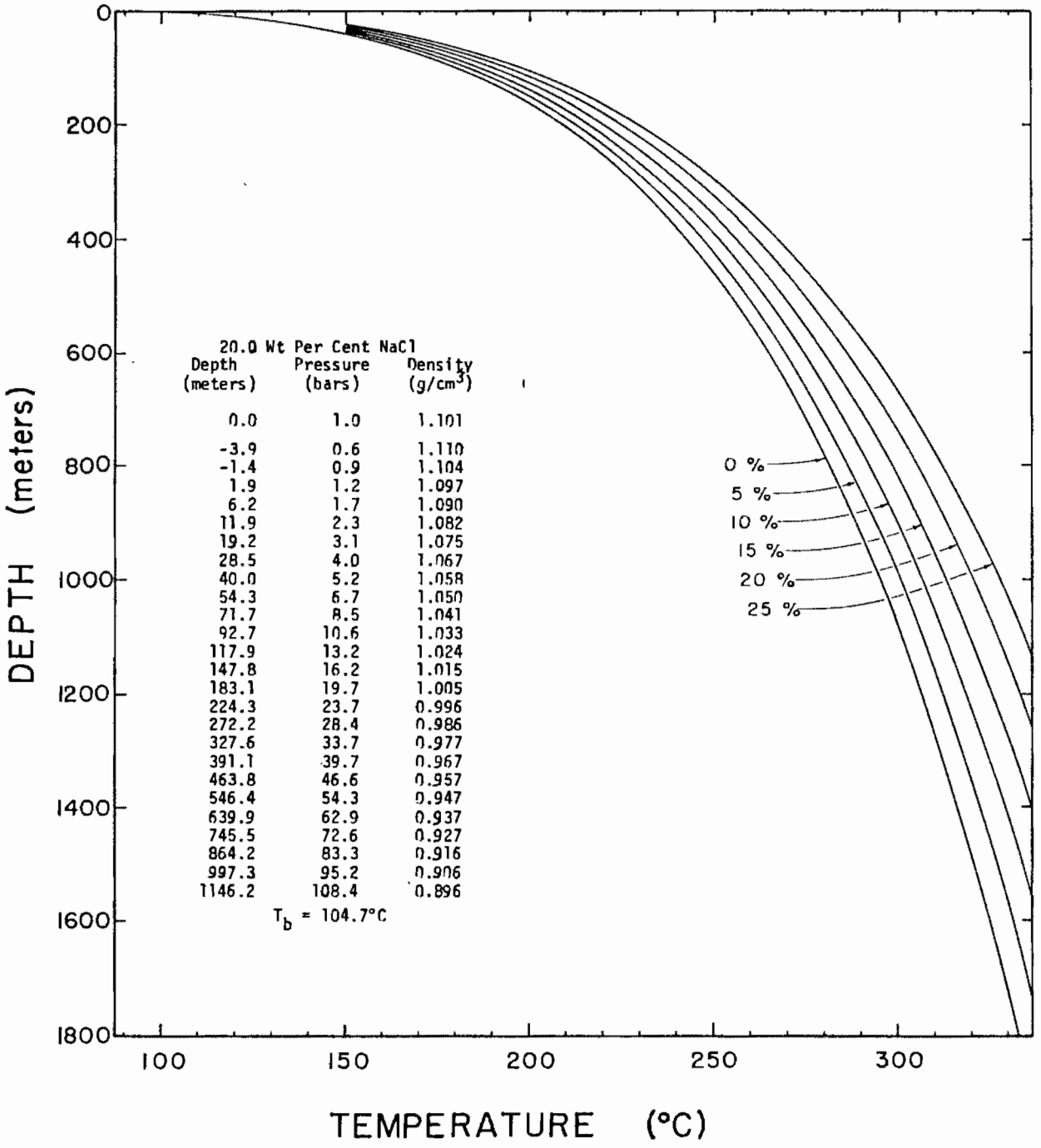

20.0 Wt Per Cent NaCl

Depth (meters)	Pressure (bars)	Density (g/cm^3)
0.0	1.0	1.101
-3.9	0.6	1.110
-1.4	0.9	1.104
1.9	1.2	1.097
6.2	1.7	1.090
11.9	2.3	1.082
19.2	3.1	1.075
28.5	4.0	1.067
40.0	5.2	1.058
54.3	6.7	1.050
71.7	8.5	1.041
92.7	10.6	1.033
117.9	13.2	1.024
147.8	16.2	1.015
183.1	19.7	1.005
224.3	23.7	0.996
272.2	28.4	0.986
327.6	33.7	0.977
391.1	39.7	0.967
463.8	46.6	0.957
546.4	54.3	0.947
639.9	62.9	0.937
745.5	72.6	0.927
864.2	83.3	0.916
997.3	95.2	0.906
1146.2	108.4	0.896

T_b = 104.7°C

Fig A3.2 Boiling curves for H_2O liquid (0 wt.%) and for brine of constant compositon given in weight % equivalent NaCl. Insert gives pressures at different depths as calculated from the cumulative density. (from Hass 1971, fig 2, table 1b.)*.

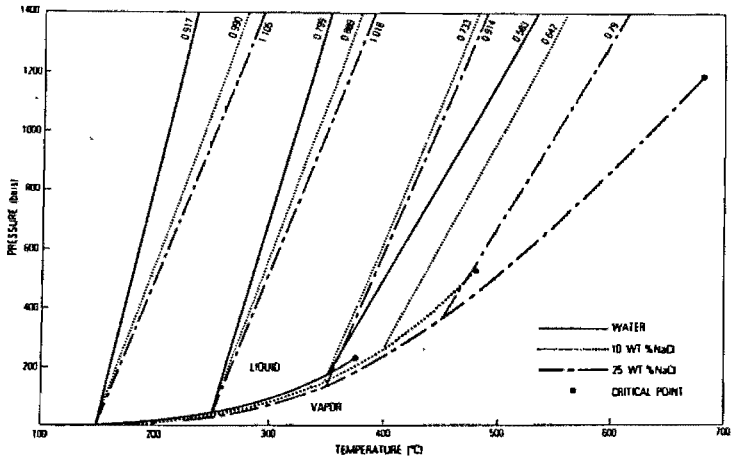

Fig A3.3 A portion of the phase diagram for water and 10 and 25 wt. % equiv. NaCl solutions showing the liquid- vapour (boiling) curves and several isochores (g cm^{-3}). (from Roedder and Bodnar, 1980, fig4.).*

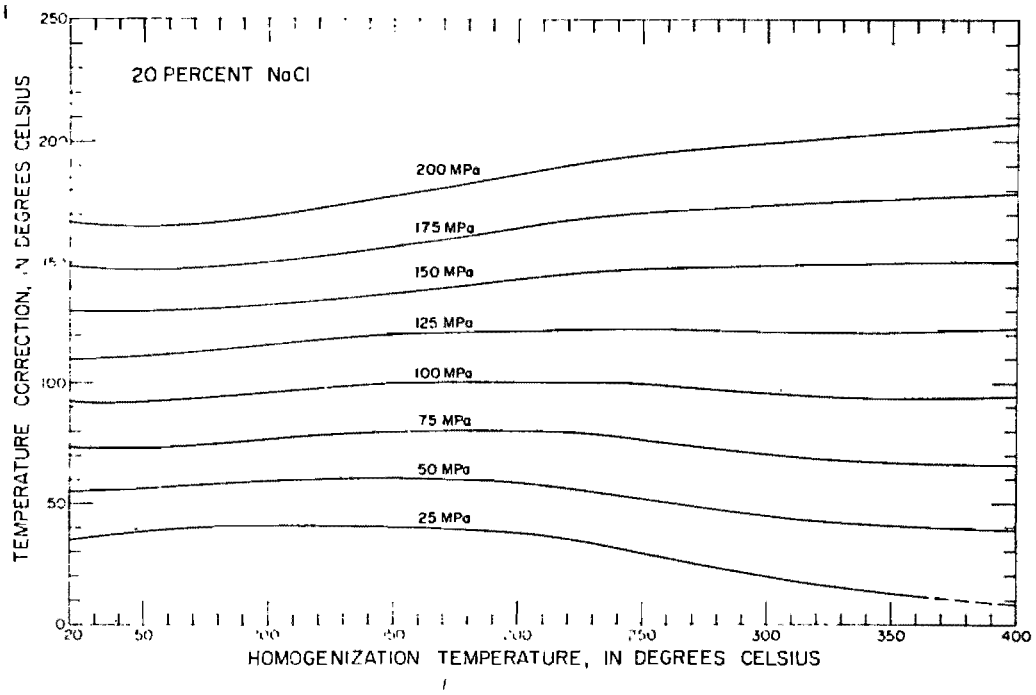

Fig A3.4 Temperature correction for a 20 wt. % equiv. NaCl solution as a function of homogenization temperature and confining pressure. (from Potter 1977.)*.

Converstion of Freezing Point Data to Salinities

For two phase inclusions consisting of an aqueous phase and a vapour bubble, freezing point depression data may be converted to salinity by the following equation of Potter et al. (1978)* -

$$W_s = 0.00 + 1.76958\theta - 4.2384 \times 10^{-2}\ \theta^2 + 5.2778 \times 10^{-4}\ \theta^3 + 0.028$$

where W_s = salinity in wt% equiv. NaCl
θ = (0 - freezing point).

Geobarometry

Homogenization pressure may be estimated by locating the position of the solvus (boiling curve) at the temperature of homogenization and for a known salinity. Appropriate diagrams from which homogenization pressure may be calculated are shown in figs A3.2 and A3.3.

Pressure-Salinity Corrections

If salinity, homogenization temperature T_H, and pressure are known or may be estimated, a temperature correction can be established so that the trapping temperature T_T may be derived, i.e. $T_T = T_H$ + (pressure-salinity correction). The appropriate diagram for 20 wt% NaCl is given in fig. A3.4.

---

* references given in main reference section

APPENDIX A4

SULPHUR ISOTOPE EXPERIMENTAL METHODS

Sulphur isotope studies of sulphide- and sulphate-bearing mineral phases of the Gourlays Creek Prospect were performed in the Central Science Laboratory, University of Tasmania. All vacuum line and mass spectrometry work was kndly undertaken by Sharon Adrichem while conversion of S values to $S^{34}S_{CDT}$ was performed by Philip Robinson (Analytical Chemist, Geology Department).

Sulphide and sulphate samples were with hand picked or drilled using tungsten carbide or diamond tipped drills and a dentist drill handpiece from polished slabs of drill core and outcrop samples. Twelve, 16 and 20 mg of pyrite, chalcopyrite and pyrrhotite respectively are required for quantitative analyses. Sulphide samples were combusted directly to SO_2 by reaction with Cu_2O in a vacuum at 1000°C by the method of Robinson and Kusakabe (1975). The SO_2 liberated was analyzed by mass spectrometric techniques giving standard deviations in the range of ± 0.02 - ± 0.05‰.

Similar techniques to those used for sulphide analysis are used for barite analysis. Fifteen mg of barite is required and combustion is by reaction with a SiO_2/Cu_2O mixture at 1120°C under vacuum.

Important Equations

$$\delta^{34}S_{sample} = \frac{(^{34}S/^{32}S)_{sample}}{(^{34}S/^{32}S)_{standard}} - 1 \quad \times 1000 \qquad \ldots(1)$$

Pyrite-pyrrhotite sulphur isotope geothermometer*:

$$T = \frac{(0.55 + 0.04)}{\Delta^{1/2}} \times 10^3 \qquad \ldots(2)$$

$$\Delta = \delta^{34}S_{py} - \delta^{34}S_{po} = \left[\frac{(0.55 + 0.04) \times 10^3}{T}\right]^2$$

put $\delta^{34}S_{py} = 0$

then $\delta^{34}S_{po} = -0.8$ at 350°C (623°K)

$= -1.1$ at 250°C (523°K)

Sulphates-pyrite sulphur isotope geothermometer**:

$$T = \frac{2.16 \times 10^3}{(\Delta - 6 \pm 0.5)^{1/2}} \qquad \ldots(3)$$

$$\Delta = \delta^{34}S_{barite} - \delta^{34}S_{py} = \left|\frac{2.16 \times 10^3}{T}\right|^2 + 6$$

put $\delta^{34}S_{py} = 0$

then $\delta^{34}S_{barite} = +18.0$ at $350^{\circ}C$ ($623^{\circ}K$).

References

* Robinson, B.R. and Kusakabke, M. (1975), Quantitative preparation of sulphur dioxide for $^{34}S/^{32}S$ analyses from sulphides by combustion with cuprous oxide: **Analyt. Chem., 47**: 1179-1181.

** Ohmoto, H. and Rye, R.O. (1979), Isotopes of sulphur and carbon: in Barnes, H.L. (Ed.), **Geochemistry of Hydrothermal Ore Deposits**: 509-567.

APPENDIX A5

Analytical Procedures

Sample preparation: All samples used for X.R.F. analysis were thoroughly trimmed and cleaned before crushing. Samples were initally crushed in a jaw crusher and then reduced to a fine powder using a vibrating swingmill. A tungsten carbide mortar was used and the crushing time was restricted to 30 second runs.

Fused borate glass discs for major element analysis were prepared from a mixture of lithium borate flux and rock powder as described by Norrish and Hutton (1969). Trace elements were analyzed in pills prepared by packing 4 gms. of rock powder into a boric acid backing.

X-ray fluorescence analysis: X.R.F. analysis of rock samples was completed under the supervision of Mr. P. Robinson on a Phillips PW 1410 x-ray spectrometer. The major elements analysed were SiO_2, Al_2O_3, Fe_2O_3, CaO, K_2O, MgO, TiO_2, P_2O_5, MnO and Na_2O. Trace elements analyzed for were Nb, Zr, Y, Sr, Rb, Ni, Cr and V.

Electron microprobe analysis: Microanalysis of mineral specimens were carried out on a JEOL JXA-50A scanning electron probe analyser operatingg in conjunction with an energy dispersive analysis system (EDAX). Accuracy of analysis is approximately $\pm$2% (relative) for concentrations above 10%, $\pm$5% for concentrations in the range 1-5% and $\pm$10% for concentrations below 1%.

Microprobe analysis given in the following pages are representative analysis for the dominant skarn minerals in the Gourlays Creek skarn. The columns are from left to right; analyzed molecule, analyzed molecular percentages, molecular number and correctrd to 100% molecular percentages. Not that for hydrous minerals, eg amphiboles, the molecular percentages are low and that they are not recalculated back to 100%.

References:

Norrish, K. and Hutton, T.T.,(1969), An accurate X-ray spectrographic method for analysis of a wide range of geochemical samples: **Geochem. Cosmochim. Acta.**, 33, 431-453.

Garnet

SIO2	35.40	2.9908	35.30
FE203	31.73	2.0172	31.64
MNO	0.44	0.0316	0.44
CAO	32.71	2.9613	32.62
SUMME	100.28	8.0008	100.00

CORR: 0

SIO2	34.97	2.9927	35.32
FE203	31.14	2.0112	31.54
MNO	0.52	0.0379	0.53
CAO	32.19	2.9601	32.61
SUMME	98.73	8.0019	100.00

CORR: 0

SIO2	38.57	2.9469	38.08
TIO2	0.34	0.0195	0.34
AL203	17.56	1.5815	17.34
FE203	8.30	0.4772	8.19
MNO	0.62	0.0398	0.61
CAO	35.91	2.9394	35.45
SUMME	101.29	8.0042	100.00

CORR: 0

SIO2	38.22	2.9828	38.05
AL203	14.44	1.3278	14.37
FE203	11.82	0.6943	11.77
MNO	0.35	0.0230	0.35
CAO	35.62	2.9783	35.46
SUMME	100.44	8.0062	100.00

CORR: 0

SIO2	37.34	2.9724	36.60
AL203	8.11	0.7612	7.95
FE203	21.53	1.2895	21.10
MNO	0.54	0.0362	0.53
CAO	34.51	2.9430	33.82
SUMME	102.04	8.0023	100.00

CORR: 0

SIO2	38.73	2.9724	37.90
AL203	14.85	1.3435	14.54
FE203	11.88	0.6863	11.63
MNO	0.47	0.0308	0.46
CAO	36.23	2.9727	35.46
SUMME	102.17	8.0127	100.00

CORR: 0

Clinopyroxene

SIO2	54.68	1.9944	54.75
FEO	2.02	0.0617	2.02
MGO	17.19	0.9344	17.21
CAO	25.97	1.0151	26.01
SUMME	99.86	4.0056	100.00

SIO2	52.22	1.9879	51.56
FEO	13.94	0.4438	13.76
MNO	0.61	0.0197	0.60
MGO	9.62	0.5458	9.50
CAO	24.89	1.0150	24.57
SUMME	101.28	4.0121	100.00

SIO2	49.41	1.9933	50.62
FEO	17.91	0.6043	18.35
MNO	0.78	0.0266	0.80
MGO	6.32	0.3799	6.47
CAO	23.19	1.0024	23.76
SUMME	97.61	4.0066	100.00

SIO2	51.31	1.9983	51.75
FEO	13.93	0.4538	14.05
MNO	1.40	0.0463	1.42
MGO	8.98	0.5211	9.05
CAO	23.53	0.9820	23.73
SUMME	99.16	4.0016	100.00

SIO2	50.32	1.9849	50.30
FEO	18.39	0.6066	18.38
MNO	0.93	0.0311	0.93
MGO	6.48	0.3812	6.48
CAO	23.93	1.0112	23.92
SUMME	100.05	4.0150	100.00

SIO2	52.68	1.9767	52.07
AL203	0.20	0.0089	0.20
FEO	9.59	0.3008	9.48
MNO	1.47	0.0466	1.45
MGO	12.02	0.6721	11.88
CAO	25.22	1.0138	24.93
SUMME	101.17	4.0189	100.00

Epidote

SIO2	36.79	6.1836
TIO2	0.23	0.0287
AL203	22.01	4.3599
FEO	13.12	1.8438
CAO	23.28	4.1914
SUMME	95.42	16.6074

SIO2	37.43	6.1755
TIO2	0.22	0.0268
AL203	22.64	4.4035
FEO	13.20	1.8212
CAO	23.58	4.1685
SUMME	97.06	16.5956

Axinite

SIO2	41.60	8.7666
AL203	17.77	4.4130
FEO	8.71	1.5352
MNO	4.14	0.7385
MGO	0.22	0.0688
CAO	19.95	4.5047
SUMME	92.38	20.0268

SIO2	41.53	8.7679
AL203	17.83	4.4379
FEO	8.26	1.4590
MNO	4.28	0.7645
MGO	0.24	0.0768
CAO	19.92	4.5069
SUMME	92.07	20.0130

Tremolite

SIO2	56.42	7.8823
AL203	0.47	0.0778
FEO	4.29	0.5016
MGO	22.24	4.6323
CAO	13.26	1.9849
SUMME	96.69	15.0788

SIO2	57.21	7.9594
AL203	0.39	0.0636
FEO	4.69	0.5461
MGO	21.79	4.5177
CAO	12.89	1.9220
SUMME	96.97	15.0088

Hornblende

SIO2	47.28	7.4473
AL203	4.23	0.7845
FEO	26.67	3.5137
MNO	0.59	0.0793
MGO	5.70	1.3383
CAO	11.71	1.9769
K20	0.20	0.0408
SUMME	96.39	15.1807

SIO2	48.68	7.6263
AL203	2.88	0.5316
FEO	28.45	3.7269
MNO	0.81	0.1076
MGO	4.92	1.1493
CAO	11.60	1.9462
K20	0.20	0.0399
CL	0.10	0.0266
SUMME	97.64	15.1543

Granville Harbour

GEOLOGICAL INTERPRETATION MAP

by RG Norris

2/85

Scale 1:5000

MN
TN

SEDIMENTARY LITHOLOGIES

- Myrtle Schist (Austhur Lineament)
- Gonah Formation
- Duck Creek Sequence*
- Zeehan Conglomerate
- Gordon Limestone
- Eldon Group**
  - Crotty Quartzite
  - Amber Slate
  - Keel Quartzite
  - Austral Creek Siltstone
  - Florence Quartzite
- Quarternary Cover
- Beach Sand

IGNEOUS LITHOLOGIES

- Heemskirk Granite
- Tertiary Basalt

SYMBOLS

- lithological boundary
- F — Fault
- conformable contact
- unconformable contact
- CRA/Geopeko grid lines
- ▲ massive magnetite-(hematite) pyrite- quartz outcrop
- DDHGC2 ⊕ diamond drill hole
- limit of outcrop
- ■ shack
- road/ track

INTERPRETED MAGNETIC HORIZONS***

- magnetite- pyroxene-quartz- garnet skarn
- banded magnetite- pyrite barite-magnetite and magnetite-garnet horizons.
- axis of (300- 1360nT) aeromagnetic anomaly.

* Defined by Blissett (1962) as Gonah Formation.

** As befined by Blissett (1962).

*** Interpreted from Kendall (1984).

APPENDIX A.6